DIAGNOSTIC ACCURACY OF CHEST COMPUTED TOMOGRAPHY IN DIAGNOSIS OF LUNG TUMORS AMONG ADULTS BASED ON HISTOPATHOLOGY AT MOI TEACHING AND REFERRAL HOSPITAL.

BY

AKORA ROSEMARY MORAA

A RESEARCH SUBMITTED IN PARTIAL FULFILLMENT OF THE REQUIREMENTS FOR THE AWARD OF A MASTERS OF MEDICINE DEGREE IN RADIOLOGY AND IMAGING, MOI UNIVERSITY, KENYA.

DECLARATION

Student's Declaration:

I declare that this research is my original work, and that it has not been presented elsewhere for academic purposes or otherwise, to the best of my knowledge. The research was carried out while pursuing my Master of Medicine in Radiology and Imaging course at the School of Medicine, Moi University. No part of this work may be reproduced without the permission from the author and/ or Moi University.

Dr. Akora Rosemary

SM/PGR/08/18

Signature:……Date:……

Supervisors Declaration

This thesis has been submitted for examination with my approval as a University supervisor.

Dr. Abuya Joseph M.

Senior Lecturer, Department of Radiology and Imaging, School of Medicine, Moi University

Signature:……Date:……

Dr. Ouma Victor

Consultant Radiologist, Directorate of Radiology and Imaging, Moi Teaching and Referral Hospital

Signature:……Date:…….

DEDICATION

I dedicate this work to my loving parents Henry Siro and Eunice Angote, for their support, encouragement and motivation throughout my entire life and education journey and in preparing this thesis, as well as my lovely daughter, Corinne Isla for her constant presence, positivity and inspiration in my life.

I also dedicate this work to my fellow radiologists who are committed to providing prompt radiological diagnoses that enable timely patient management and subsequent improvement of clinical outcomes.

Unfortunately, my loving dad passed on before completion of my postgraduate studies.

ACKNOWLEDGEMENT

I would wish to thank the Almighty God for giving me the opportunity to do this study. I want to thank Moi University, School of Medicine and Moi Teaching and Referral Hospital for the opportunity to do the study. I sincerely wish to thank my Supervisors Dr. Joseph Abuya and Dr.Victor Ouma, for their guidance and support in this research. I would also like to acknowledge the Dean, School of Medicine at Moi University for this opportunity. My gratitude is extended to all the lecturers in the Department of Radiology and Imaging, the consultant radiologists at the Directorate of Radiology and Imaging in MTRH as well as the pathologist at the Histopathology Department. I am grateful to my biostatistician for his invaluable input during the data mining and analysis process. I am thankful to the Kisii County Government and National Government for granting me the study leave. I thank my fellow colleagues and support staff for their invaluable support and guidance in this research, as well as Chandaria Faraja Lung Cancer Care Programme, for their immense support on following up on the care of the lung tumor patients.

TABLE OF CONTENTS

LIST OF TABLES

LIST OF FIGURES

SAMPLE IMAGES

ABSTRACT

Background: Globally, lung cancer is the leading cause of cancer incidence and mortality, accounting for about 2 million diagnoses and 1.8 million deaths (18.4% of cancer deaths). In Kenya, lung cancer is ranked as the fourteenth cause of cancer morbidity and mortality. The burden of lung cancer in the adult population is largely unknown, as most patients are managed for pulmonary tuberculosis because of similar clinical manifestations. Most lung cancer patients in Kenya are diagnosed late when the disease is in its advanced stages, due to the long waiting time for definitive diagnosis from biopsy and histopathology studies. Chest Computed Tomography (CT) scan comprehensively evaluates lung tumors based on morphology and can stage the disease due to ability to reduce overlap from lung lesions, bones and mediastinal structures, and identify adenopathy. Image-guided biopsy and histopathology studies give definitive diagnosis when pre-biopsy evaluation and imaging highly suggests a lung tumor, but these services are limited mostly to referral hospitals.

Objectives: To describe the chest CT and histopathologic findings of lung tumors, and to determine the diagnostic accuracy of chest CT in the diagnosis of lung tumors based on histopathology among adults at Moi Teaching and Referral Hospital (MTRH).

Methods: This was a cross-sectional study conducted at the Radiology and Imaging Department between October 2021 and September 2022. A consecutive sampling method was used to enroll 86 participants. Chest CT images were acquired using the 128 slice Neo-soft 4000 Dual CT machine. Adults with suspected lung tumors from chest CT scan underwent image guided biopsy at the Interventional Radiology (IR) unit and histopathology results were obtained from histopathology laboratory. Data was collected using a data collection form, where demographics, chest CT findings and histopathological findings were recorded. Continuous variables were summarized using mean, median and standard deviation whereas categorical variables were summarized in frequency tables, percentages, charts and bar graphs. Analysis of data was done using STATA version 16 to determine correlation between chest CT and histopathology findings. The sensitivity, specificity, positive predictive value (PPV), negative predictive value (NPV), positive likelihood ratio (PLR), and negative likelihood ratio (NLR) were determined from the 2X2 table. The diagnostic accuracy was determined by Cohen's kappa statistic.

Results: The female to male ratio was 9:8 (52.3:47.7%). The mean age of the participants was 55 years (range 23-86 years, S.D. of 15.57). Malignant features were seen in 76.7% of chest CT scans and benign in 23.3%. Suspicious features of lung tumors on chest CT included: solid components, intense homogenous enhancement, irregular margins and lymphadenopathy. On histopathology, malignant tumors accounted for 86.0% while benign tumors were 14.0%. The commonest malignant lesion on histopathology was adenocarcinoma (51.2%). Chest CT had a diagnostic accuracy of 91.86%, sensitivity of 98.46%, specificity of 71.43 %, PPV of 91.43%, NPV of 93.75 %, with a PLR and NLR of 3.38 and of 0.17 respectively, in the detection of lung tumors. There was substantial agreement between CT and histopathology findings with Cohen's kappa, $\kappa = 0.764$, $p < 0.0001$.

Conclusion: The common tumor on chest CT findings was the malignant type. The prominent tumor on histopathology findings was also the malignant type, with the major histopathologic sub-type being adenocarcinoma. Chest CT demonstrated a high diagnostic accuracy, sensitivity and specificity in detecting lung tumors based on the obtained histopathology results.

Recommendation: There should be increased awareness among radiologists and clinicians on high index of suspicion for lung malignancy based on the salient chest CT features, especially where IR and histopathology services are limited. Chest CT can be used for pre-biopsy screening of lung tumors owing to its high sensitivity and specificity.

LIST OF ABBREVIATIONS

AAH	Atypical Adenomatous Hyperplasia
ADC	Adenocarcinoma
AIS	Adenocarcinoma in situ
ASC	Adenosquamous Carcinoma
CI	Confidence Interval
COVID Test	Coronavirus Disease Test
CT	Computed Tomography
CXR	Chest X-ray
FHG	Full Haemogram
FNAC	Fine Needle Aspiration Cytology
GGO	Ground Glass Opacification
GGN	Ground Glass Nodule
INR	International Normalised Ratio
IR	Interventional Radiology
IREC	Institutional Research Ethics Committee
KNH	Kenyatta National Hospital
LCC	Large Cell Carcinoma
LMIC	Little and Middle Income Countries
LPG	Liquefied petroleum gas
METS	Metastasis

MIA	Minimally invasive adenocarcinoma
MTRH	Moi Teaching and Referral Hospital
MUSOM	Moi University School of Medicine
PTNB	Percutaneous transthoracic needle biopsy
NSCC	Non-Small Cell Carcinoma
SQCC	Squamous Cell Carcinoma
SMCC	Small Cell Carcinoma
UECs	Urea, Electrolytes and Creatinine
WHO	World Health Organization

OPERATIONAL DEFINITION OF TERMS

Adult An individual aged 18 years and above.

Diagnostic accuracy The ability of a test to discriminate between the target condition and health. It measures the ability of a test to detect a condition when it is present and detect the absence of a condition when it is absent. Test result correctly identifies the presence of the condition and incorrectly identifies the presence of the condition when it was absent. Comparison of the result of a diagnostic test to the true known condition of each subject classifies each outcome as: true positive (TP) test result correctly identifies the presence of the condition; false positive (FP) test result identifies the presence of the condition when it was absent; true negative (TN) test result correctly identifies the absence of the condition and false negative (FN) test result incorrectly identifies the absence of the condition when it was present.

Chest CT scan It is an imaging modality that uses special X-ray equipment to visualize the lungs and the surrounding structures to help diagnose the cause of unexplained cough, shortness of breath, chest pain, fever and other symptoms. It is painless, non-invasive and fairly accurate.

Histopathology It is the study of signs of a disease using the microscopic examination of a biopsy or surgical specimen that is processed and fixed onto glass slides.

Benign	This describes tumors that stay in their primary location without invading the other sites of the body. They do not spread to nearby local structures or to distant parts of the body. They tend to grow slowly and often have distinct borders.
Lung tumor	An abnormal proliferation of cells that form within the lungs and surrounding lung structures which can either be benign (non-cancerous) or malignant (cancerous).
Malignant	This describes tumors whose cells grow uncontrollably and spread locally and/or to distant sites. They are cancerous in nature. They invade other sites.
Metastasis	The spread of cancer cells from their original site (primary tumor) to another part of the body via lymphatic or hematogenous spread.
Primary lung tumor	Tumors arising from the cells and tissues of lung and surrounding lung tissues.
Sensitivity	It is the ability of a test, CT in this case, to correctly classify an individual as having a disease as compared to the goal standard (histopathology).
Specificity	It is the ability of a test to correctly classify an individual as not having a disease.
Gold standard	It is the time honored diagnostic test that is considered to be the definitive test for the disease in question. A hypothetical ideal "gold standard" test has a sensitivity of 100% with respect to the presence of the disease (it identifies all individuals with a well-

	defined disease process; it does not have any false-negative results) and a specificity of 100% (it does not falsely identify someone with a condition that does not have the condition).
Positive predictive value	It is the probability of patients with true positive results (having the condition of interest) to test positive.
Negative predictive value	It is the probability of patients with true negative results (have no disease) to test negative.
Triple Serology	A blood screen for Hepatitis B, Hepatitis C and Syphilis.

CHAPTER ONE: INTRODUCTION

1.1 Background of the study

Lung cancer poses one of the greatest challenges in the overall public health globally, because of its high incidence, steep financial implications, poor outcomes and a great burden to the caregivers. In addition to the significantly high mortality associated with lung tumors, there is a considerable need for terminal care and palliative care for patients which are expensive. There is also resultant psychological stress that comes about due to the aforementioned implications (Gaafar, 2017).

Information on cancer patterns in the Sub-Saharan Africa is very sparse (Korir et al., 2015). The low overall survival rate of lung cancer is linked to late diagnosis and metastasis. Comprehensive data within the African continent is limited due to the lack of a registry, financial constraints, and low public awareness of lung cancer as well inadequate screening and treatment facilities. Additionally, there is lack of conclusive data in our setting (Said, 2023).

Lung cancer diagnosis has been a great challenge in Kenya at large due to the technicalities that are related to the screening and diagnostic procedures. The burden of lung cancer in the adult population is largely unknown, as most of the patients are managed for Pulmonary Tuberculosis, because they both have similar clinical manifestations (Atundo et al., 2018).

1.1.1 Lung tumors

A solitary pulmonary nodule is defined as a circumscribed pulmonary opacity with no associated pulmonary, pleural, or mediastinal abnormality and measures less than 3 cm in diameter. Many of the nodules are discovered incidentally, but up to 40% may be discovered to be malignant.

Benign intrapulmonary lymph nodes are nodules that are less than 15mm from the pleural surface, are ellipsoid in shape and are normally connected to the pleural surface by a fine linear opacity.

Ground-glass nodules are classified into three categories:

1. Ground-glass density, which is a focal area of increased lung attenuation that can be well or poorly defined, through which normal lung structures can be seen.
2. Pure ground-glass nodule, which has no soft tissue component
3. Part solid ground-glass nodule, which demonstrates a solid component obscuring lung architecture

The main way of differentiating between benign and malignant lung masses/tumors are two primary criteria that is, the rate of growth (stability over time) and the attenuation of the nodule. The patient's age also plays a significant distinguishing feature (a carcinoma is likely seen in less than 1% of patients under the age of 35 years.

Regarding the rate of growth/stability over time, benign lesions show a doubling time of less than 1 month or more than 18 months. However, the bronchoalveolar

carcinomas are an exemption in that they may have very slow growth rates. The bronchial carcinomas usually have a doubling time of between 1 and 18 months.

On matters attenuation or enhancement, a dense central nidus or lamellated calcification indicates a granulomatous process (e.g. tuberculosis, histoplasmosis) while an irregular 'popcorn' calcification may suggest a hamartoma. Fat is virtually diagnostic of a hamartoma. A lack of enhancement with Hounsfield Units (HU) of less than 15 post contrast enhancement is highly indicative of benignity.

Granular calcification can be seen on CT scans in up to 7% of carcinomas. This can represent either tumor calcification or a granuloma that is engulfed by tumor. Eccentric or stippled calcification within soft tissue may be highly indicative of malignancy. A mixture of soft tissue and ground-glass attenuation nodules is more likely to be malignant than if its soft tissue nodules alone.

Size is of little diagnostic value since most benign nodules are less than 2cm. Round, flat or tubular nodules tend to be mostly benign. With regard to margins, a well-defined mass with a smooth pencil-sharp margin is likely to be benign. Carcinomas tend to have ill-defined margins which are irregular, spiculated, or lobulated and may also exhibit umbilication or a notch. Unfortunately all these features can also be seen with benign disease.

FDG-PET is useful for nodules more than 1 cm. A positive result is 97% sensitive and 82% specific for malignancy. False-positive result can occur secondary to an infectious or inflammatory process (e.g**.** tuberculosis, sarcoid or rheumatoid nodules). A false-negative result: this can occur if a nodule is less than 1cm. It can also occur

due to a carcinoid tumor or a slow growing adenocarcinoma sub-type.(Grainger 2019, n.d.)

The Fleischner Society guidelines for nodule management released in 2017 are based on creating a much better understanding of the morphologic features of pulmonary nodules, reliable size measurements, recognition of sub-solid components, an understanding of interval growth or change in nodule morphology, and knowledge of the patient's risk factors. They are aimed at expanding the flexibility of the ordering clinicians and subsequently individualize the management of nodules. The new criteria demand a better understanding and knowledge of pulmonary nodules and the factors that may influence their behavior over time (Bueno et al., 2018).

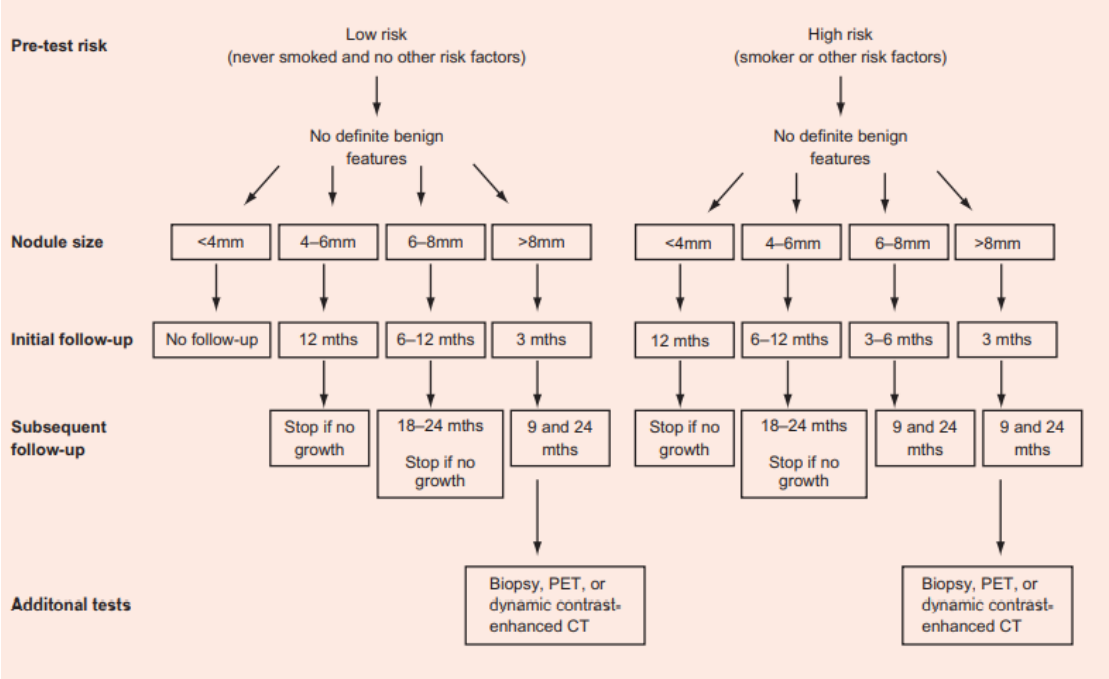

Figure 1: The Fleischner Society guidelines provide a strategy for follow-up and management of pulmonary nodules in patients over 35 years of age with no known malignancy.

The 2021 WHO Classification of Thoracic Tumors contains the classification of lung tumors in one of the chapters. The principles entail those of using morphology first, supported by immunohistochemistry, and then molecular techniques. In 2015, the use of immunohistochemistry made a clear-cut emphasis on the accuracy of classification. In 2021, there is greater emphasis on advances in molecular pathology across all the tumor types (Nicholson et al., 2022).

The tumor types are classified as shown below according to (Nicholson et al., 2022).

Epithelial tumors	
Papillomas	
Squamous cell papilloma, NOS	8052/0
Squamous cell papilloma, inverted	8053/0
Glandular papilloma	8260/0
Mixed squamous cell and glandular papilloma	8560/0
Adenomas	
Sclerosing pneumocytoma	8832/0
Alveolar adenoma	8251/0
Papillary adenoma	8260/0
Bronchiolar adenoma/ciliated muconodular papillary tumor	8140/0
Mucinous cystadenoma	8470/0
Mucous gland adenoma	8480/0
Precursor glandular lesions	
Atypical adenomatous hyperplasia	8250/0
Adenocarcinoma in situ	
Adenocarcinoma in situ, nonmucinous	8250/2
Adenocarcinoma in situ, mucinous	8253/2
Adenocarcinomas	
Minimally invasive adenocarcinoma	
Minimally invasive adenocarcinoma, nonmucinous	8256/3
Minimally invasive adenocarcinoma, mucinous	8257/3

Invasive nonmucinous adenocarcinoma	
Lepidic adenocarcinoma	8250/3
Acinar adenocarcinoma	8551/3
Papillary adenocarcinoma	8260/3
Micropapillary adenocarcinoma	8265/3
Solid adenocarcinoma	8230/3
	8253/3
Invasive mucinous adenocarcinoma	
Mixed invasive mucinous and nonmucinous adenocarcinoma	8254/3
Colloid adenocarcinoma	8480/3
Fetal adenocarcinoma	8333/3
Adenocarcinoma, enteric type	8144/3
Adenocarcinoma, NOS	8140/3
Squamous precursor lesions	
Squamous cell carcinoma in situ	8070/2
Mild squamous dysplasia	8077/0
Moderate squamous dysplasia	8077/2
Severe squamous dysplasia	8077/2
Squamous cell carcinomas	
Squamous cell carcinoma, NOS	8070/3
Squamous cell carcinoma, keratinizing	8071/3
Squamous cell carcinoma, non-keratinizing	8072/3
Basaloid squamous cell carcinoma	8083/3
Lympho-epithelial carcinoma	8082/3
Large cell carcinomas	
Large cell carcinoma	8012/3
Adenosquamous carcinomas	
Adenosquamous carcinoma	8560/3

Sarcomatoid carcinomas	
Pleomorphic carcinoma	8022/3
Giant cell carcinoma	8031/3
Spindle cell carcinoma	8032/3
Pulmonary blastoma	8972/3
Carcinosarcoma	8980/3
Other epithelial tumors	
NUT carcinoma	8023/3
Thoracic SMARCA4-deficient undifferentiated tumor	8044/3
Salivary gland-type tumors	
Pleomorphic adenoma	8940/0
Adenoid cystic carcinoma	8200/3
Epithelial-myoepithelial carcinoma	8562/3
Mucoepidermoid carcinoma	8430/3
Hyalinizing clear cell carcinoma	8310/3
Myoepithelioma	8982/0
Myoepithelial carcinoma	8982/3
Lung neuroendocrine neoplasms	
Precursor lesion	
Diffuse idiopathic neuroendocrine cell hyperplasia	8040/0
Neuroendocrine tumors	
Carcinoid tumor, NOS/neuroendocrine tumor, NOS	8240/3
Typical carcinoid/neuroendocrine tumor, grade 1	8240/3
Atypical carcinoid/neuroendocrine tumor, grade 2	8249/3
Neuroendocrine carcinomas	
Small cell carcinoma	8041/3
Combined small cell carcinoma	8045/3
Large cell neuroendocrine carcinoma	8013/3

Combined large cell neuroendocrine carcinoma	8013/3
Tumors of ectopic tissues	
Melanoma	8720/3
Meningioma	9530/0
Mesenchymal tumors specific to the lung	
Pulmonary hamartoma	8992/0
Chondroma	9220/0
Diffuse lymphangiomatosis	9170/3
Pleuropulmonaryblastoma	8973/3
Intimal sarcoma	9137/3
Congenital peribronchialmyofibroblastic tumor	8827/1
Pulmonary myxoid sarcoma with EWSR1-CREB1 fusion	8842/3
PEComatous tumors	
Lymphangioleiomyomatosis	9174/3
PEComa, benign	8714/0
PEComa, malignant	8714/3
Hematolymphoid tumors	
MALT lymphoma	9699/3
Diffuse large B-cell lymphoma, NOS	9680/3
Lymphomatoid granulomatosis, NOS	9766/1
Lymphomatoid granulomatosis, grade 1	9766/1
Lymphomatoid granulomatosis, grade 2	9766/1
Lymphomatoid granulomatosis, grade 3	9766/3
Intravascular large B-cell lymphoma	9712/3
Langerhans cell histiocytosis	9751/1
Erdheim–Chester disease	9749/3

1.1.2 Neoplastic lung tumors

Lung tumors are majorly classified according to their histopathological type. Generally, lung carcinomas are categorized by their size and appearance. Two major classes have been distinguished: small cell lung carcinoma (SCLC) and non-small cell lung carcinoma (NSCLC) (Stapelfeld et al., 2020).

The more predominant type is the NSCLC, which accounts for 85% of all cases. NSCLC includes histopathologic subtypes that include: squamous cell carcinoma, which arises from the proximal airway epithelium; large cell carcinoma, which arises from atypical epithelial cells lining the bronchi, and adenocarcinoma, which develops from gland tissue of bronchial glands located in the peripheral regions of the lung. Of these types, adenocarcinoma is the most common subtype of lung cancer (Stapelfeld et al., 2020).

SCLC is also termed as small (oat) cell carcinoma. It originates from submucosal neuroendocrine cells and it rapidly spreads via haematogenous and lymphatic spread. It manifests like a systemic disease and is usually disseminated by the time of patient presentation (Grainger 2019, n.d.).

1.1.3 Pulmonary metastases

Adult pulmonary metastases are usually from the following primary sites: breast, gastrointestinal tract, kidney, testes, head and neck tumors as well as from a variety of bone and soft tissue sarcomas. There are 3 modes of spread: haematogenous (commonest), lymphatic and endobronchial (rare). Their growth rates can be very variable, and range from very slow (e.g. metastatic thyroid carcinoma) to very rapid (e.g. metastatic choriocarcinoma or an osteosarcoma) (Grainger 2019, n.d.).

1.1.4 Benign lung tumors

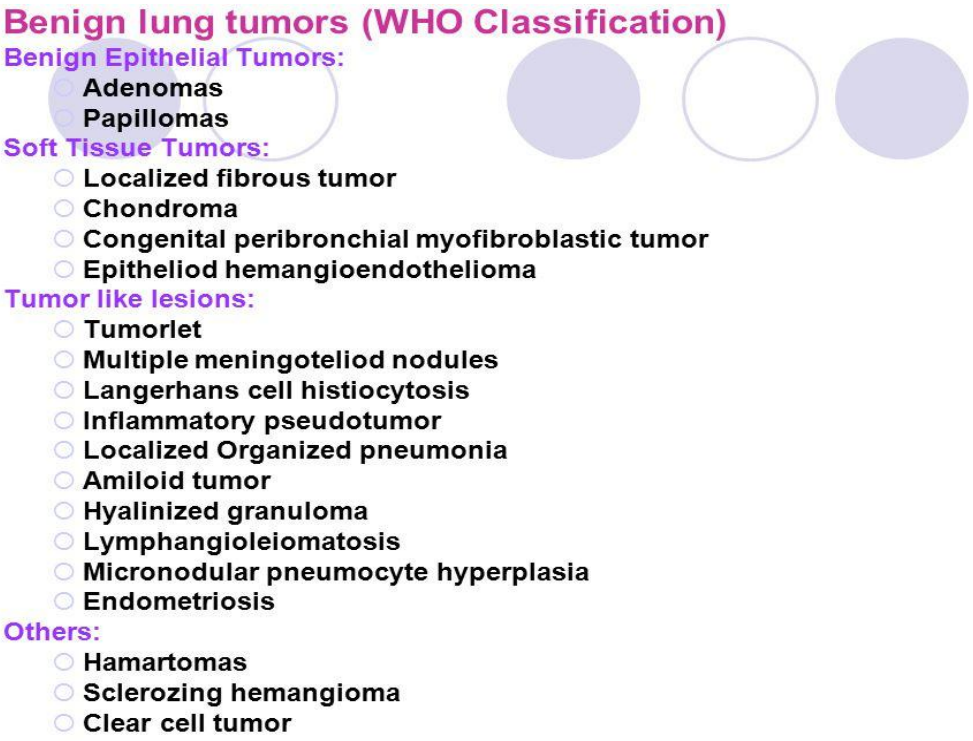

Figure 2: Classification of benign tumors of the respiratory system *(Nicholson et al., 2022).*

Benign lung tumors include but not limited to pulmonary hamartomas, leiomyoma of the lung and plasma cell granuloma of the lung (inflammatory pseudo-tumor).

Pulmonary hamartoma-A hamartoma is a tumor-like malformation that is composed of abnormal mature tissues that are normally found within the concerned organ. Pulmonary hamartomas consist of predominantly cartilage, bronchial epithelium and fat and they demonstrate slow growth. Malignant transformation is extremely rare and they can very occasionally be multiple.

Leiomyoma of the lung may appear as a solitary lesion or as multiple lesions which can present as multiple discrete lung nodules. They are also called benign

metastasizing leiomyomas) and are radiographically indistinguishable from the other benign connective tissue neoplasms

Plasma cell granuloma of the lung (inflammatory pseudo-tumor) is reactive inflammatory granulomatous tissue which appears as an asymptomatic solitary pulmonary nodule. It can demonstrate occasional cavitation or calcification (Grainger 2019, n.d.).

1.2 Problem statement

Lung cancer in Kenya is leading in incidence (11.6% of all cancer cases), seconded by breast cancer (11.6%) while colorectal (10.2%) and prostrate (7.1%) are the third and fourth respectively. Mortalities that result from lung cancer are highest mutually in both genders (18.4% of all cancer deaths), followed by colorectal cancer (9.2%), stomach cancer (8.2%) and liver cancer with (8.2%) (Warui et al., 2021).

Lung cancer is ranked 14th among all the other sites of cancer, with a prevalence of 1.75 per 100,000 and a case fatality of 92%. (KNCCS, 2017)

Lung cancer is reported to have the highest mortality rate, which corresponds to one-fifth of the overall share of the cancer-related deaths. (Said & Degu, 2023)

Lung cancer is considered to have one of the lowest survival rates, along with liver and pancreatic cancer. The 5-year relative survival rate for all the stages combined was about 12% for lung cancers diagnosed from the year 1975–1977. It was estimated to be 18% for new cancer diagnoses between the year 2003 and 2009. Lung cancer is often not diagnosed until it gets to the advanced stages of disease. This is even more so in blacks compared to whites. Advanced lung cancer has extremely poor prognosis, with a 5-year survival of only 5% (de Groot et al., 2018).

Over the last few years, there has been an increase in the incidence of patients diagnosed with lung cancer possibly resulting from outreach programs that have made it easier for patients seek the health services, as well as the establishment of referral systems. However, the referral system is not very effective in identifying the possibility of lung tumors at an early stage. Most of the patients end up being treated for infectious conditions such as tuberculosis, and by the time they get referred for CT scan of the chest, there is considerable progress of disease to the late stages. (Gaafar, 2017) Consequentially, minimal can be done to halt or control the disease progress. The patients end up with a poor prognosis and a reduced overall 5-year survival rate from the time of diagnosis.

Changes in the therapeutic scenario in the last few years have emphasized the need for a multidisciplinary approach in lung cancer management. Data from various studies show that high-volume centers and multidisciplinary teams are more efficient at managing patients with lung cancer than low-volume or non-multidisciplinary canters, by providing more complete staging, better adherence to guidelines and increased survival rates. The multidisciplinary tumor boards influence health care providers' initial plans in 26%–40% of cases. The absolute need to reach a proper and precise morphological and biological definition often requires tissue sampling. This can be quite challenging with most of the treatment decisions depending on the information obtained from the specimen collected at diagnosis (Planchard et al., 2018).

There is a lag time of several years between the beginning of smoking and the clinical manifestation of cancer. This may end up distorting the perception of lung cancer risk factors by an individual. Moreover, the lag makes clinical intervention studies to reduce the cancer risk more difficult to design and to interpret. Thus, most of the

current knowledge concerning lung cancer prevention in humans is based on observational studies (Biesalski et al., 1998).

Inadequate management and mostly under-diagnosis of lung cancer are alarming issues in the health care of most African settings. Access to timely cancer screening and treatment is one of the major challenges in Kenya (Said & Degu, 2023).

The diagnostic accuracy of CT chest scan in the diagnosis of lung cancer has not been studied in Kenya. Most of the lung chest CT scan reports usually indicate a suspicious lung mass as the tentative diagnosis without specifying if it's cancerous or non-cancerous lesion.

Most patients who require these services come from resource-limited settings. They cannot afford both the CT chest scan as well as the image guided biopsy and histopathology procedures at one point in time. They end up having progressive disease by the time the histopathology results are back, and advanced stages of the disease result in more complications and financial implications to both the patient and caregiver.

The county health facilities in Kenya offer CT scan services but there are limited centers where the interventional radiology and histopathological services are offered.

In addition to the above, the paucity of local research has resulted in inadequate knowledge on a high index of suspicion for lung tumors on chest CT scans of patients, resulting in adverse health and financial implications and higher incidence and mortality rates.

1.3 Justification of the study

Worldwide, lung cancer, its complications, the resultant health burden and a high mortality have continued to be on the rise. (Barta et al., 2019) Despite the high incidence lung cancers, very limited research has been done on their radiological appearance and prevailing types in Kenya. In depth knowledge on the prevailing patterns and the CT chest appearances can help in early and correct diagnosis and treatment of lung cancer, resulting in better outcomes and fewer complications for patients. Early detection of lung cancer may improve the patient's morbidity and mortality. Computed tomography (CT) being used as a screening tool, has been evaluated in several large screening trials for early detection of lung cancer (Rosado de Christenson, 2008).

In most lung tumors, especially in the case of peripheral lesions, transthoracic percutaneous fine needle aspiration and/or core biopsy, under imaging guidance is associated with a diagnostic accuracy of > 88% yield, a sensitivity of 90% and a false-negative rate of 22%. In the presence of a pleural effusion, thoracentesis could represent both a diagnostic tool and a palliative treatment. If fluid cytology examination is negative, image-guided pleural biopsy should be carried out.

The surgical candidates with lung tumor can be referred for percutaneous thoracic needle biopsy to provide preoperative confirmation of malignancy before definitive resection. This confirmation allows a more streamlined approach to planning and consenting for surgery and also avoids surgical resection of benign lesions, infection, and lymphoma. The nonsurgical candidates with lung cancer or metastases may be referred for PTNB to confirm malignancy before radiotherapy, ablation, or chemotherapy. In patients with known lung cancer, PTNB provides adequate tissue

for molecular analysis to identify biomarkers and mutations amenable to treatment with targeted agents and enrollment into clinical trials (Planchard et al., 2018).

This study will therefore generate information on the prevailing types of lung tumors, their appearance on chest CT scan and their confirmatory histological diagnosis. This will create awareness among the radiologists on what exactly to look out for in such cases.

With the evolution of CT scanners to high resolution, very subtle features suspicious of lung cancer can be detected. This study will guide radiologists with know-how on which suspicious lung masses may warrant histopathological attention.

This will reduce the additional cost of having to do image guided lung biopsy and histopathological services which may not be affordable for every patient.

It will also reduce the likelihood of the complications that may arise from the image guided lung biopsy such as pneumothorax, pulmonary hemorrhage, pneumothorax, infections, air embolism and tumor seeding (Winokur et al., 2013).

This study will form a basis of planning the management of such cases at all the health care levels.

This study aims to determine the diagnostic accuracy of chest in determining a conclusive histopathologic diagnosis of lung tumors among the adult patients presenting at MTRH.

1.4 Research Question

What is the diagnostic accuracy of chest CT in the diagnosis of lung tumors among adults based on histopathology at MTRH?

1.5 Objectives of the study

1.5.1 General Objective

To determine the diagnostic accuracy of chest CT in the diagnosis of lung tumors among adults based on histopathology at MTRH.

1.5.2 Specific Objectives

1. To describe CT chest findings of adult patients with lung tumors at MTRH
2. To highlight the histopathological findings of adult patients with lung tumors at MTRH
3. To evaluate the diagnostic accuracy of chest CT in the diagnosis of lung tumors among adults based on histopathology at MTRH.

CHAPTER TWO: LITERATURE REVIEW

2.1Embryology of the lungs

2.1.1 Respiratory primordium

The respiratory system starts off as a median outgrowth, the laryngotracheal groove which appears in the floor of the caudal end of the primordial pharynx. This primordium of the tracheobronchial tree develops caudal to the fourth pair of pharyngeal pouches. The endoderm lining of the laryngotracheal groove gives rise to the pulmonary epithelium and glands of the larynx, trachea, and bronchi. The connective tissues, cartilages, and smooth muscles in these structures develop from the splanchnic mesoderm surrounding the foregut.

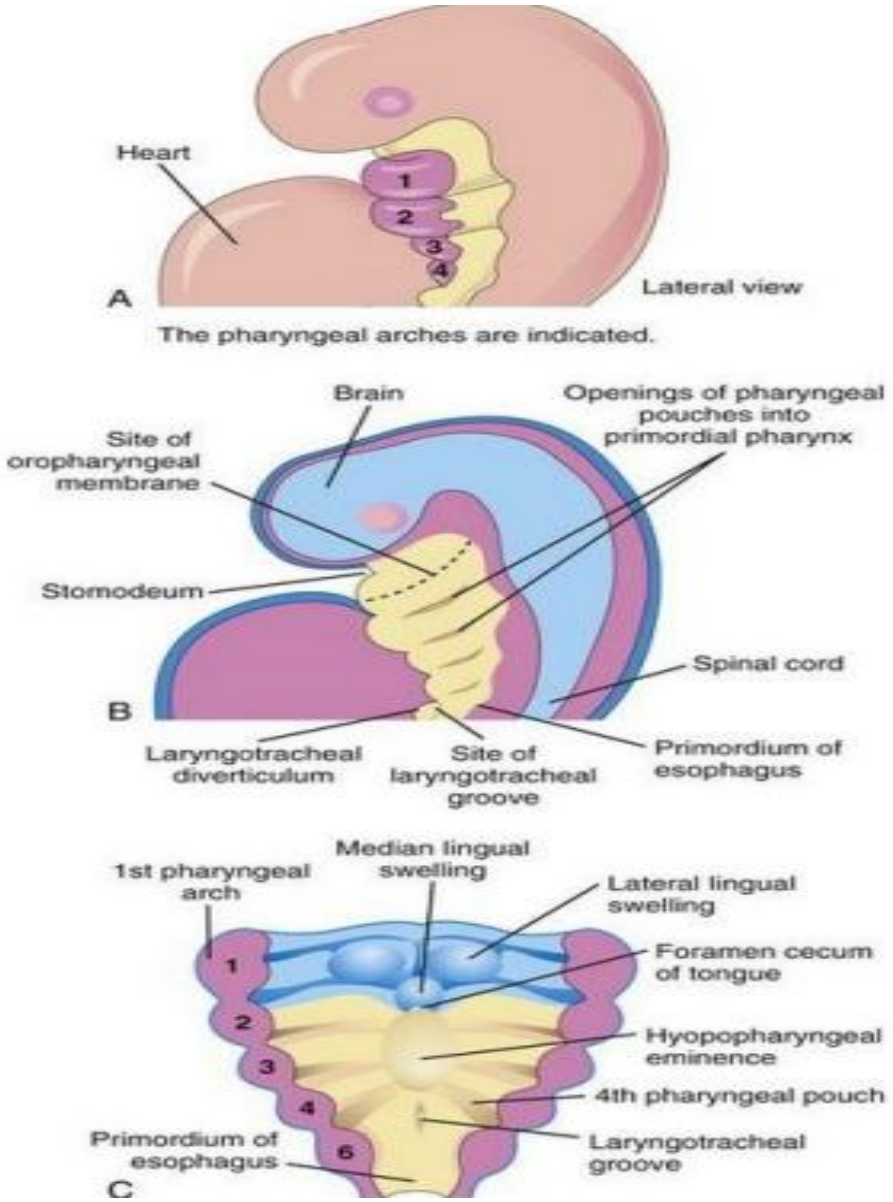

Figure 3: A shows a lateral view of a 4-week embryo illustrating the relationship of pharyngeal apparatus to the developing respiratory system. B shows a sagittal section of the cranial half of the embryo. C shows a horizontal section of the embryo illustrating the floor of primordial pharynx and location of the laryngotracheal groove *(Moore, 2019).*

By the end of the fourth week, the laryngotracheal groove evaginates (protrudes) to form a pouch-like laryngotracheal diverticulum (lung bud). This is usually located ventral to the caudal part of the foregut. As this diverticulum elongates, it becomes invested with splanchnic mesenchyme (primordial embryonic connective tissue), and

its distal end enlarges to form a globular respiratory bud; this bud denotes the single bud from which the respiratory tree originates.

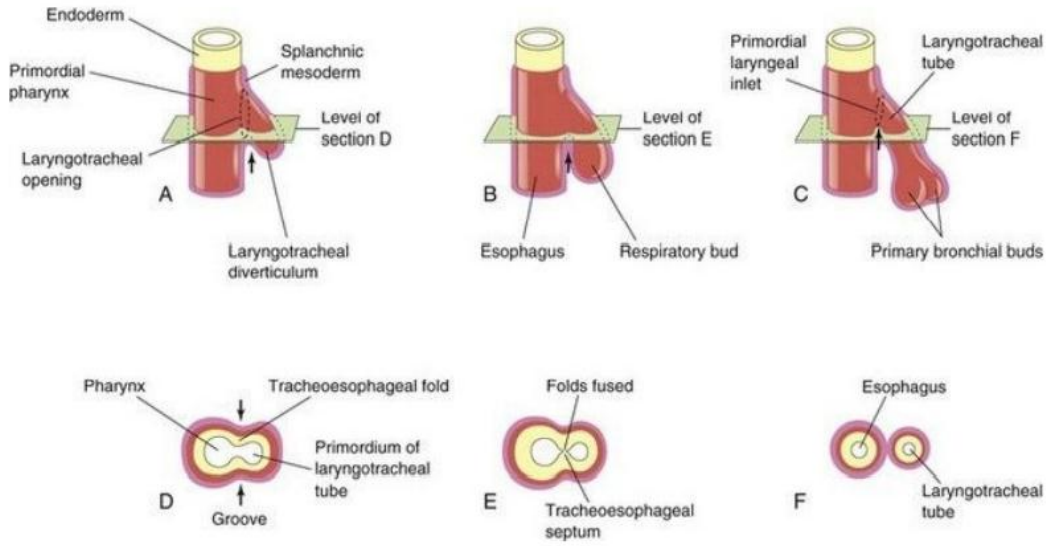

Figure 4: The successive stages in development of the tracheoesophageal septum in the fourth and fifth weeks. A to C demonstrates lateral views of the caudal part of the primordial pharynx. It shows the laryngotracheal diverticulum and then the partitioning of the foregut into esophagus and laryngotracheal tube. D to F demonstrates transverse sections illustrating formation of the tracheoesophageal septum and shows how it separates the foregut into laryngotracheal tube and esophagus. The arrows indicate the cellular changes that result from growth *(Moore, 2019)*.

The laryngotracheal diverticulum then separates from the primordial pharynx but maintains a communication with it through the primordial laryngeal inlet. Longitudinal tracheoesophageal folds develop in the laryngotracheal diverticulum, then they approach each other and fuse to form a partition called the tracheoesophageal septum. This happens by the end of the fifth week. This septum divides the cranial portion of the foregut into a ventral part, the laryngotracheal tube (primordium of larynx, trachea, bronchi, and lungs), and a dorsal part (primordium of oropharynx and esophagus. The opening of the laryngotracheal tube into the pharynx now becomes the primordial laryngeal inlet.

Development of Bronchi and Lungs

The respiratory bud develops at the caudal end of the laryngotracheal diverticulum in the fourth week. The bud soon divides into two outpouchings, the primary bronchial buds. These buds grow laterally into the pericardioperitoneal canals, the primordia of the pleural cavities. Secondary and tertiary bronchial buds develop soon after this (Moore, 2019).

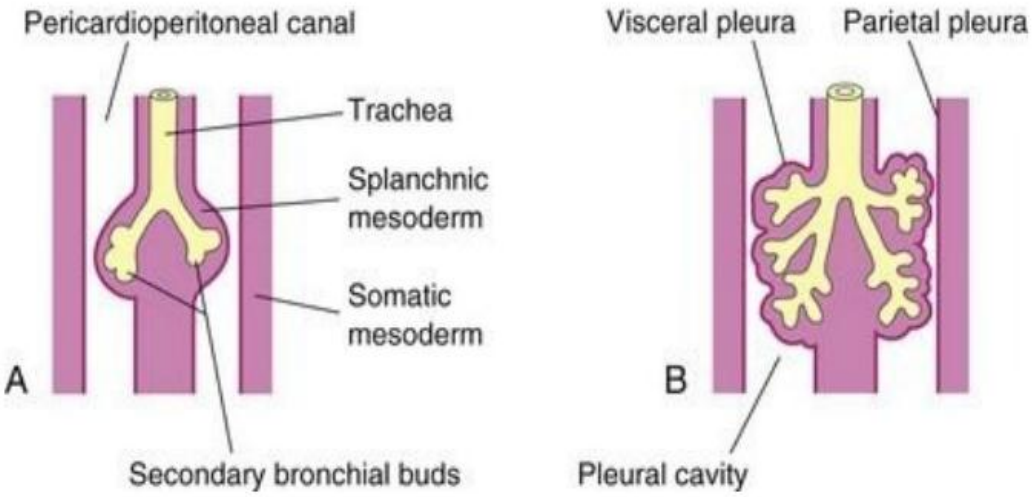

Figure 5: The diagrammatic representation of growth of the developing lungs into the splanchnic mesenchyme which is adjacent to the medial walls of the pericardioperitoneal canals (primordial pleural cavities). The development of the layers of the pleura is also demonstrated at A, 5 weeks and B, 6 weeks *(Moore, 2019).*

Together with their surrounding splanchnic mesenchyme, the bronchial buds eventually differentiate into the bronchi and their ramifications in the lungs. Early in the fifth week, the connection of each bronchial bud with the trachea enlarges to form the primordia of the main bronchi. The embryonic right main bronchus is usually slightly larger than the left one and it is oriented more vertically. This relationship still persists in the adult; consequently, a foreign body is highly likely to enter the right main bronchus than the left one.

The main bronchi then subdivide into secondary bronchi that form lobar, segmental, and intrasegmental branches. On the right, the superior lobar bronchus will supply the upper (superior) lobe of the lung, whereas the inferior bronchus subdivides into two bronchi, one to the middle lobe of the right lung and the other to the lower (inferior) lobe. On the left, the two secondary bronchi supply the upper and lower lobes of the lung. Each lobar bronchus undergoes progressive branching.

The segmental bronchi, 10 in the right lung and eight or nine in the left lung, begin to develop by the seventh week. As this occurs, the surrounding mesenchyme is also dividing. The segmental bronchi, together with the surrounding mass of mesenchyme, form the primordial of the bronchopulmonary segments. By 24 weeks, approximately 17 orders of branches are formed and respiratory bronchioles are developed. An additional seven orders of airways develop after birth. (Moore, 2019)

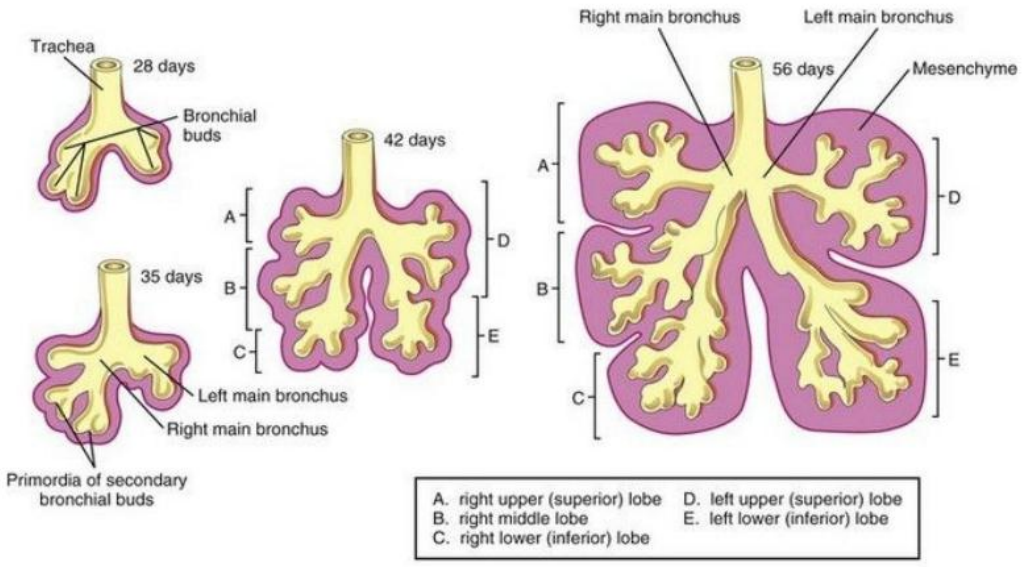

Figure 6: Successive stages in development of the bronchial buds, bronchi, and lungs *(Moore, 2019).*

As the bronchi develop, the cartilaginous plates develop from the surrounding splanchnic mesenchyme, from which the bronchial smooth muscle and connective tissue and the pulmonary connective tissue and capillaries are also derived. As lungs develop, they acquire a layer of visceral pleura from the splanchnic mesenchyme. With expansion, the lungs and pleural cavities grow caudally into the mesenchyme of the body wall and thereafter lie close to the heart. The thoracic body wall becomes lined by a layer of parietal pleura, derived from the somatic mesoderm. The space between the parietal and visceral pleura is the pleural cavity.

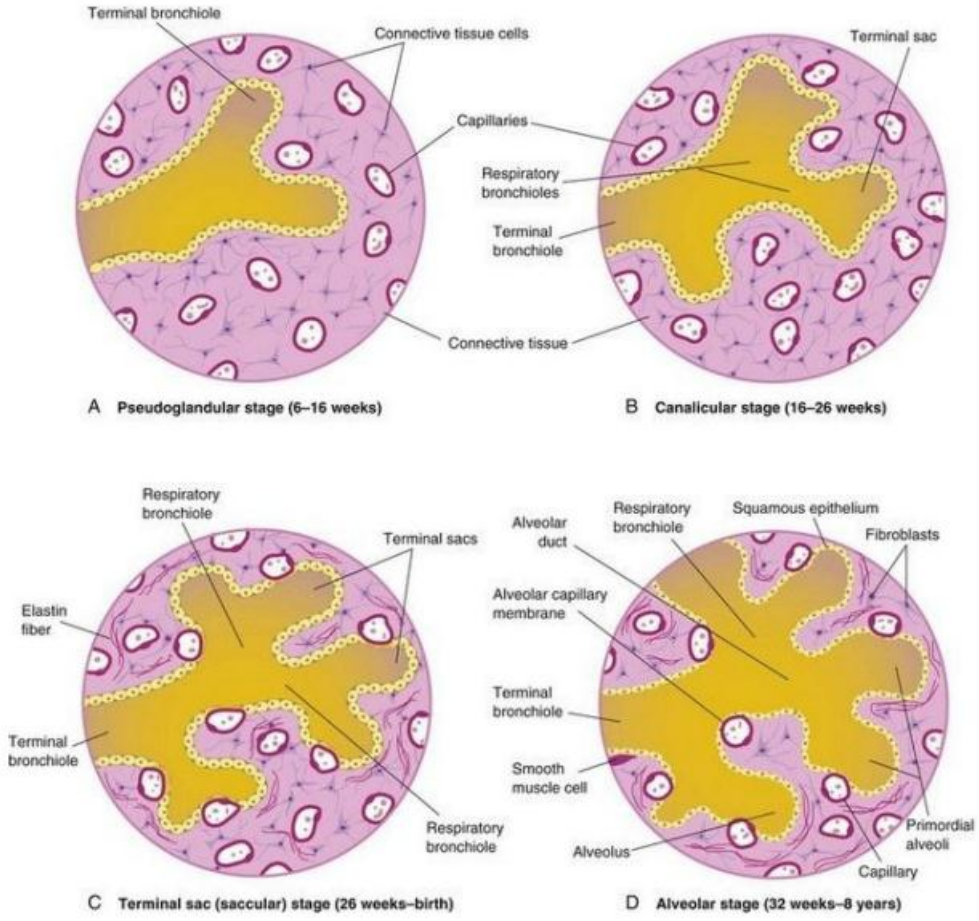

Figure 7: Diagrammatic sketches of histologic sections illustrating stages of lung development. Image A and B demonstrate the early stages of lung development. C and D demonstrate the later stages. Note that the alveoli-capillary membrane is thin and some of the capillaries bulge into terminal sacs and alveoli *(Moore, 2019).*

2.1.2. Gross anatomy of the lungs

The lungs are the organs of respiration which are located in the thorax on either side of the mediastinum within the thoracic cavity. Their function is to oxygenate blood. They achieve this function by bringing inspired air into very close contact with oxygen-poor blood in the pulmonary capillaries.

Each lung is surrounded by a pleural cavity formed by the visceral and parietal pleura. They are suspended from the mediastinum by the lung root which is a collection of structures entering and leaving the lungs. The medial surface of the lungs lies close to mediastinal structures.

The left lung is slightly smaller than the right due to the presence of the heart and has two lobes with the right having three. The lungs are roughly cone shaped and have an apex, a base, three surfaces and three borders.

Apex – This is the blunt superior aspect of the lung. It projects upwards, above level of the 1st rib and into floor of the neck.

Base – This is the inferior surface of the lung, which normally sits on the diaphragm.

Lobes (two or three) – The lobes are separated by fissures within the lung.

Surfaces (three) – These correspond to the area of the thorax that they face. They are named the costal, mediastinal and diaphragmatic.

Borders (three) – These are the edges of the lungs, named the anterior, inferior and posterior borders.

2.1.2.1. Lobes

The right lung has three lobes; the superior, middle and inferior. The lobes are divided from each other by two fissures:

An oblique (major) fissure runs from the inferior border of the lung in a superior-posterior direction, until it meets the posterior lung border. It extends from T4/T5 posteriorly to the diaphragm anterior-inferiorly.

A transverse (minor) fissure separates the upper and middle lobes of the right lung. It runs horizontally from the hilum to the anterior and lateral surfaces of the right lung, at the level of the fourth costal cartilage, to meet the oblique fissure.

The left lung contains superior and inferior lobes, which are separated by a similar oblique fissure. The lingula of the left upper lobe corresponds to the medial lobe on the right lung.

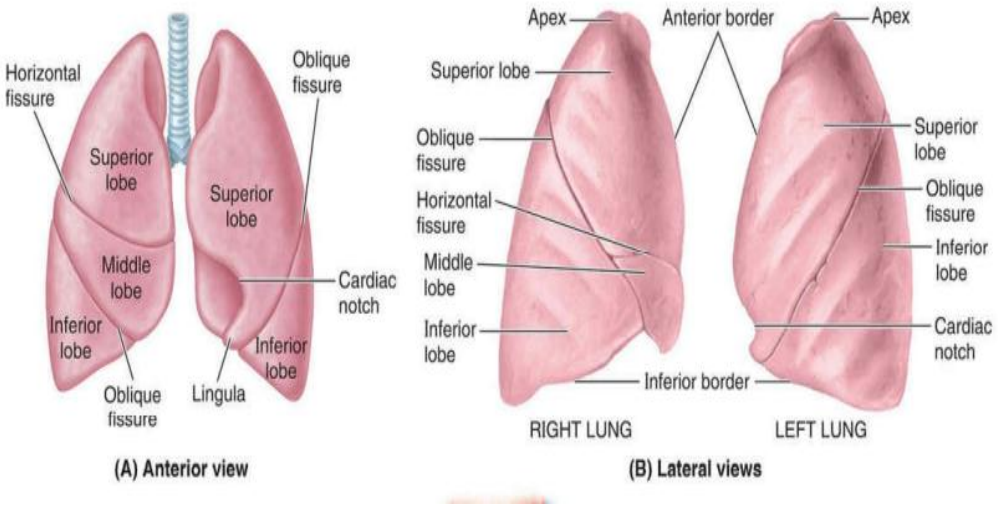

Figure 8: The costal surfaces of lungs. The lungs are demonstrated in anterior (A) and lateral views (B) showing the lobes and fissures *(Moore, 2019)*.

2.1.2.2. Bronchopulmonary segments

The lobes of each lung are divided into bronchopulmonary segments each supplied by a bronchus, artery and vein. Each segment takes its name after the supplying bronchus.

Segmental bronchi are subject to variation with the most common being the apical segmental bronchi from the trachea especially on the right.

There is very little connection between segments except through pores of Kohn-the openings in the alveolar walls connecting adjacent alveolar lumens and the canals of Lambert-connections between terminal bronchioles and adjacent alveoli.

The bronchopulmonary segments are considered as the largest subdivisions of a lobe. They are pyramidal-shaped segments of the lung with their apices facing the lung root and their bases located at the pleural surface. They are separated from the adjacent segments by connective tissue septa. They are each supplied independently by a segmental bronchus and a tertiary branch of the pulmonary artery. They derive their names from the segmental bronchi that supply them.

Venous drainage is by the intersegmental parts of the pulmonary veins which usually lie in the connective tissue in between and drain the adjacent segments. The bronchopulmonary segments are usually 18–20 in number (10 in the right lung; 8–10 in the left lung, depending on the combination of segments). They are surgically resectable (Moore et al., n.d.).

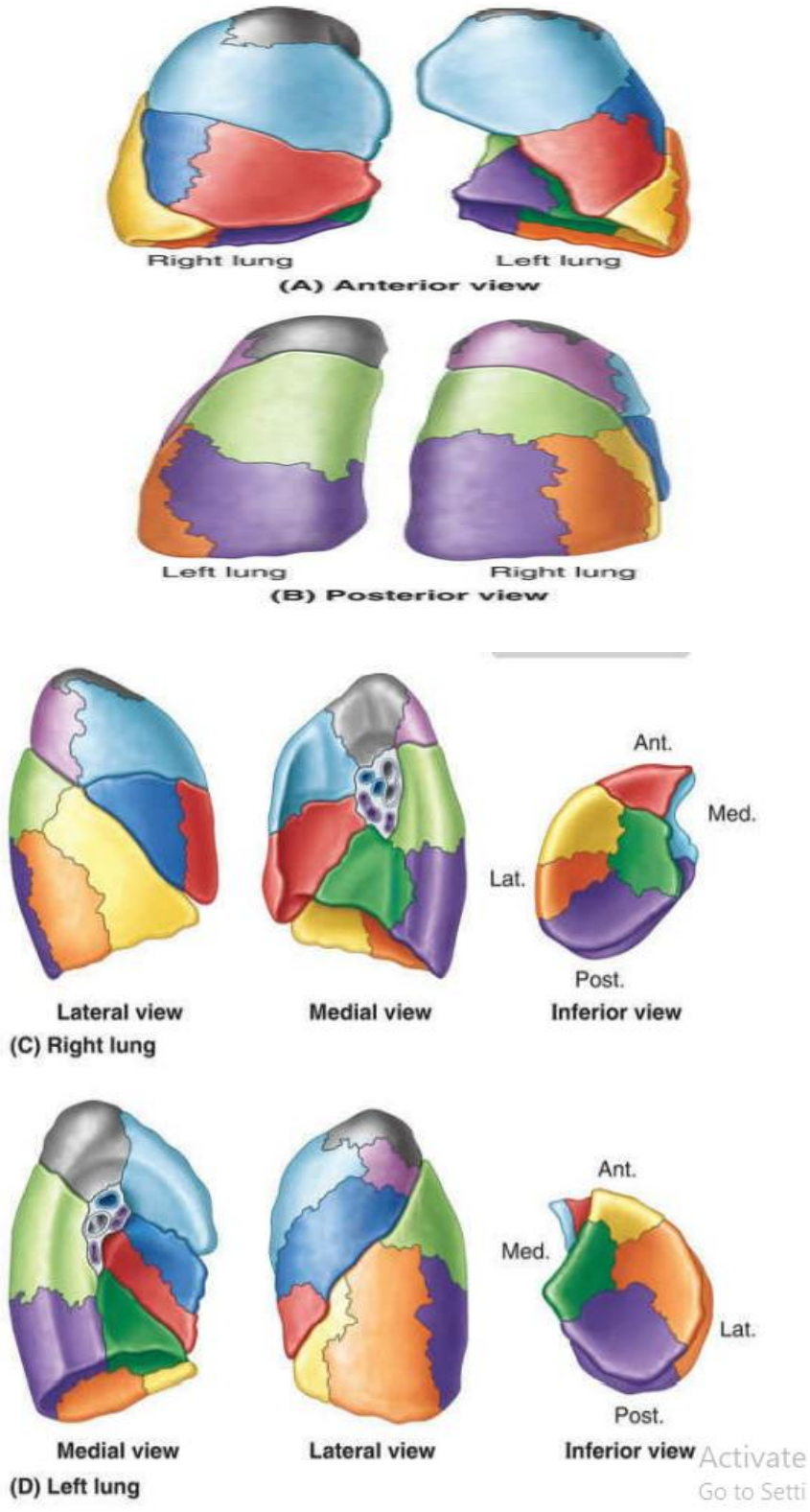

Figure 9: Tracheobronchial tree and bronchopulmonary segments A to D *(Moore, 2019).*

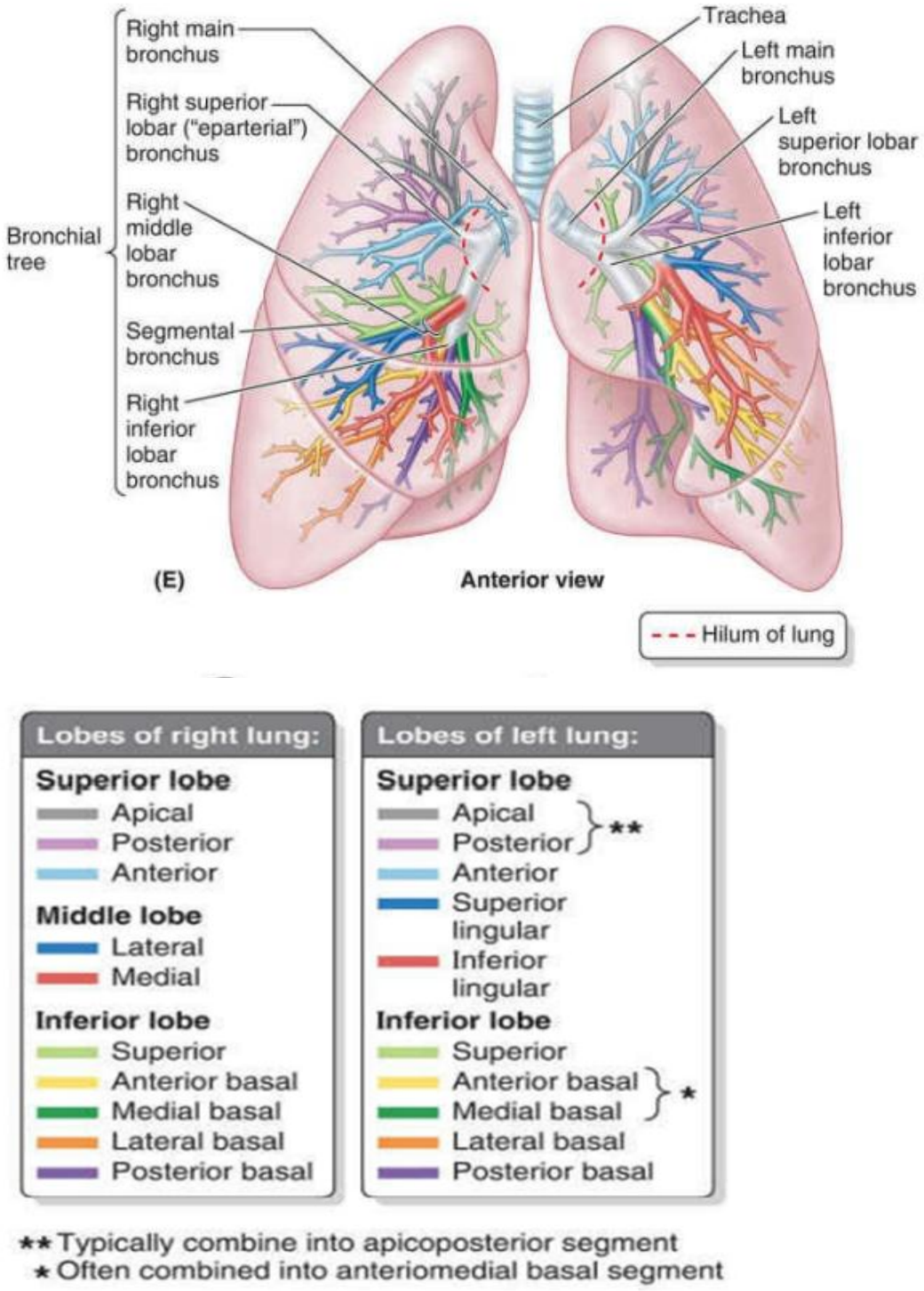

Figure 10: The bronchopulmonary segments are further demonstrated after injection of different color latex into each of the tertiary segmental bronchus, as demonstrated in figure (E). The right main bronchus gives off the right superior lobar (lobe) bronchus, before it enters the hilum of the lung *(Moore, 2019)*.

2.1.2.3 Surfaces and pleurae

There are three lung surfaces that correspond to an area of the thorax. The mediastinal surface, which faces the lateral aspect of the middle mediastinum, is where the lung hilum is located. The diaphragmatic surface forms the base of the lung. It's concave in shape and rests on the dome of the diaphragm. The concavity is deeper in right lung due to the higher position of the right dome which overlies the liver. The costal surface of the lung, which is convex and smooth, faces the internal surface of the chest wall. It is related to the costal pleura which it separates from the innermost intercostal muscles and the ribs.

Pleurae refer to the serous membranes that form the lining of the lungs and the thoracic cavity.

There are two pleurae in the body, one associated with each lung. They serous membrane which constitutes the pleurae is made up of simple squamous cells (mesothelium) supported by connective tissue. Each pleura has two parts: the visceral pleura that covers the outer surface of the lungs and the parietal pleura which covers the internal surface of the thoracic cavity. The two parts are continuous with each other at the hilum of each lung. The parietal pleura are thicker than the visceral pleura. It is divided into four parts depending on the body part it lies in contact with.

Cervical pleura line the extension of the pleural cavity into the neck.

Costal pleura cover the inner aspect of the ribs, costal cartilages and intercostal muscles.

Diaphragmatic pleura cover the superior surface of the diaphragm (thoracic surface).

Mediastinal pleura cover the lateral aspect of the mediastinum.

The visceral pleura extend into the inter-lobar fissures and continue with the parietal pleura at the hilum of the lungs.

The pleural cavity is described as a potential space between the visceral and parietal pleura. It contains serous fluid whose function is to lubricate the surfaces of the pleurae allowing them to slide over each other and produce surface tension thus pulling the parietal and visceral pleura together. This ensures that when the thorax expands the lung is able to expand too and fill with air.

There are two pleural recesses in each pleural cavity. The costo-diaphragmatic recess is located between the costal and diaphragmatic pleurae and the costo-mediastinal recess is between the costal and mediastinal pleura, behind the sternum. The recesses provide a location where fluid such as pleural effusion can collect in some conditions.

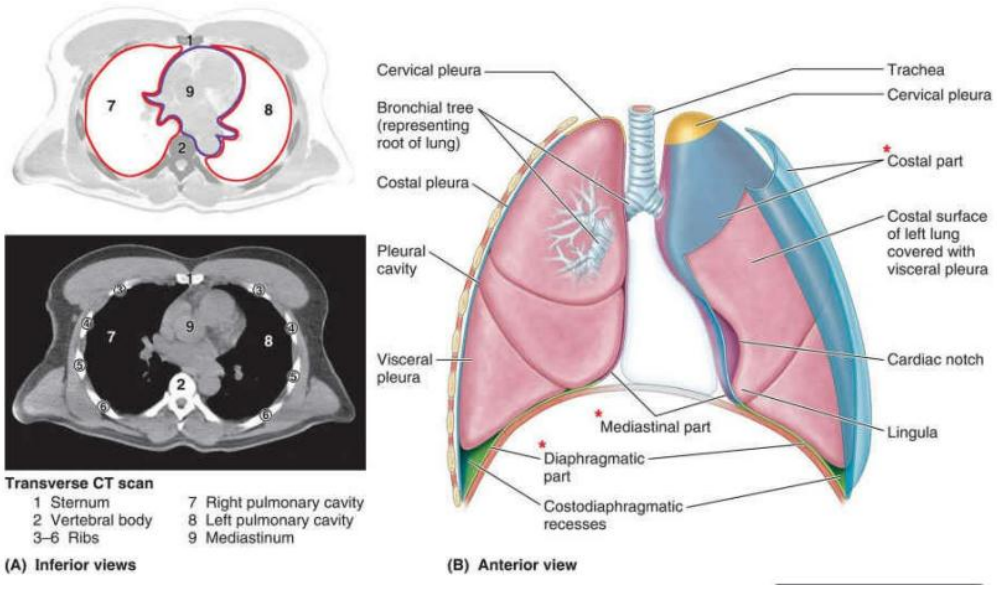

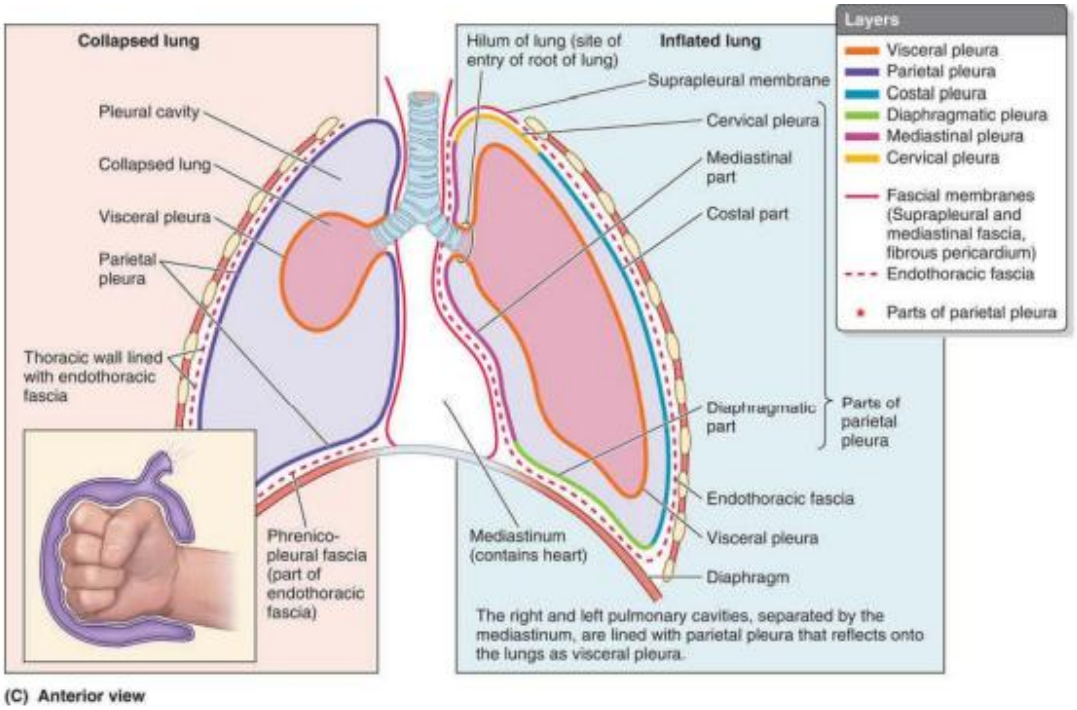

Figure 11: The divisions of thoracic cavity and the lining of pulmonary cavities.

A. CT scan with an interpretive diagram above it, demonstrating transverse cross-sectional views of the thoracic cavity outlining its kidney-like shape. This results from the protrusion of the vertebral bodies, and division into three compartments *(Moore, 2019)*.

(B) Dimensional and (C) coronal cross-sectional diagrams showing the linings of the pleural cavities and lungs (pleurae). Each lung is invested by the inner layer of a closed sac which has been invaginated by the lung *(Moore, 2019)*.

Inset: A fist invaginating an underinflated balloon. This demonstrates the relationship of the lung (represented by the fist), to the walls of the pleural sac (parietal and visceral layers of pleura) *(Moore, 2019)*.

2.1.2.4 Borders of the lungs

The anterior border of the lung is formed by the convergence of the costal and mediastinal surfaces. Left lung anterior border has the cardiac notch.

The inferior border separates the base of the lung from the costal and mediastinal surfaces.

The posterior border formed by the costal and mediastinal surfaces meeting posteriorly.

2.1.2.5 The root and hilum

Lung root consists of structures that suspend the lung from the mediastinum. They comprise a bronchus, a pulmonary artery, two pulmonary veins, bronchial vessels, pulmonary plexus of nerves and the lymphatic vessels. These structures enter or leave the lung via the hilum.

They lie at vertebral levels T5-T7. The right lung root lies below the arch of the Azygos vein and posterior to the superior vena cava and the right atrium. The left lung root lies below the arch of the aorta and anterior to the descending aorta.

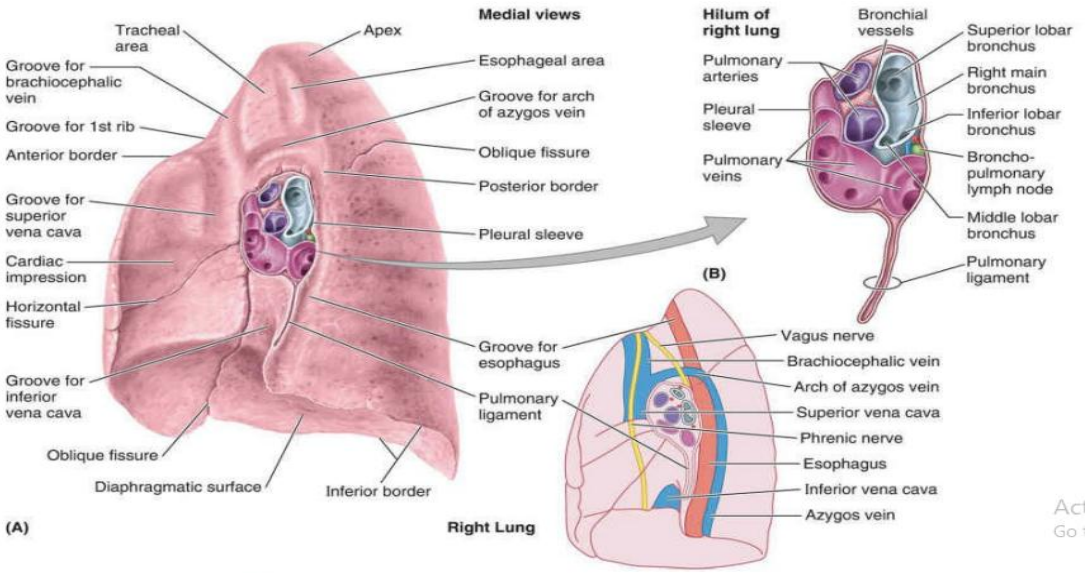

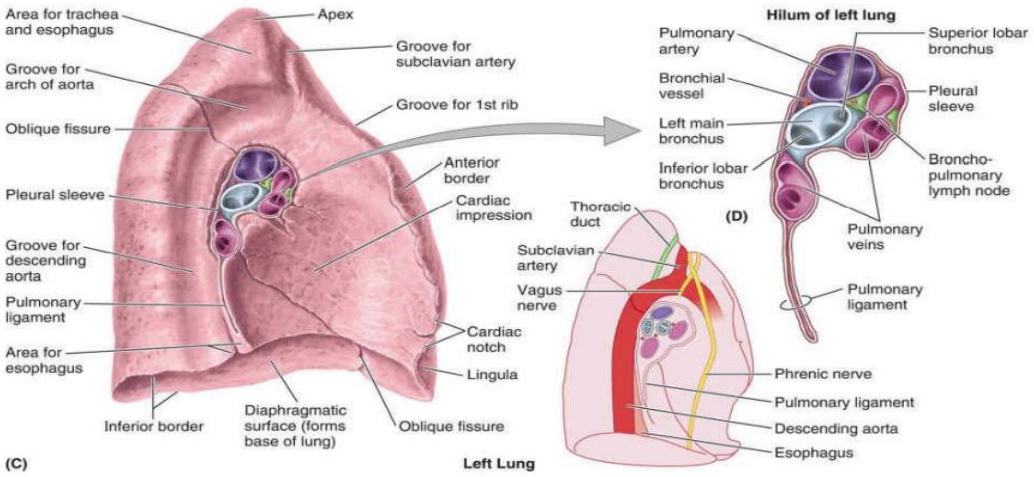

Figure 12: Mediastinal surfaces and hila of the lungs. The impressions are formed in embalmed lungs by being in contact with the adjacent structures. Superior to the root of the right lung (A), a groove is formed by the arch of the azygos vein as it courses anteriorly to enter superior vena cava (SVC), whereas in the left lung (C), a similar but larger groove is formed more superior to the root as the aorta arches posteriorly before it descends as the thoracic aorta. The visualized hilum of each lung is centered in the mediastinal surface. At the hilum (B and D), the root of each lung is then surrounded by a pleural sleeve that descends inferior to that root as the pulmonary ligament. The pulmonary veins are the most anterior and inferior in the lung root, with the bronchi being central and posteriorly placed *(Moore, 2019)*.

2.1.2.6 Bronchial tree

The bronchial tree is a series of passages that supplies air to the lung alveoli. It begins off as the trachea which divides into right and left bronchus. These divide into lobar bronchi supplying each lobe of the lungs. Each lobar bronchus subdivides into segmental bronchi that supply each bronchopulmonary segment – the functional units of the lungs. The segmental bronchi give rise to conducting bronchioles that eventually lead to the terminal bronchioles. Each terminal bronchiole gives rise to the respiratory bronchioles which have thin walled out-pocketings extending from their lumens called alveoli. These are the sites for gaseous exchange.

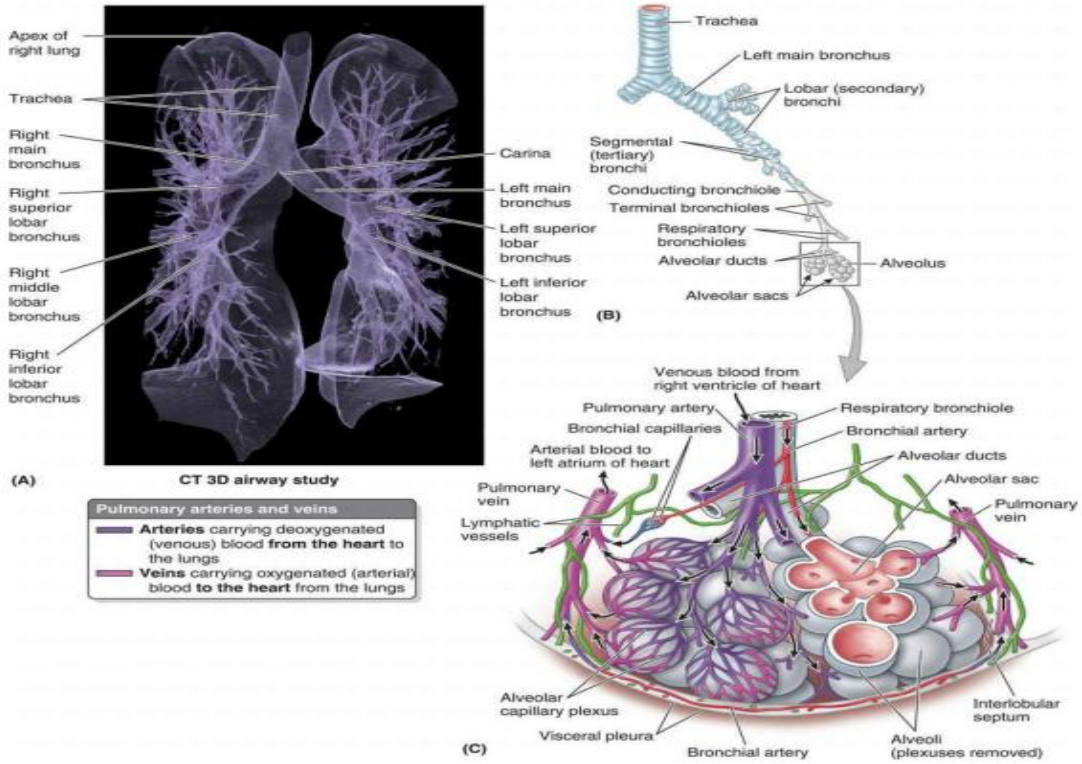

Figure 13: The internal structure and the organization of the lungs. (A) 3D CT airway study. (B) The subdivisions of bronchial tree. (C) The alveoli. Within the lungs, the bronchi and the pulmonary arteries are paired and branch in unison. Tertiary segmental branches supply the bronchopulmonary segments. Each intrasegmental pulmonary artery, while carrying poorly oxygenated blood, ends in a capillary plexus in walls of the alveolar sacs and alveoli, where oxygen and carbon dioxide are exchanged. The intersegmental pulmonary veins, arising from the pulmonary capillaries, carry well-oxygenated blood to the heart *(Moore, 2019).*

2.1.2.7 Blood supply

Blood supply to the lungs is via the paired pulmonary arteries. After oxygenation, the blood leaves the lungs via the paired pulmonary veins. Bronchial arteries from the descending aorta supply the bronchi, lung roots, visceral pleura and connective tissues of the lungs. Parietal pleura are supplied by intercostal arteries and visceral pleura by the branchial arteries.

2.1.2.8 Venous drainage

The lung structures are drained by the bronchial veins. The deep veins form a network of veins around the pulmonary interstitium and communicate freely with the pulmonary veins. They as well form a bronchial vein trunk that drains to the pulmonary system. The superficial bronchial veins drain into the azygos vein on the right and into the accessory hemi-azygos vein on the left.

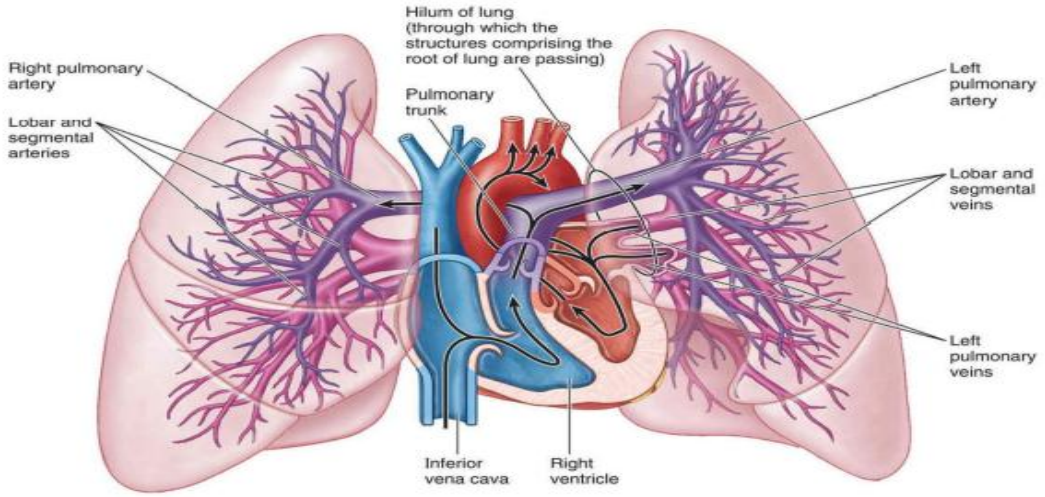

Figure 14: Pulmonary circulation. Note that the right pulmonary artery passes under the arch of the aorta to reach the right lung and the left pulmonary artery lies completely to the left of the arch *(Moore, 2019)*.

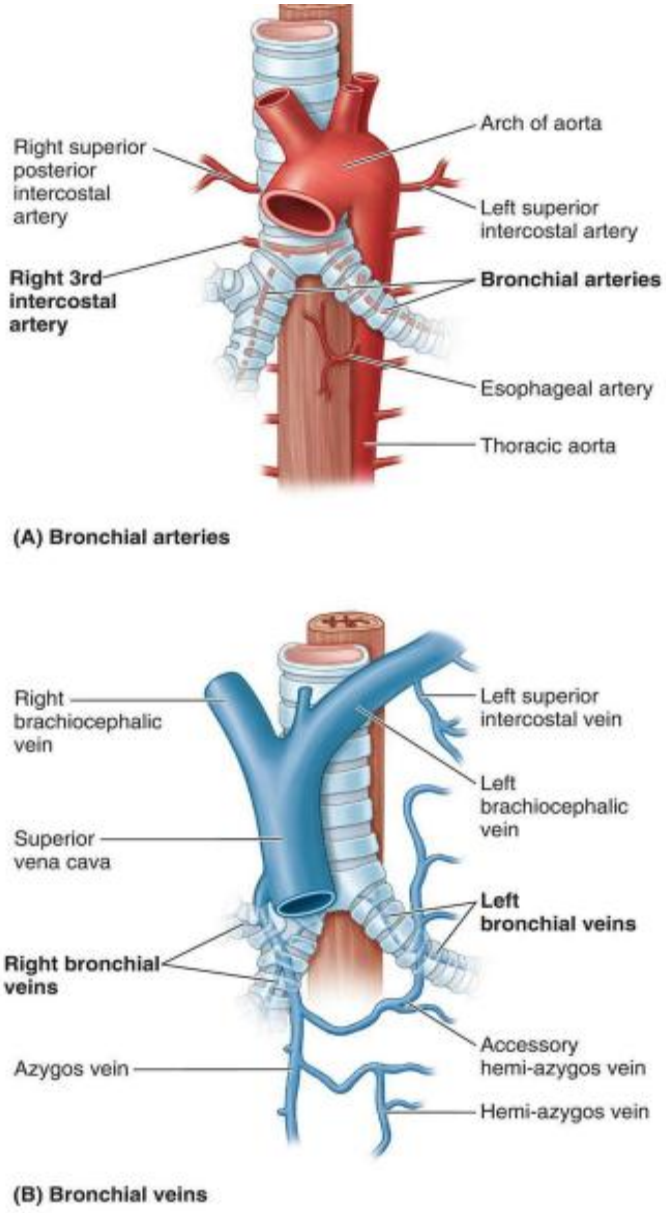

Figure 15: The bronchial arteries and veins. A. The bronchial arteries supply the supporting tissues of the lungs and visceral pleura. B. The bronchial veins drain the more proximal capillary beds that are supplied by the bronchial arteries; the rest is drained by the pulmonary veins (Moore, 2019).

2.1.2.9 Lymphatic drainage.

Mediastinal lymph nodes that drain the lung are named according to their position:

- Pulmonary nodes: within the lung substance
- Bronchopulmonary nodes: at the hilum
- Carinal nodes: below the hilum
- Tracheobronchial nodes: above the tracheobronchial junction
- Right and left paratracheal nodes: on either side of the trachea.

Superficial lymphatic plexus located beneath the pleura and drains around the surface of the lungs and fissure margins, to converge at the hila and the bronchopulmonary nodes.

Deep lymphatic plexuses drain with pulmonary vessels towards the hila. They also drain structures at the lung root.

There are few connections between the superficial and deep plexuses except at the hila.

The bronchopulmonary nodes drain into the tracheobronchial and paratracheal nodes and thence into the broncho-mediastinal trunks.

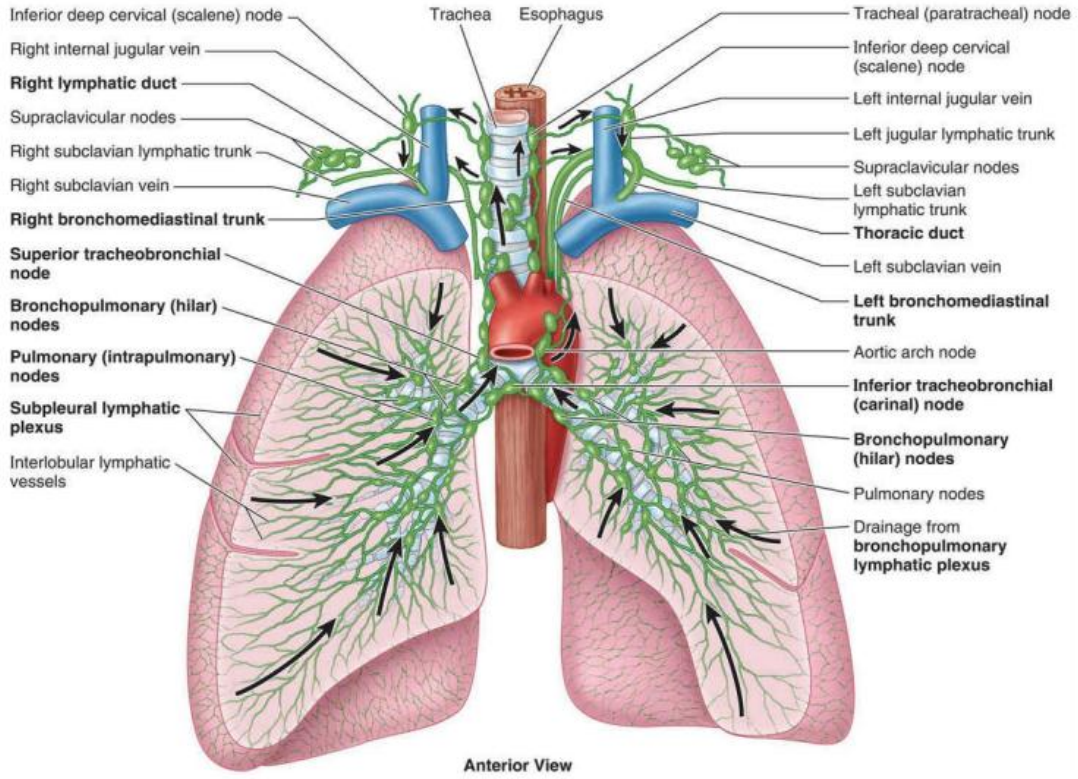

Figure 16: Lymphatic drainage of the lungs. The lymphatic vessels originate from superficial, the sub-pleural and the deep lymphatic plexuses. All lymph from the lung leaves along the lung root and drains into the inferior or superior tracheobronchial lymph nodes. The inferior lobe of both lungs drains into the centrally placed inferior tracheobronchial (carinal) nodes, which primarily drain to the right side. The other lobes of each lung drain primarily into the ipsilateral superior tracheobronchial lymph nodes. Thereafter, the lymph then traverses a variable number of paratracheal lymph nodes and enters into the bronchomediastinal trunks *(Moore, 2019)*.

2.1.2.10 Nerve supply

The nerves supplying the lungs are derived from the pulmonary plexuses. They have sympathetic, parasympathetic and visceral afferent fibers.

Sympathetic supply is from the sympathetic trunks and stimulates the bronchial smooth muscle relaxation and pulmonary vasoconstriction.

Parasympathetic supply is from the vagus nerve and stimulates bronchial glands secretions, bronchial smooth muscle contraction and pulmonary vasodilation.

Visceral afferent nerves conduct impulses of pain to the sensory ganglion of the vagus nerve.

Parietal pleura are sensitive to pain, pressure and temperature and is supplied by phrenic and intercostal nerves. The visceral pleura are sensitive to stretch and receive autonomic innervation from the pulmonary plexus derived from the sympathetic trunk and vagus nerve.(Stephanie, 2011)

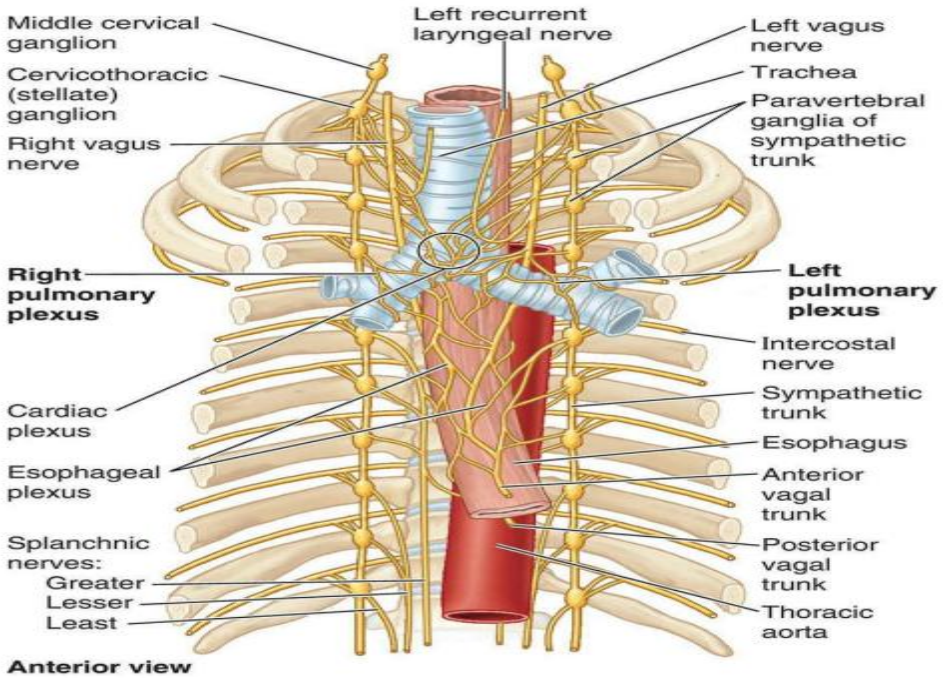

Figure 17: The nerves supplying the lungs and visceral pleura. The right and left pulmonary plexuses, located anterior and posterior to the roots of the lungs, receive sympathetic contributions from right and left sympathetic trunks and parasympathetic contributions from right and left vagus nerves (CN X). After it contributes to the posterior pulmonary plexus, the vagus nerves continue inferiorly and then become part of the esophageal plexus, lose their identity and subsequently reform as the anterior and posterior vagal trunks. Branches of the pulmonary plexuses accompany the pulmonary arteries and especially the bronchi to and within the lungs parenchyma (Moore, 2019).

2.1.3 Radiological anatomy of the lung

Chest Radiography

Chest radiography remains to be the most commonly used imaging modality for screening a variety of pulmonary diseases such as pneumonia, emphysema tuberculosis and lung cancer. It boasts of the advantages of being fast, easy, non-invasive and inexpensive. It is therefore widely available in emergency rooms, the ambulatory care centers and in some community health care centers (Mittal et al., 2017).

Despite being easy to acquire, a chest radiograph (CXR) is one of the most complex imaging modalities to interpret. Its successful interpretation heavily depends on the level of training and expertise of the person interpreting it (Delruei L, Gosselin R, Ilsen B, Landeghem A Van, Mey J De, 2001).

Lung field segmentation (LFS) is paramount because it precisely defines the region of interest to be examined. The specific radiologic signs include cephalization of pulmonary vessels, cavities, consolidations, Kerley B-lines, pulmonary opacities, and lung nodules. Additionally, the outlines of the lung fields and other quantitative parameters including the size, shape, texture, and volume are directly viewed as an indicator of various medical conditions such as emphysema, cardiomegaly or pneumothorax. However, segmenting the lung field in CXRs has proven to be extremely challenging due to factors such as:

i. Overlapping of anatomical structures like clavicles and the rib cage,
ii. Variations in its shape and size affected by gender, age, and physical structure of the subject,

iii. The presence of foreign objects such as pacemakers, catheters, buttons, brassier clips and jewelry

iv. Various radiographic artefacts (Mittal et al., 2017).

Some of the anatomical structures (such as heart and lungs) are apparently visible on a CXR; some are obscured or invisible, while some of them (such as pleura) become visible only when abnormal.

A. *Airways*: The airways contain air and appear to be of lower density as compared with the surrounding soft tissues. Thus, the airways appear darker on a CXR. The trachea is the largest airway and located midline in a normal CXR. Tracheal shift may indicate abnormalities such as pleural effusion, pneumothorax, atelectasis, as well as pleural fibrosis. Normally, radiologists locate the upper end of the trachea and its centre line, and delineate it to detect abnormalities. The trachea then branches into the left and right bronchus at the carina.

B. *Bones*: Bones are dense, and thus appear brighter than soft tissues on a chest radiograph. . The bones visible on a CXR include the clavicles, ribs, part of the spine, scapula, and the proximal humerus.

C. *Cardio-mediastinal region*: Cardio-mediastinal region is the area between the lungs that consists of major blood vessels, trachea with stem bronchi, muscular esophagus, thymus gland, and the heart. This region is denser as compared with the surrounding air-filled lungs, and thus appears brighter on a CXR. Although most of the constituents of the mediastinal region, except the heart, are not apparently visible on a normal CXR, the cardio-mediastinal silhouette plays an important role in diagnosing various diseases. Radiologists look for subtle deviation in the mediastinal

silhouette to detect cardiomegaly, and pericardial effusion .Mediastinal contours can also be outlined.

D. *Diaphragm*: The diaphragm separates the relatively denser abdominal region below it from the less dense lung region above it. Each of the hemidiaphragms should appear as a crisp dome-shaped contour on a normal CXR. Obscured, flattened, or raised hemi-diaphragm. Abnormalities that can be visualized include consolidation of lower lobes, congenital diaphragmatic hernia, phrenic nerve palsy, and lung hyper-expansion. The angle between the diaphragm and the chest wall at the bottom of the lung, known as cardio phrenic angle also provides critical information regarding lung pathology. Blunt CP angle helps in the detection of pleural effusion that can be caused by pneumonia, cirrhosis, pulmonary embolism, and pulmonary tuberculosis.

E. *Expanded lung*: Chest radiographs are generally acquired after the patient inhales and hold their breath. The expanded air-filled lungs appear less dense, and thus appear darker on a CXR. In normal cases, a lung boundary consists of lung apices, the mediastinal edges, the hemi diaphragms and the costal edges. The mediastinal region, heart, aorta, and the structures below the diaphragm are not included in the lung field. However, there is a difference in opinion amongst radiologists about what constitutes the lung field in abnormal cases. Some radiologists consider only the air cavities as a part of lung field, while others consider the air cavities and the area obscured by the pleural fluid as a part of the lung field.

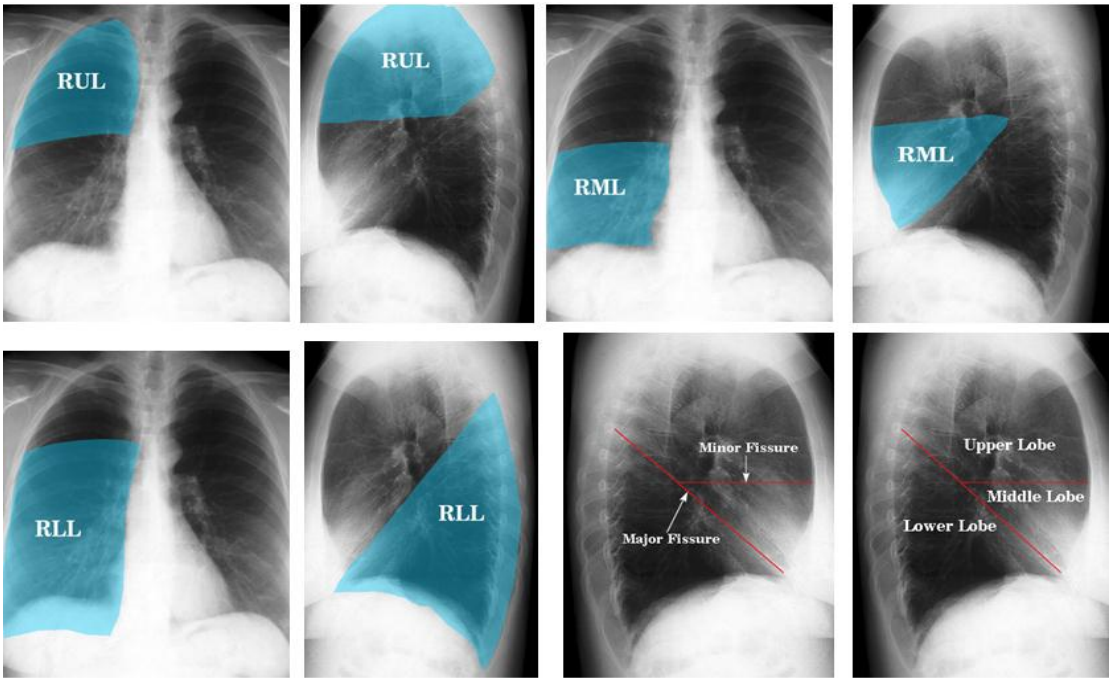

Figure 18: Chest radiographs of normal lung anatomy on posterior-anterior (PA) and lateral views. The lungs are divided into lobes by the fissures *(Stephanie, 2011)*.

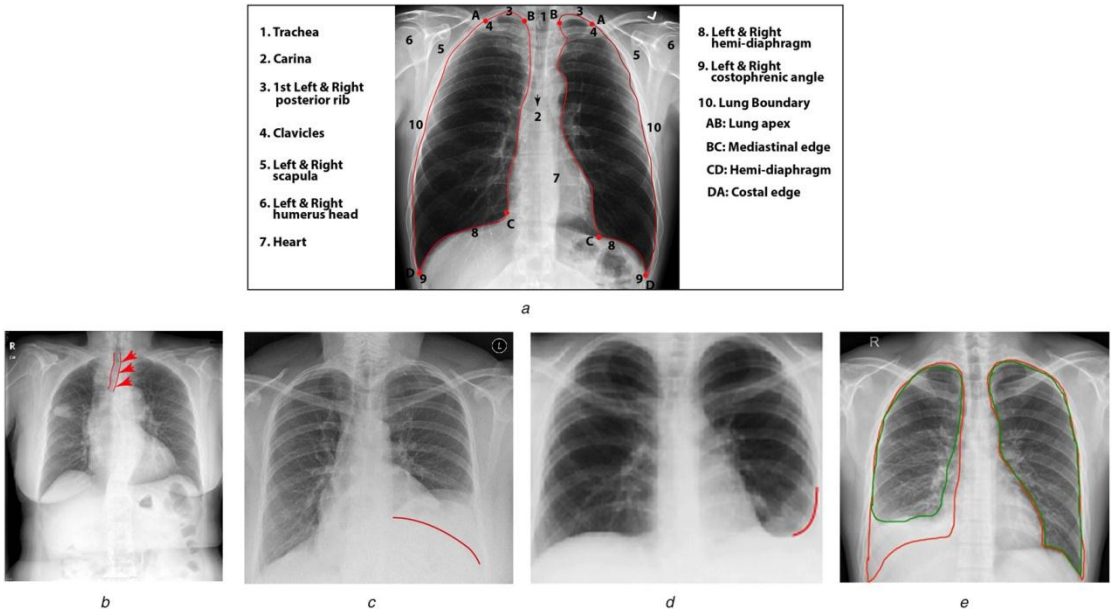

Figure 19: Chest anatomy(a) A normal labelled chest radiograph, (b) A chest Radiograph indicating the tracheal shift toward the right, (c) Raised left hemidiaphragm due to left phrenic nerve palsy, normal position is delineated in red, (d) Blunted cardiophrenic angle indicating pleural effusion, delineated in red, (e) Two different ways of delineating lung boundary in abnormal cases (Stephanie, 2011).

Computed tomography (CT) of the chest

Computed tomography (CT) of the chest is a diagnostic medical imaging method of radiography that uses special x-ray equipment to examine the abnormalities found in the lungs. It is commonly known as a CT or CAT scan. Like traditional x-rays, it produces multiple images or pictures of the inside of the body that can be reformatted in multiple planes. It can as well generate three-dimensional images. CT images of internal organs, bones, soft tissue, and blood vessels provide a greater detail than traditional x-rays. This follows symptoms of unexplained cough, chest pain, shortness of breath, fever, and other chest symptoms.

CT scanning is a fast, painless, noninvasive and accurate imaging method. This is because of its ability to detect very small nodules in the lung; chest CT is especially effective for diagnosing lung cancer at its earliest, most curable stage (Nanavaty et al., 2014).

Lung fissures are less visible on conventional CT than on plain radiographs. They appear as regions of relative avascularity on the outer cortex of the lobe, where tapering vessels are less visible. Discrete lines can only be seen if the vertical axis of the fissure is perpendicular to plane of the CT slice. This can sometimes occur in parts of the oblique fissure but not in the transverse fissure or can occur on coronal and sagittal images acquired at multi-detector CT. On the high-resolution CT scans, the fissures are seen as sharp lines.

The bronchi may be seen depending on their size and orientation. Narrow slices improve their visualization. The horizontally orientated bronchi, such as the anterior segment bronchus of the upper lobes, the superior segmental bronchi of the lower lobes and the proximal part of the middle lobe bronchus, may be seen as tubular

structures. The vertically orientated bronchi, such as the main bronchi, bronchus intermedius, lower-lobe bronchi and apical segmental bronchi may be seen as circular air-filled structures. The posterior wall of the right main bronchus and its divisions into upper-lobe bronchus and bronchus intermedius should be outlined by lung as it invaginates into the azygooesophageal recess. Lung fields appear as areas of hypodensity, in comparison to the surrounding soft tissues (Stephanie, 2011).

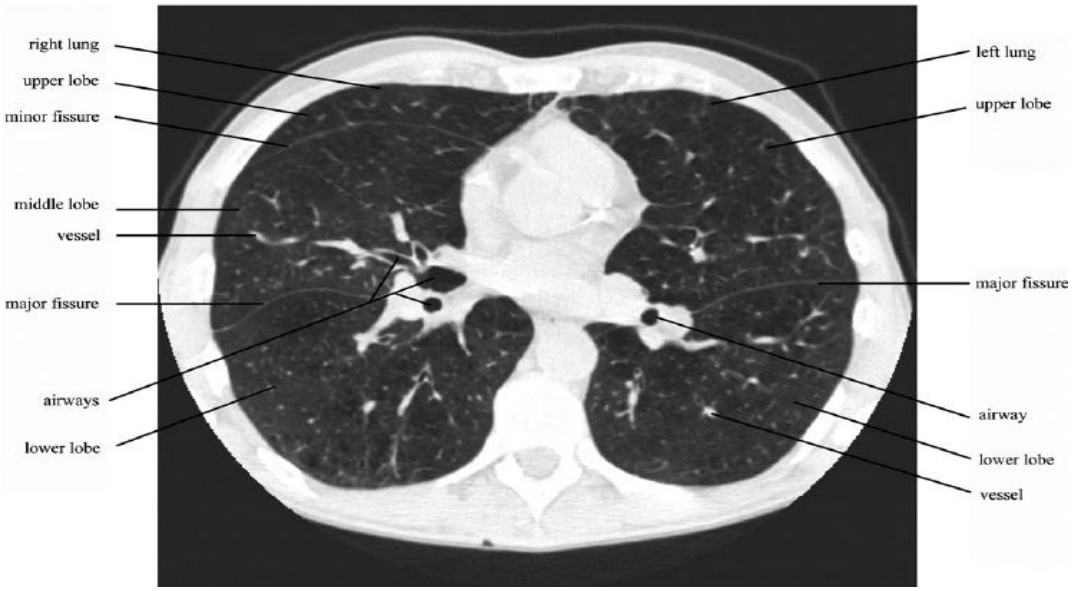

Figure 20: A lung window axial slice of a chest CT scan at the level of the mediastinum, with labeled normal anatomical structures *(Stephanie, 2011)*.

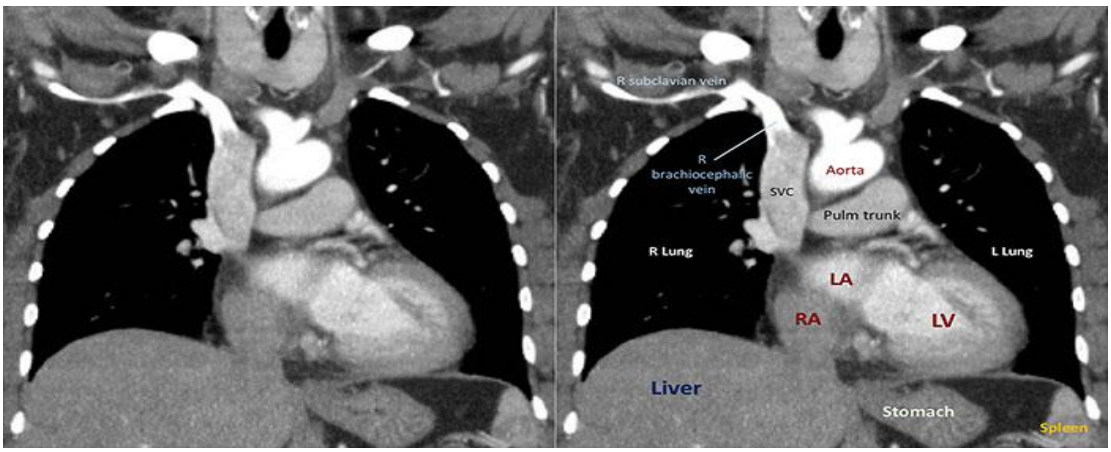

Figure 21: Coronal reconstruction of a chest CT scan in arterial phase showing normal anatomy of the labeled structures *(Stephanie, 2011)*.

2.1.4 Histology of the normal lung tissue

There are four main histological layers within the respiratory system: respiratory mucosa, which includes (epithelium and supporting lamina propria), submucosa, cartilage and/or muscular layer and adventitia.

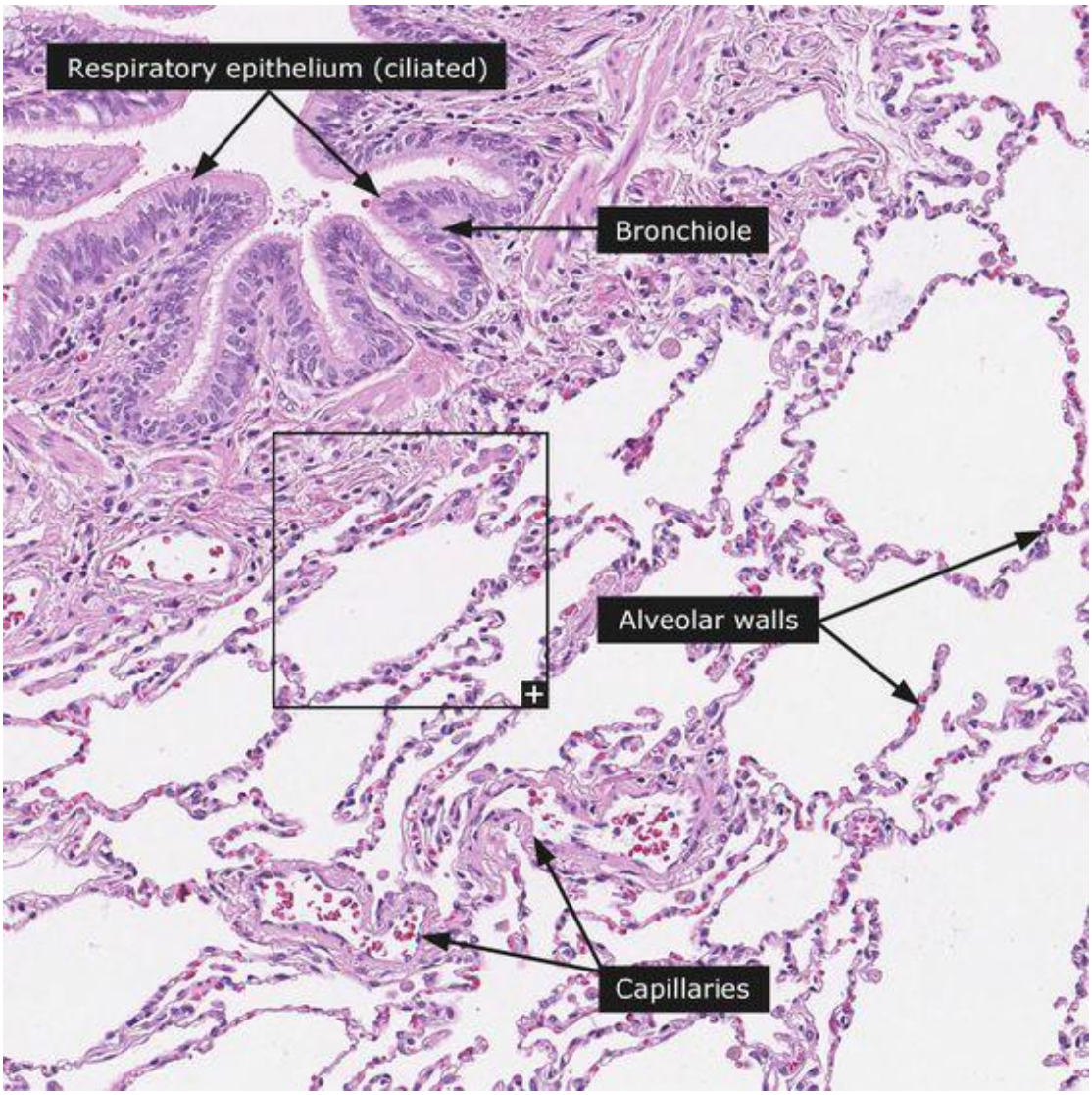

Figure 22: Normal histological features of the normal lung tissues. ***(The Human Protein Atlas)***

2.1.5 Epidemiology

Globally, lung cancer continues to be the leading cause of cancer-related deaths in both men and women. Lung cancer incidence and mortality are both tightly linked to cigarette smoking patterns. As smoking rates peak more in men than women – lung cancer incidence and mortality have risen in the past few decades (de Groot et al., 2018).

Lung cancer accounts for an estimated 2 million diagnoses and 1.8 million deaths globally (Wheless et al., 2013).

The new lung cancer cases in the US were estimated to be 121,680 for men and 112,350 for women, for a total of 234,030 cases in 2018. This is close to an equivalent of 641 lung cancers diagnosed daily. Lung carcinoma is the 2nd most common diagnosis by gender, behind prostate cancer in men and breast in women. In 2018, lung cancer accounted for nearly 14% of new cancers in men and about 13% of new cancers in women in the US.

The estimated cases of mortality in the US in 2018 were 83,550 deaths for men and 70,500 for women, accounting for around 25% of annual cancer fatalities (de Groot et al., 2018).

Internationally, lung cancer has continued to be the leading cause of cancer-related deaths in men and women. There is no much difference in cancer deaths in men and women but there is a higher rate of lung cancer deaths in women in the industrialized countries in comparison to those in developing nations. In developing countries, lung cancer deaths are the second most common after breast cancer in females and prostate cancer in men. The higher incidence and mortality from lung cancer are tightly linked

to cigarette smoking patterns. As the smoking rates peak first in men then followed by women, lung cancer incidence and mortality has been on the rise in subsequent decades before starting to decline following the initiation of comprehensive tobacco control programs. These trends have occurred earlier in industrialized countries compared to the developing world. Lung cancer incidence and mortality rates have been falling since the 1990s in the United States (US) and the United Kingdom (UK). However, emerging nations including Russia, Brazil, India, China, and South Africa, continue to have higher rates of cigarette smoking both in men and women. They exhibit a lower incidence of lung cancer but a higher mortality burden as compared to developed countries. The reasons postulated for these patterns include unequal access to good healthcare leading to a delay in diagnosis and treatment, environmental contamination as well as sociocultural barriers (Barta et al., 2019).

The 5-year total survival rate for lung cancer in the United States from 2001 to 2007 was 15.6%. Patients with localized disease at diagnosis have a 5-year survival rate of 52%; however, the more than 52% of patients with distant metastasis at diagnosis have a dismal 5-year survival rate of 3.6%, which begs for the need for better screening methods to detect early-stage cancers (Dela Cruz et al., 2011).

In the year 2012, lung cancer mortality was estimated at 1,098,700 men and 491,200 women globally, which corresponded to 24% and 14% of all cancer deaths in males and females, respectively. The leading cause of lung cancer is tobacco smoking. However, the proportion of lung cancer deaths attributed to smoking varies across populations. It ranges from >80% in the United States and France to about 61% in a pooled analysis of 21 Asian cohorts and approximately 40% in sub-Saharan Africa (Islami et al., 2015).

Despite this malignancy being known to have a poor survival rate, an improvement in the overall survival rates can be highly attributed to personalized treatment and the introduction of targeted therapy. In a study done in Scandinavia, an improvement in 1-year survival was seen in non-squamous cell carcinoma regardless of the stage of the disease at diagnosis. However, only those with the stages I and II of the malignancy showed a longer-term 5-year survival rate. Previous studies have mostly reported poor overall survival among lung cancer patients. Several factors have been associated with the survival outcomes of lung cancer, including age, gender, the performance status, detailed tumor location, histopathological sub-type, and initial treatment modality, which are crucial predictive variables in the survival of lung cancer patients (Said & Degu, 2023).

In the Middle East and North Africa region (MENA), lung cancer is less than international rates with a range that is between 4.2 per 100,000 in Yemen and 23 per 100,000 in Lebanon. The lack of up-to-date population registries in many of those countries in the region leads to a major challenge in obtaining accurate data about the cancer incidence in general. The sources of epidemiologic data may include the national, local and international registries. However, available literature suggests more male predominance as well as presentation at advanced stages. Lung cancer was ranked among the top 10 cancers in all the countries except one country. The estimated numbers of new lung cancer cases were 79,887 in 2018. Despite significant advances in the understanding and treatment of lung cancer, the 5-year survival rate in MENA is only relatively around 8%. The highest death percentages occurred in Morocco and Tunisia while the lowest were in Yemen and Egypt. Most of lung cancer patients present at the advanced stages in the region (Jazieh et al., 2019).

Cancer in Africa is an emerging health problem. Recently, there has been an estimate of 715,000 new cancer cases and 542,000 cancer mortalities. About 847,000 new cancer cases and 591,000 deaths occurred in the year 2012 and about three quarters of these occurred in the sub-Saharan region (Nwagbara et al., 2020).

There were an estimated 752,000 new cancer cases (approximately 4% of the global incidence) and 506,000 cancer deaths in sub-Saharan Africa in 2018. The overall cancer burden in this region is dominated by breast, cervical, and prostate cancers. However, the cancer profile in sub-Saharan Africa is diverse with incidence rates increasing for several major cancer sites i.e., in Zimbabwe, cervical cancer rates increased by 80% in Zimbabwe and by 36% in South Africa in 2018 (Warui et al., 2021).

In Kenya, cancer ranks third as a cause of death, after infectious and cardiovascular diseases, and in 2012 there was an estimated 37,000 new cancer cases, and 28,500 cancer deaths reported (Macharia et al., 2019).

The Eldoret Cancer Registry (ECR) has the epidemiological profile and statistics across western region of Kenya. Lung cancer diagnosis has proven to be a challenge in the western Kenya region due to the technicalities related to the screening and diagnostic procedures. The burden in the adult population remains largely unknown. This is because most patients are primarily managed for Pulmonary Tuberculosis, since both have similar manifestations clinically.

A retrospective review done at MTRH for all lung cancer cases diagnosed from 2012 to 2016 from the ECR revealed that out of the 60 cases the highest incidence was among age cohort of 50-59 years i.e., 17 cases representing 28.3%. This was attributed to the slow disease progression and the delays in early diagnosis. The

incidence was higher among males at 63.3% (38 cases), likely associated with susceptibilities to risk factors like smoking and exposure to industrial fumes. On the incidence of the staging at diagnosis, most of the cases (54) were unknown at 90% while 10% were at stage IV likely due to the late diagnosis (Atundo et al., 2018).

2.1.7 Risk factors

The risk factors for lung cancer include smoking, lifestyle, environmental and occupational exposures. These factors play a role depending on the geographic location, gender and race characteristics, the genetic predisposition and their synergistic interactions. Cigarette smoking is so far the most recognized risk factor for development of lung cancer. Unprocessed biomass fuels, including wood, crop residues, dung, and coal, create indoor emissions also lead to an increased lung cancer risk. Occupational hazards such as exposure to asbestos are a well-recognized occupational cause of lung cancer. A higher risk is on the workers in asbestos mining and milling industries, shipbuilding, construction, textiles and insulation, and in automobile repair sector. Genetic factors and poor diet may also contribute to an increased susceptibility to lung cancer. (Barta et al., 2019)

Lung cancer caused by secondhand tobacco smoke, results in an estimated 21,400 lung cancer deaths in non-smokers annually. “Other risk factors for lung cancer include indoor air pollution due to unventilated combustion of coal in households used for heating and cooking, outdoor air pollution, the exposure to hazardous chemicals in some occupations, like coal gasification and aluminum production, exposure to radiation from indoor radon released from soil and building mortalities resulting from second-hand smoke and indoor air pollution occur in the low- and middle-income countries (LMICs) (Islami et al., 2015).

Smoking

Smoking has been found to be the major risk factor, accounting for about 90% of lung cancer incidence. There are also other additional exogenous and endogenous factors contributing to the individual risk, such as the following: Low consumption of fruits and vegetables, the genetic predisposition of a person, the exposure to non-tobacco pro-carcinogens, carcinogens, and tumor promoters, a previous lung disease such as chronic obstructive pulmonary disease (COPD), a previous tobacco-related cancer as well as passive smoking. The increase of lung cancer mortality noted in the last few decades can almost entirely be attributed to the trend of tobacco consumption that has been on the rise. However, there is a lag time of several years between the beginning of smoking and the time of clinical manifestation of cancer. This fact may end up distorting the perceived risk factors for lung cancer at an individual level. Moreover, the lag makes clinical intervention studies that reduce the cancer risk difficult to design and to interpret. Therefore, most of our current knowledge concerning lung cancer prevention in the human is based on observational studies. (Biesalski et al., 1998)

Approximately half of the world's population is significantly reliant on biomass (primarily wood and the agricultural residues) or coal fuel (collectively termed as solid fuels) for heating, lighting, and cooking. The incomplete combustion of such materials releases the byproducts that have well-known adverse health effects, thus increasing the risk of many diseases and death. Some of the conditions include: acute respiratory infections, heart disease, chronic obstructive pulmonary disease, , stroke, asthma, cataracts and blindness, tuberculosis, asthma, adverse pregnancy outcomes and worst of all, lung cancer (Kaplan, 2010).

Passive smoking

In passive smoking, environmental tobacco smoke is considered a human carcinogen. However, the extent of the lung cancer risk that's obtained from passive smoking remains a thoroughly discussed subject (Biesalski et al., 1998).

Exposure to non-tobacco pro carcinogens

Indoor air pollution that results from the incomplete combustion of the mentioned coal and unprocessed biomass (wood, sticks, twigs and crop residues) used to heat homes or cook food is a major public health concern in developing countries. The smoke that is generated from incomplete combustion of such fuels contains constituents that have been identified as either known or suspected carcinogens in studies of lung cancer among Chinese patients and also those of other countries. In China, an increased risk of lung cancer has been linked to exposure to polycyclic aromatic hydrocarbons, from coal smoke and benzo(a)pyrene, a known lung carcinogen produced from unvented soft, smoky coal used for both cooking and heating (Blegen et al., 2019).

There are four identified classes of indoor air pollution based on the derivation of the pollutants. The first class is chemical pollution which results from building materials, furnishings, pesticides, formaldehyde, and volatile organic compounds. The second class is termed radon that emanates from the ground under a building. The third class entails the biological processes derived from mold, mildew, and mites, among other things. The fourth and final class, and the one with the main focus, comprises the byproducts of incomplete combustion, such as carbon monoxide (CO), particulate matter(PM), nitrogen dioxide (NO_2), sulfur dioxide (SO_2), and other organic compounds. The inefficient burning of solid fuels

while heating or cooking on the open fires or traditional simple stoves results in extremely high levels of indoor air pollution. The lack of ventilation in the homes where such fuels are used and the poor design of stoves that do not have flues or hoods to remove excessive smoke form the living area, intensify such exposures (Kaplan, 2010).

Exposure to radon, asbestos, and chemical carcinogens has been found to stimulate the development of lung cancer. The lung cancer risk from non-tobacco carcinogens is multiplicative with the risk increase from smoking both passively and actively (Biesalski et al., 1998).

Low consumption of vegetables and fruits

A large number of observational studies worldwide have consistently found that an increased consumption of fruits and vegetables has an associated reduction in lung cancer risk in smokers, ex-smokers, and never-smokers. However, the specific mechanisms of the epidemiological association between personal diet and lung cancer incidence remain to be elucidated. So far, no single dietary compound has been identified to exert any chemo-preventive action on lung cancer acquisition. It has been found that low intake of vitamin A may contribute to the metaplastic changes in the respiratory mucosa. It is advised that, while avoiding smoking is the most important behavior for reducing lung cancer risk, the daily consumption of a variety of fruits and vegetables provides a combination of vitamins C, E and retinoids as well as other potential protective factors. These may offer the best dietary protection against lung cancer (Yong et al., 1997).

Genetic predisposition

Individual risk for getting lung cancer depends on both inherited and environmental factors. Improved understanding of the molecular genetics of lung cancer may have major implications for both risk assessment and prevention of lung cancer in the near future. Subjects with a genetic pre-disposition might be in a position to reduce their lung cancer risk by a proper intake of fresh fruits and vegetables.

Previous cancer

The increased risk for a secondary metastasis from a primary cancer at different sites of the body is explained by both genetic predisposition and the effect of an unhealthy lifestyle, which has been alluded to smoking and low intake of vegetables and fruit.

Previous inflammatory lung disease

Some chronic inflammatory lung diseases, such as COPD, asthma, and tuberculosis, are associated with an increased lung cancer risk in later life. The possible explanations for increased cancer risk from chronic inflammation are the mutagenic effect of free radicals that are produced by inflammatory cells as well as the stimulation of cell proliferation during tissue regeneration. In the National Health and Nutrition Ex- amination Survey (NHANES) II study it was demonstrated that a low intake of vitamin A is associated with increased COPD risk and thus subsequent level of risk for getting lung cancer (Yong et al., 1997).

2.1.8 Chest CT findings of lung tumors

The commonest and most important recognized primary lung tumor is the bronchogenic carcinoma. Lung cancer is the only visceral malignancy that gives an early radiographic clue of its existence. Most patients are referred for further evaluation of a lung mass after an incidental finding of a spot or abnormality on a

chest radiograph. CT scan of the chest serves a role in a patient suspected to have a lung mass based on the plain chest radiograph. Initially, it may help to facilitate the diagnostic evaluation, by giving a more precise characterization of the extent, size, and contour and possible tissue composition of the suspicious lesion. Subsequently, an indeterminate pulmonary mass/nodule can either be classified as cancerous or non-cancerous. It has been estimated that close to 40% of all resected pulmonary nodules are malignant (Dr. Dinesh K. Gupta , Dr. Sudha Gupta, 2019).

A large spectrum of lung tumors translates into the various CT presentations and features. These generally show a good correlation with histopathology findings, stressing the key role of the radiologist in the diagnosis and management of these patients. This is helpful for radiologists to understand the up-to-date basics of lung tumor pathological classifications, the radio-pathological correlations and how to use them in our clinical setting (Cohen et al., 2016)

A study was undertaken in Mahatma Gandhi Medical College, Hospital, Jaipur by Dr. Dinesh K. Gupta , Dr. Sudha Gupta, 2019 to establish the role of CT in the comprehensive evaluation of lung masses. The CT scan results revealed that 37(82.2%) of patients had malignant features and 8(17.7%) of the lung masses were of benign nature. The sensitivity of CT in diagnosing malignancy was found to be 97.36%, specificity of 100%, positive predictive value at 100% and negative predictive value of 88.89%. The final diagnosis with FNAC showed 38(84.4%) malignant & 7(15.5%) benign - lesions with a sensitivity and specificity of 100%.

Aoki et al., 2000 conducted a study to evaluate the evolution of peripheral lung adenocarcinomas using CT chest findings and histologic classification, in relation to tumor doubling time. Out of the 34 patients studied, five of the six adenocarcinomas

(83%) with tumor types A or B showed localized ground-glass opacity on a high-resolution CT scan. All the six tumors had a tumor-doubling time of more than 1 year. Fifteen of the 21 tumors with type C (71%), showed partial ground-glass opacities mixed with localized solid attenuation on a high-resolution CT. Ten of these 21(48%) type C tumors had a tumor doubling time of more than 1 year. In the types B and C, the solid component or development of vascular convergence and pleural indentation increased during observation before undergoing surgery. All the seven tumors with types D, E, and F showed solid attenuation mostly, and the tumor doubling time was less than 1 year in six (87%) of the seven tumors.

On the CT features, the atypical adenomatous hyperplasia (AAH) appears as a pure ground-glass nodule, a well-defined oval or round shape. It usually measuring ≤ 5 mm in diameter but can exceed 10 mm. It can be solitary but it is mostly multiple and bilateral, often found incidentally. It has a low attenuation and small size. Adenocarcinoma in situ (AIS) appears in the majority of cases on CT as a pure GGN > 5 mm to < 30 mm. AIS presents more frequently with bubble-like patterns, higher attenuation and a larger diameter (> 5 mm) than AAH. Minimally invasive adenocarcinoma (MIA) in most cases is non-mucinous and appears as a pure or a part-solid GGN, with a solid portion usually measures less than 5 mm. Mucinous MIA is a very rare and may present as a solid nodule. Invasive adenocarcinomas can appear as a pure GGN, a part-solid GGN or a solid nodule.(Cohen et al., 2016)

A study was done in Japan at the Toranomon Hospital and Toho University to evaluate the clinical, radiological and histopathological characteristics of small lung tumors 1cm or less in diameter. 44 lung tumors of 1 cm or less in diameter resected from 38 adult patients over a 4year period, were analyzed. According to the Noguchi's classification.(Travis et al., 2011) the adenocarcinomas were further sub

classified into histological sub types A to F. Thirty-tumors were adenocarcinomas, eight were atypical adenomatous hyperplasia and four were squamous cell carcinomas. All carcinoma cases were proved to be stage IA. In that study, more of AAH and type A showed HRCT scan findings of pure ground-glass attenuation, whereas types B to F and the SCC frequently showed malignant signs on CT such as population and the convergence of peripheral vessels. Two adenocarcinomas (types D and F) and two SCC types showed lymphatic or vascular invasion. HRCT scan done on these four tumors appeared to have more than two-thirds of soft-tissue attenuation in each nodule. (Kishi et al., 2004)

A retrospective study was done to evaluate the computed tomography (CT)-determined size, the morphology and the location of lung tumors in high-risk individuals who underwent annual chest CT screening for duration of five years. In that study, the most common CT morphologic features were as follows: for bronchioloalveolar carcinoma (BAC) ground glass attenuation and smooth, irregular or spiculated margin were seen. The non-BAC adenocarcinomas had semisolid or solid attenuation and irregular margins. For the squamous cell carcinoma, solid attenuation and irregular margin identified. Small cell or mixed small and large cell neuroendocrine carcinoma demonstrated solid attenuation and irregular margin and for non–small cell carcinoma not otherwise specified, solid attenuation and irregular margin. The large cell carcinomas had solid attenuation and spiculated shapes were demonstrated. (Rosado de Christenson, 2008)

Both primary and the metastatic lung tumors can present with cavitation on CT images. The cavitation usually arises from tumor necrosis in the majority of cases, but it can also occur as a result of bacterial colonization or growth in the necrotic center of tumors (W. Y. Liao et al., 2000).

Another study reported the frequency of cavity formation in primary lung cancer to be 2-16%. Squamous cell carcinoma and adenocarcinoma accounted for 45-63 and 30-53% of the cavitation, respectively. The possible mechanisms of cavity formation include that were noted included: i) ischemic necrosis due to occlusion of the feeding vessels, ii) check-valve mechanism of the conducting bronchus, iii) elastic traction by the surrounding lung tissue, iv) tumor development in pre-existing lesions such as bullae, and v) neoplastic cell autophagism (Goto et al., 2011).

A study was done to evaluate thin-section computed tomographic characteristics of malignant nodules based on overall appearance (pure ground-glass opacity [GGO], mixed GGO, or solid opacity) in comparison with the appearance of benign nodules. It was noted that among the nodules with pure GGO, a round shape was found to be more frequent in malignant lesions (11 of 17, 65%) than in benign lesions (two of 12, 17%; $P = .02$; PPV, 85%); mixed GGO, a subtype with GGO in the periphery and a high-attenuation zone in the center, was seen much more often in the malignant lesions (11 of 27, 41%) than in the benign lesions (two of 29, 7%; $P = .004$; PPV, 85%). Among the solid nodules, a polygonal shape or a smooth or nearly smooth margin was present less frequently in the malignant than in benign lesions (polygonal shape: 7% vs 38%, $P = .02$; smooth or somewhat smooth margin: 0% vs 63%, $P < .001$), and 98% (46 of 47) of polygonal nodules and 100% (77 of 77) of nodules with a smooth or somewhat smooth margin were benign in nature (Li & Abe, 2004).

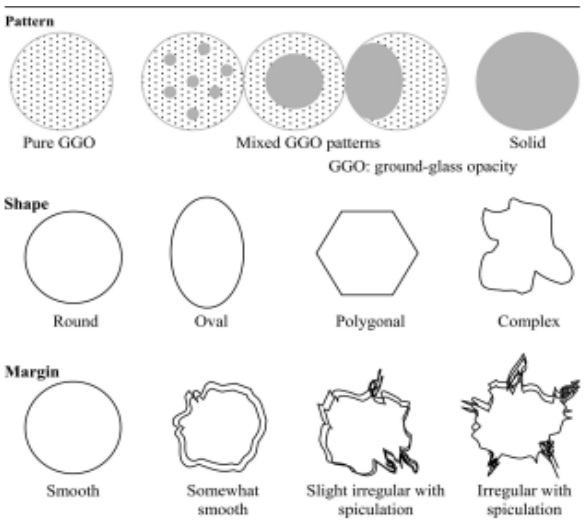

Figure 23: Typical appearance of the three patterns, four shapes, and four margins used to classify lung tumor description on CT (Li & Abe, 2004).

It is reported that there are three criteria for diagnosing vascular invasion on CT: 1) the disappearance of the fat layer; 2) the angle of tumor contact >90; and 3) stenosis and deformation of the vascular lumen. The degree of vascular invasion is classified as follows: 1) invasion outside the outer membrane; 2) invasion of inflammatory cells; 3) invasion of the outer membrane; 4) invasion of the media membrane; 5) invasion of the inner space (Oka et al., 2017).

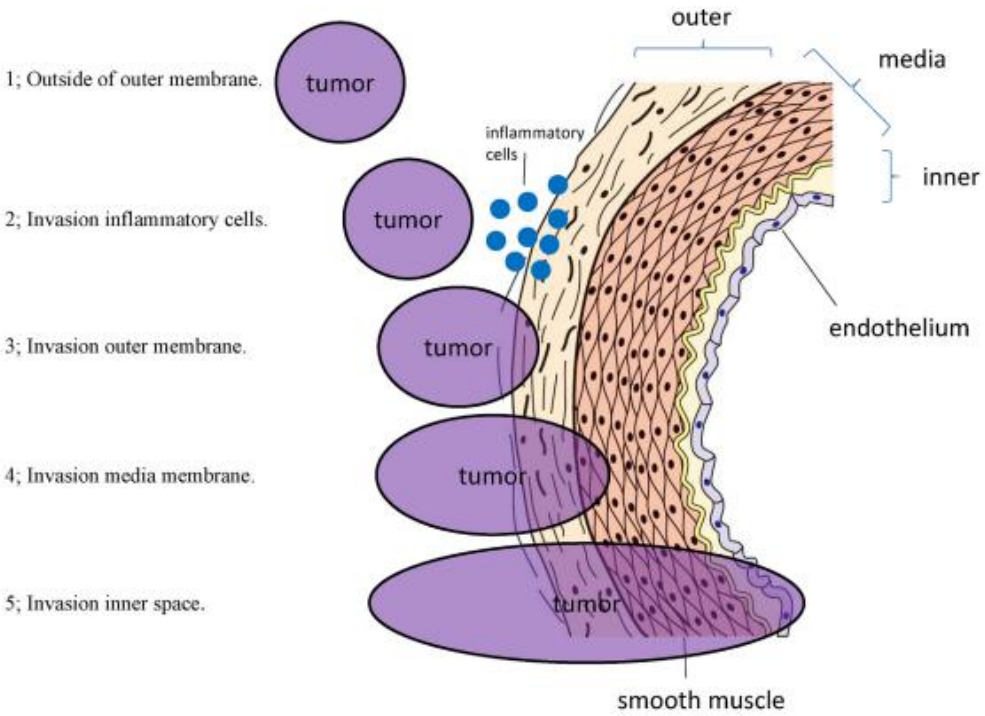

Figure 24: Diagram showing the various degrees of vascular invasion: 1) invasion outside the outer membrane; 2) invasion of inflammatory cells; 3) invasion of the outer membrane; 4) invasion of the media membrane; 5) invasion of the inner space.

However, (Munden et al., 2018) reported that the CT-based diagnosis of vascular and mediastinal tumor invasion was of limited use in current management of patients because most are incidental findings frequently seen on chest CT.

The skeleton is one of the commonest sites of metastasis in patients with lung cancer. It has been documented that the incidence of bone metastases in lung cancer patients is approximately 30-40%, and the median survival time (MST) of those patients with such type of metastases is 6-7 months. Metastatic bone disease may lead to various complications or skeletal related events including pain, pathological fractures, vertebral deformities and (or) collapse, hypercalcemia of malignancy and spinal cord compression. Lytic bone metastases are secondary to a variety of primary tumors and are found to be more common than sclerotic metastases. Most of the cases seen in the

literature up to date were found to have lytic bone metastasis or mixed lytic sclerotic bone metastasis with primary pulmonary adenocarcinoma (Tsuya et al., 2007).

There are certain limitations of CT scan when used for diagnosis and staging of lung cancer. The use of CT scan for detection of tumor invasion to adjacent structures such as pleura and chest wall is less specific and less sensitive. Also, it has low sensitivity and specificity for determination of nodal status based on the fact that enlarged lymph nodes may be hyperplastic rather than neoplastic and normal sized lymph nodes may contain neoplastic cells (Singh et al., 2004).

2.1.9 Histopathology of lung tumors

Lung cancer mostly arises from the cells of the respiratory epithelium and this can be divided into two broad categories. Small cell lung cancer (SCLC) is a highly malignant tumor derived from cells that exhibit neuroendocrine characteristics and it accounts for 15% of lung cancer cases. Non–small cell lung cancer (NSCLC), accounts for the remaining 85% of cases, and is further divided into 3 major pathologic subtypes: adenocarcinoma, squamous cell carcinoma, and large cell carcinoma. Adenocarcinoma accounts for about 38.5% of all lung cancer cases, with squamous cell carcinoma accounting for almost 20% and large cell carcinoma accounting for 2.9%. In the past several decades, the incidence of adenocarcinoma has increased greatly, and it has replaced squamous cell carcinoma as the most prevalent type of NSCLC (Dela Cruz et al., 2011).

Subsequently, adenocarcinoma has been found to be the most common histopathologic subtype of lung cancer, both in the smokers and non-smokers. Currently, it comprises nearly half of all diagnosed cases of lung cancer globally (J. H. Liao et al., 2015)(Aoki et al., 2000).

Traditionally, lung cancer was classified into two primary groups, the small cell and the non–small cell types. This grouping was then progressively specified by use of histopathologic features and immunohistochemical markers. Progress is being made in distinguishing invasive adenocarcinomas from pre-invasive lesions. The higher rates of adenocarcinoma compared to squamous and small cell lung cancer are greater in women. These findings may reflect the differences in the types of cigarettes more frequently used by women including filtered and low-tar versions, as well as genetic predisposition and the environmental exposures in female non-smokers (Barta et al., 2019).

Previously, there were six main subtypes of adenocarcinoma labeled A through F, which were used to describe the varying patterns of tumor growth. Type A through C described the bronchioloalveolar carcinoma (BAC). Type A, termed as localized BAC, described tumors that grew along the alveolar wall with only minimal to mild thickening of the alveolar septa; (no evidence of invasion/lepidic pattern). Type B described the localized BACs that demonstrated some evidence of structural collapse of alveolar. Type C was as type B BACs but with additional characteristic of fibroblastic proliferation. No lymph node involvement was described in type A or B tumors. Type C described BACs that had acquired invasive capabilities with around 28% having spread to lymph nodes. Their 5-year survival rate of these patients was 74.8%. The Types D to F described solid adenocarcinomas with poorer prognoses. Type D described poorly-differentiated adenocarcinomas. Type E (tubular adenocarcinomas), appeared to originate from bronchial gland cells, and the type F (papillary adenocarcinomas), resembled tall columnar cells of the bronchial epithelium (Noguchi et al., 1995).

In 2011, the International Association for the Study of Lung Cancer, American Thoracic Society, and European Respiratory Society ((IASLC/ETS/ERS) proposed a new categorization adenocarcinoma based on the histological evidence of invasion. Pre-invasive lesions are classified from atypical adenomatous hyperplasia (AAH) to adenocarcinoma in situ (AIS), and minimally invasive adenocarcinoma (MIA) in a continuum. Squamous cell lung cancer is the second most common sub-type. These tumors are distinguished histologically by the squamous pearl formation, keratin production, and intercellular bridging. Squamous cell lung cancer occurred and has an aggressive clinical course. It comprises 14% of lung cancers and it typically presents as a peri-hilar mass associated with both early and extensive lymph node metastases. It has a strong association with history of smoking and causes paraneoplastic syndromes commonly. Less frequent subtypes of lung cancer histologically include large cell (3%), adenosquamous (1–2%), and carcinoid tumors. (Barta et al., 2019)

According to the 2016 IASLC/ETS/ERS and WHO classifications lung-adenocarcinoma-spectrum, adenocarcinomas are categorized into three groups. The first category is the pre-invasive lesions. This entails the atypical adenomatous hyperplasia (AAH) a precursor lesion of a subset of adenocarcinomas that arise from the terminal respiratory units. It was defined as a peripheral small focal (≤ 5 mm) proliferation of the atypical type II pneumocytes and/or Clara cells that line the alveolar walls and respiratory bronchioles, with no sign of invasion. It is usually found incidentally. Another pre-invasive lesion is the adenocarcinoma in situ (AIS) formerly the bronchiolo-alveolar carcinoma. It is a purely lepidic proliferation of the type II pneumocytes/Clara cells. This implies no stromal, vascular or pleural invasion and is a rare occurrence (3 to 4%) of all non-small cell carcinomas (NSCLC). They

are mostly non-mucinous and measure 5-20 mm (but less than 30 mm). AIS have a 5-year survival rate of 100% 5-year survival after surgery due to its non-invasiveness.

The second category is the Invasive tumors. This includes the minimally invasive adenocarcinoma (MIA) which describes an ADC of less than 30 mm in diameter and a predominant lepidic pattern. Unlike AIS, it harbors an invasive area less than 5 mm and is usually a solitary tumor and harbors excellent prognosis post-surgery (98 -100 %.) It also describes the Invasive ADC defined by the presence of an invasive component larger than 5mm and are pathologically heterogeneous (a complex mixture of acinar, papillary, micropapillary, lepidic and solid patterns.) the lepidic predominant ADCs have an excellent 5-year post-resection survival of around 90%. On the contrary, a micropapillary pattern significantly worsens the prognosis. The third category is the adenocarcinoma variants. This includes the Invasive mucinous adenocarcinoma which is composed of mucinous cells, growing along alveoli secreting a lot of mucus filling alveoli. It measures more than 3 cm and has an invasive area of more than 5 mm. Other rare variants include the colloid, enteric and fetal type adenocarcinomas (Cohen et al., 2016)(J. H. Liao et al., 2015).

The 8th edition of the TNM classification of lung cancer was considered as the worldwide standard as of January 1, 2017. The T component is subdivided by the primary tumor size in 1cm increments, and other descriptors of invasion into the adjacent lung structures. The N component is determined by the location of the lymph nodes involved. The M component is subdivided into a single extra-thoracic metastasis, intrathoracic dissemination and multiple metastases. These are then coalesced into stage groups. This system provides a universal language to describe the anatomic extent of disease. (Detterbeck et al., 2017)

The definitions for T, N and M descriptors are as below:

T (Primary Tumor)

T0 No primary tumor,

Tis Carcinoma in situ (Squamous or Adenocarcinoma)

T1 Tumor ≤3 cm,

T1a (mi) Minimally Invasive Adenocarcinoma

T1a Superficial spreading tumor in central airways

T1a Tumor ≤1 cm

T1b Tumor >1 but ≤2 cm

T1c Tumor >2 but ≤3 cm

T2 tumor >3 but ≤5cm or tumor involving the visceral pleura, main bronchus but not carina and atelectasis to hilum

T2a tumor >3 but ≤4cm

T2b tumor >4 but ≤ 5cm

T3 tumor >5 but≤ 7cm or invading the chest wall, pericardium, phrenic nerve or separate tumor nodules in the same lobe

T4 tumor > 7cm or tumor invading mediastinum, diaphragm, heart, great vessels, recurrent laryngeal nerve, carina, trachea, esophagus, spine; or tumor nodule(s) in a different ipsilateral lobe

N (Regional Lymph Nodes)

N0 No regional node metastasis

N1 Metastasis in ipsilateral pulmonary or hilar nodes

N2 Metastasis in ipsilateral mediastinal/subcarinal nodes

N3 Metastasis in contralateral mediastinal/hilar, or supraclavicular nodes

M (Distant Metastasis)

M0 No distant metastasis

M1a Malignant pleural/pericardial effusion or separate tumor nodule(s) in a contralateral lobe.

M1b Single extra thoracic metastasis

M1c Multiple extra thoracic metastases

Histological diagnosis of NSCLC is crucial to many treatment decisions and should be as exact and detailed as the samples and available technology allow. Diagnosis should be based upon the criteria laid out in the WHO classification. This classification entails the complete diagnostic approach for surgically resected tumors and provides guidance for assessing and reporting small biopsy and cytology samples where complete morphological criteria for specific diagnosis may not be met accurately.

Most patients with NSCLC present with advanced stage unresectable disease, therefore all treatment-determining diagnoses must be made on small biopsy and/or cytology-type samples. Sampling may be carried out of the primary tumor or any accessible metastases, taken under direct vision or more usually with image-guided assistance, which greatly increases the diagnostic yield (hit rate). Sampling metastatic disease may facilitate staging, as well as diagnosis. These diagnostic samples frequently have limited tumor material and must therefore be handled accordingly; ensuring processing is suitable for all likely diagnostic procedures and that material is

used sparingly at each step, since many diagnostic tests may be required (Planchard et al., 2018).

Percutaneous thoracic needle biopsy (PTNB) is a safe and effective method of obtaining tissue for histopathology in pulmonary nodules. Major complications are rare. The factors that increase the likelihood of success include proper communication with the clinical team, optimization of the patient factors, the use of conscious sedation, adherence to careful technique, and on-site cytology. PTNB provides invaluable information for biomarker-based targeted therapy and for enrollment into clinical trials. It can aid radiation planning and preoperative localization of nodules with image-guided percutaneous fiducial marker placement. Such advances have expanded the role of the interventional thoracic radiologist in managing patients with lung cancer (Sharma & Shepard, 2018).

Immunohistochemistry (IHC) has become a key technique in primary diagnosis as well as in predictive biomarker assessment. In those cases of NSCLC where specific subtyping is not possible by morphology alone, a limited panel of IHC is recommended to determine the subtype. For instance, thyroid transcription factor 1 (TTF1) positivity is associated with probable diagnosis of adenocarcinoma, p40 positivity with probable diagnosis of SCC; if neither are positive the diagnosis remains NSCLC-not otherwise specified (NOS). IHC staining should be used to reduce the NSCLC-NOS rate to < 10% of cases diagnosed. Pathologists are advised to conserve tissue at every stage of diagnosis, to use only two tissue sections for IHC NSCLC subtyping and to avoid excessive IHC investigation, which may not be clinically relevant (Planchard et al., 2018).

2.1.10 CT chest and histopathology correlation of lung tumors

Studies have been done globally on CT chest diagnosis of lung tumors and their histopathological outcome correlation including studies by (Dr. Dinesh K. Gupta , Dr. Sudha Gupta, 2019)(Suzuki et al., 2011)(Kishi et al., 2004)(Asamura et al., 2003)(Cohen et al., 2016). However limited research has been conducted regarding the same in Kenya, and the Eastern Africa at large, on the diagnostic accuracy of chest CT in the final histopathological diagnosis of lung tumors.

In a retrospective study done at Samsung Medical Centre in Korea on images of 10 patients, a review was done to evaluate chest CT features of lung pleomorphic carcinomas in comparison to pathologic findings. This included location and size of tumor, the presence of calcification, attenuation values and internal architecture of the mass as well as invasion of pleura and chest wall. Attenuation values of the mass on CT scans were compared with pathologic findings in tumors in available gross specimens. On the unenhanced CT scans, attenuation of the tumor was found to be similar to that of surrounding muscle tissue. One patient had calcification visible within the tumor. Invasion of the chest wall was noted in two patients while seven patients had pleural invasion. Tumors had a peripheral location in nine patients. On contrast enhanced CT scans, lesions that had the longest diameter larger than 5 cm, showed central low-attenuation areas and a substantial enhancement in the tumor periphery. Comparatively, lesions with the longest diameter smaller than 5 cm showed a homogeneous enhancement. Low-attenuation areas on contrast-enhanced CT scans corresponded to areas of either: myxoid degeneration, necrosis or hemorrhage in pathologic specimens. Pleomorphic carcinomas of the lung were found to commonly manifest as large peripheral lung neoplasms that have a central low-

attenuation area, and frequently invade the pleura and chest wall (T. H. Kim et al., 2004).

In the National Cancer Center Hospital, Tokyo, a clinicopathological study of resected sub-centimeter lung cancers was done to determine if there was a favorable prognosis for ground glass opacity lesions.

The information obtained from the pathology files of 51 patients showed a primary tumor of 1cm or less in diameter excluding three tumors arising from the bronchial lumina of hilum and squamous cell carcinoma on histology. 48 tumors of peripheral origin were studied and the clinicopathological features were analyzed based on three types of appearance on high-resolution CT: those with non-solid ground glass opacification (GGO) were 19; those with the partly-solid GGO type were 9 and the purely solid types were 20. Non-solid GGO is made up of moderately increased density and homogenous on CT and cannot obscure the broncho-vascular structure. The partly solid GGO contains a solid part but doesn't exceed 50% of the whole area. The histologic type of the GGO lesion was bronchioloalveolar carcinoma in all the 28 cases. In solid lesions, histologically there were 16 adenocarcinomas, 2 cases of squamous cell carcinoma and 1 case each of small cell carcinoma and carcinoid tumor seen. Lymph node involvement was seen in only 3 patients with the solid lesions (N1 in 2 patients, N2 in 1 patient) (Asamura et al., 2003).

2.2 Sensitivity and specificity

The sensitivity and specificity of a diagnostic or screening test is the accuracy defined relative to a reference standard. It indicates the level of agreement of a test with respect to a chosen reference/ a gold standard. The gold standard is usually the preferred method of diagnosis or a benchmark that is normally available under reasonable conditions (Franco & Di Napoli, 2016)(Cardoso et al., 2014).

Using sensitivity and specificity provides the validity of a diagnostic test. These are obtained by comparing the diagnostic test against the gold standard in a two-by-two table. The diagnostic test is then compared with the gold standard regarding the ability to identify the disease or not.

Table 2.1: Table showing 2*2 (two-by-two) comparison of the diagnostic test and gold standard (Molinaro, 2015).

	Gold standard disease present	**Gold standard disease absent**	
Test Positive	True Positive (a)	False Positive (b)	Total test Positive (a+b)
Test Negative	False Negative (c)	True Negative (d)	Total test Negative (c+d)
	Total disease(a+c)	Total Normal (b+d)	Total Population (a+b+c+d)

Sensitivity = a/a+c
=a (true positive)/a+c (true positive +false negative)
Specificity= d/b+d
=d (true negative)/b+d (true negative+false positive)

The sensitivity of a test is the probability of the test turning out positive when the disease is present. The specificity is the probability of the test turning negative when the disease is absent (Molinaro, 2015).

A diagnostic test that is ideal has a sensitivity of 100% with respect to identification of the pathology and a specificity of 100% in pointing out absence of that pathology. However, in practice, there is no gold standard and instead, the diagnostic methods with the highest sensitivity and specificity are used. This criterion could be used to define radiologically an early adenocarcinoma of the lung.

Image-guided percutaneous thoracic needle biopsy (PTNB) is considered a safe and effective method of obtaining a diagnosis in suspected malignancy, focal benign lesions, or even infection. It is the most preferred technique for diagnosis of new or

growing pulmonary nodules, or in the cases where bronchoscopy is negative for persistent airspace opacity or a hilar mass. PTNB has a sensitivity and specificity of 93% to 98% and 98% to 100%, respectively, for the diagnosis of malignancy. The sensitivity for the evaluation of benign lesions is significantly lower than for malignant lesions and varies from 17% to 91%. Methods of image guidance include ultrasonography, computed tomography (CT), fluoroscopy and magnetic resonance imaging. Most procedures are normally performed with CT guidance but ultrasonography guidance is often preferred for sub-pleural lung masses or those that extend across the chest wall (Sharma & Shepard, 2018).

Diagnostic accuracy is determined by the kappa statistic. Kappa is one of the measures of inter-observer agreement. There are other methods of assessing this agreement, but kappa is reported to be the most commonly used measure in the medical literature.

This calculation is based on the difference between how much agreement is actually present (“observed” agreement) in comparison to how much agreement would be expected to be present by chance alone (“expected” agreement) . However, Kappa makes no distinction among various types and sources of disagreement. Since it is affected by prevalence, it may not be deemed appropriate to compare kappa between different populations or studies. Nevertheless, kappa can provide more information than a mere simple calculation of the raw proportion of agreement (Viera & Garrett, 2005).

Interpretation of Kappa Agreement :< 0 Less than chance agreement, 0.01–0.20 Slight agreement, 0.21– 0.40 Fair agreement, 0.41–0.60 Moderate agreement, 0.61–0.80 Substantial agreement, 0.81–0.99 Almost perfect agreement (Viera & Garrett, 2005).

CHAPTER THREE: METHODOLOGY

3.1. Study site

The study was conducted at the Moi Teaching and Referral Hospital, Radiology and Imaging Department, Interventional Radiology (IR) clinic and Histopathology department. MTRH is a National Referral hospital which serves patients from over 22 counties of the Western region of Kenya and the Rift Valley, as well as our Ugandan and Southern Sudan Counterparts. It is the main teaching center for Moi University Schools of Medicine, Nursing, Dentistry and Public health for both the undergraduate and postgraduate studies. The School of Medicine offers training for radiologists, radiology technologists, sonographers and interventional radiologists.

3.2 Study duration

The study was conducted for a period of 12 months, commencing in October 2021 to September 2022.

3.3 Study design

The study design employed was a cross-sectional study.

3.4 Study population

The study population included all adult patients sent for chest CT with suspicion of lung tumor for image guided biopsy and tissue diagnosis. These were recruited to the study.

3.5 Eligibility criteria

Those eligible participants who took part in the study fulfilled the following eligibility criteria.

3.5.1. Inclusion criteria

1. Adult patients sent for chest CT with diagnosis of suspected lung tumor and undergoing image guided biopsy to obtain tissue diagnosis, who consented to the study.

3.5.2. Exclusion criteria

1. Patients with confirmed diagnosis of lung tumor and on follow up.
2. Patients who were lost to follow up before biopsy.
3. Patients who opted out of the study before biopsy.

3.6 Sampling Techniques

3.6.1. Sampling procedure

Consecutive sampling was done in this study until the sample size that was required was attained, within the study duration. Hence every adult patient sent for CT chest scan with suspected lung tumor, for image guided biopsy and subsequent tissue diagnosis was recruited to the study.

3.6.2 Sample Size Determination

This was a census study based on the small number of patients who presented to MTRH with CT chest diagnosis of lung tumor for image guided biopsy. According to past the records in MTRH for the preceding three years, (2020, 2019 and 2018), the total number of patients with a chest CT and histopathological diagnosis of lung tumor 104, 90 and 86. This made an average of 90 patients per year, which was the basis for census study.

3.6.3 Study Recruitment Schema

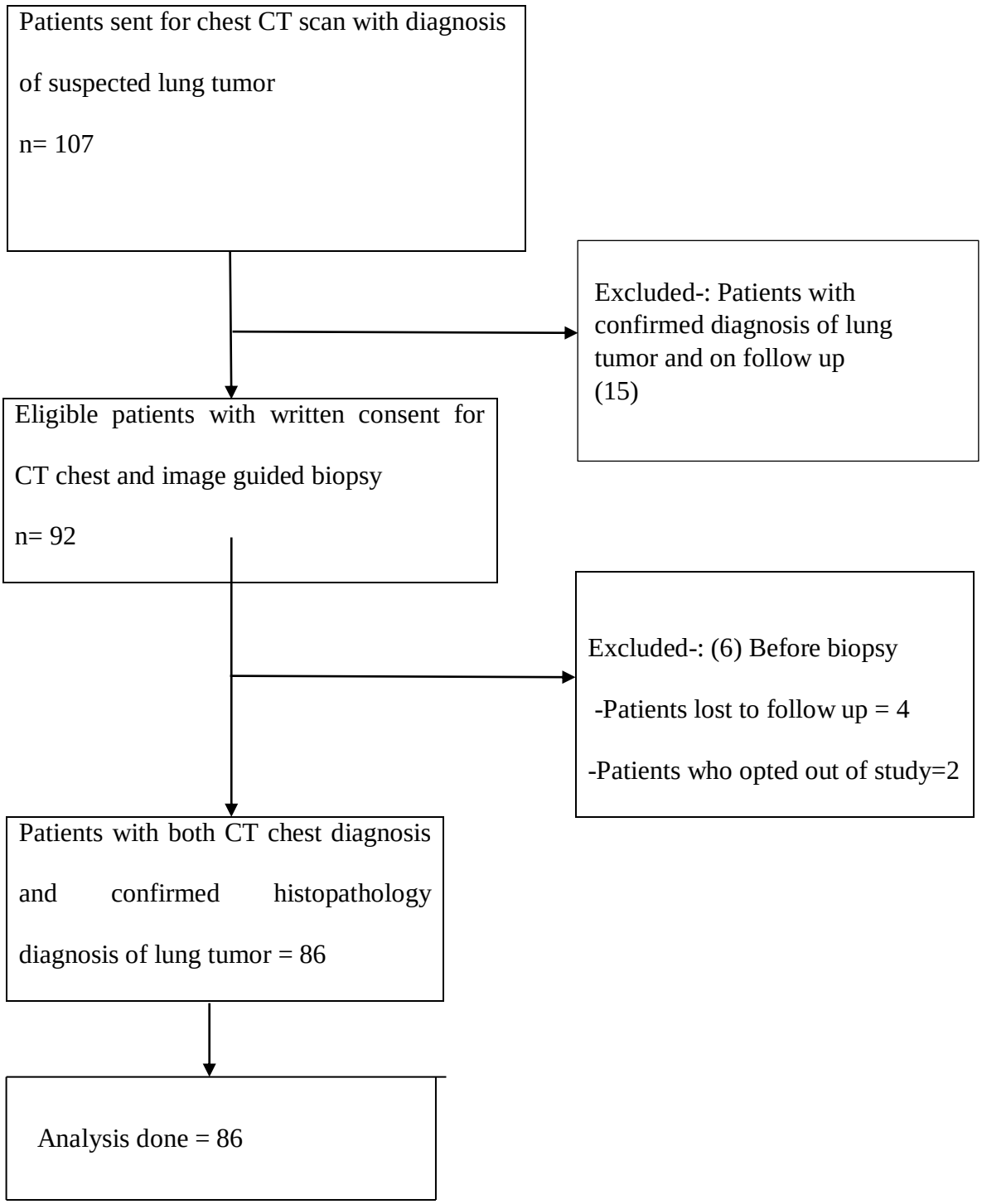

Figure 25: Study Recruitment Schema

3. 7 Study Procedure

Patients with suspected lung tumour underwent CT scan of the chest at the CT Centre in Radiology and Imaging Department of MTRH. They then underwent image guided lung biopsy at the Interventional Radiology Department and the biopsy samples were taken to the histopathology lab for a confirmatory lung tumor diagnosis.

Chest CT Scan Protocol for MTRH Radiology and Imaging Department.

CT scan images of the chest were acquired via a helical technique using a Neosoft 4000 DUAL machine that were operated by 2 qualified radiographers using the protocol as illustrated below.

Patients were positioned supine with their arms above their head and the head resting in a head cradle. The patient's body was immobilized using Velcro straps, and then the table was raised to a height of 140cm. The patient was moved into the scanner gantry whereby an automated audio system gave instructions.

A topogram was obtained antero-posteriorly with dimensions of 350-400mm. A scout view with extent from just above the lung apices to just below the diaphragm (at the level of adrenal glands) was taken. The direction of the scanning was caudo-cranial with a minimal scan delay in suspended inspiration. A standard algorithm was used. The window settings were 1500 Hounsfield units (H) for window width and window level of -500H. The technical parameters were 130 Kvp, 150 mAs, a pitch of 1.375, a typical matrix of 512 × 512 pixels and a slice thickness of 5mm. Contrast enhanced CT scans were obtained in arterial phase after administration of intravenous (IV) Iohexal 2ml/kg and a bolus of 50mls of IV normal saline at 4ml/sec. Multiplanar reconstructions were performed in all cases using a bone window and soft tissue window.

The CT images generated were interpreted by the researcher and confirmed by two independent consultant radiologists. The final chest CT scan reports were done based on the 8th edition of the TNM classification of lung cancer. The lung tumor description of chest CT included: Site (specific lung lobe), largest dimensions in cm (T), margins, configurations and enhancement patterns. Pleural involvement, local and satellite mass effect, local and distant nodal spread (N), local and distant metastasis (M), vascular and osseous involvement were described (Detterbeck et al., 2017).

Patients with suspected lung tumour from CT chest scan results were sent by the principal investigator and consultant radiologists to the IR department for biopsy.

Percutaneous thoracic needle biopsy (PTNB) protocol for Interventional Radiology Department in MTRH

Patient presenting with a chest CT result of suspected lung tumour were triaged and assessed at the IR department.

The procedure to be done was explained to the patient in terms of the benefits, risks and possible complications that may arise.

As part of assessment, the patients underwent ultrasound examination to confirm the exact location of the mass, the access technique to be used, the equipment and medications needed and the laboratory work ups required prior to the biopsy.

The biopsies were to be done under image guidance using either ultrasound or CT modalities.

The pre-procedural lab works required were full haemogram (FHG), urea/electrolytes and creatinine levels (UEC) s, international normalised ratio (INR), COVID Test and Triple Serology - (Hepatitis B, Hepatitis C and Syphilis)

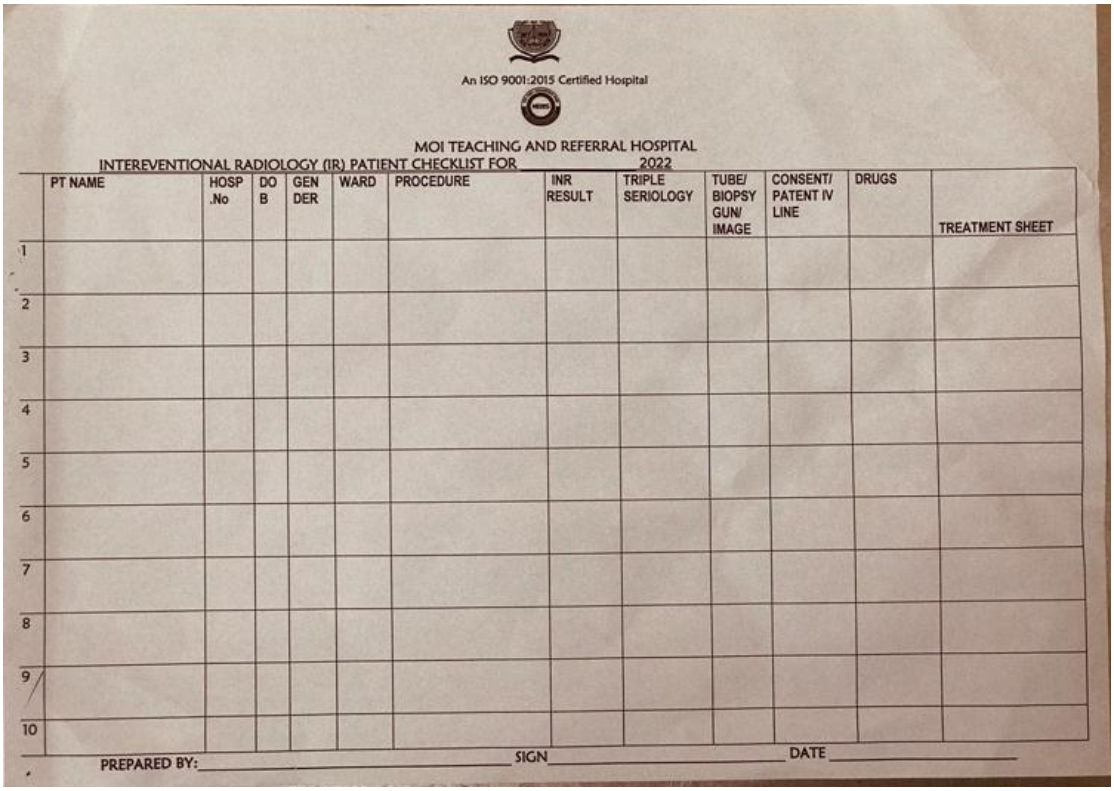

An ISO 9001:2015 Certified Hospital

MOI TEACHING AND REFERRAL HOSPITAL

INTEREVENTIONAL RADIOLOGY (IR) PATIENT CHECKLIST FOR _____ 2022

	PT NAME	HOSP .No	DOB	GENDER	WARD	PROCEDURE	INR RESULT	TRIPLE SERIOLOGY	TUBE/ BIOPSY GUN/ IMAGE	CONSENT/ PATENT IV LINE	DRUGS	TREATMENT SHEET
1												
2												
3												
4												
5												
6												
7												
8												
9												
10												

PREPARED BY:_____ SIGN_____ DATE _____

Figure 26: Interventional Radiology department assessment check list form at MTRH.

Patient preparation

Patients were required to give consent and got an explanation on the need to tolerate the procedure.

Adequate targeted history and clinical examination was done by the principal investigator.

Medications that increase the risk of pulmonary hemorrhage or hemothorax were withheld to restore normal coagulation.

Coumadin, full-dose aspirin, and nonsteroidal anti-inflammatory drugs were discontinued 5 days before biopsy. Heparin and warfarin were discontinued 6 and 12 hours before biopsy, respectively, with confirmation of normalization of blood coagulation factors. Patients using continuous positive airway pressure or bi-level

positive airway pressure ventilation were stopped for at least 24 hours following PTNB to prevent a delayed pneumothorax. Patients who were living alone or had severe comorbidities required overnight admission. Patients who received conscious sedation or general anesthesia were told to refrain from solids for 6 hours and fluids for 3 hours before the procedure as per MTRH protocol.

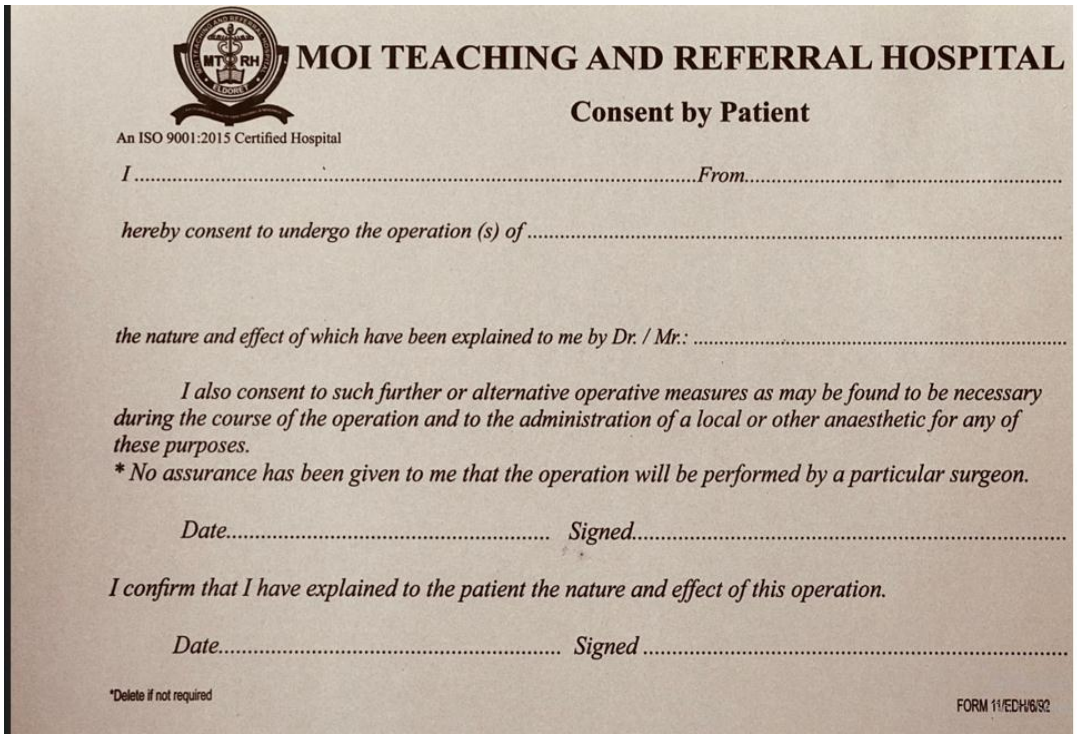

MOI TEACHING AND REFERRAL HOSPITAL

Consent by Patient

An ISO 9001:2015 Certified Hospital

I .....From.....

hereby consent to undergo the operation (s) of .....

the nature and effect of which have been explained to me by Dr. / Mr.: .....

I also consent to such further or alternative operative measures as may be found to be necessary during the course of the operation and to the administration of a local or other anaesthetic for any of these purposes.

** No assurance has been given to me that the operation will be performed by a particular surgeon.*

Date..... Signed.....

I confirm that I have explained to the patient the nature and effect of this operation.

Date..... Signed .....

*Delete if not required

FORM 11/EDH/6/92

Figure 27: Consent form used in IR department at MTRH.

Sedation

PTNB was performed with local anesthesia, conscious sedation and monitored anesthesia care. When local anesthesia was used, the patient was instructed to breathe normally during the entire procedure and notify the interventionist in-case of any pain.

Patient Positioning

Patient stability during the procedure was best achieved in the supine, lateral or prone position. When prone, the rib spaces are wide and the patient cannot see the needle, this increased patient comfort. The subclavian vessels, prominent costochondral cartilages, and breast tissue can hinder the anterior approach in the upper zones. The lateral approach renders the patient less stable; the ribs are closer together, reducing the access and there is a higher incidence of pneumothorax compared with the supine or prone approach. Recovery was in the dependent, supine position which is often easier for patients to tolerate.

a) CT guided biopsy

Localizing the Nodule

Review of prior imaging confirmed the position of the nodule. A radio-opaque grid was placed on the patient's skin at the level of the suspected nodule. Localized 5-mm sections were obtained during gentle respiration to localize the nodule. Then 2.5-mm sections were obtained and centered on the nodule to find a window for biopsy. Dose reduction was achieved by using the optimum millamperage and kilovoltage.

Finding the Window

An appropriate path from the skin to the nodule was visible on at least 3 axial 2.5-mm sections. This window avoids ribs, vessels, and fissures. Once the required table position was defined, a line was drawn from the nodule upward to the skin to mimic the trajectory of the biopsy needle. The corresponding line on the grid was determined and the table was moved to the required table position. Using the scanner's laser light, a cross was marked on the patient's skin that intersected with the table position with the line on the grid.

Preparation of the Biopsy Site

The marked skin was sterilized with iodine following removal of the grid. Sterile drapes were used to cover the remainder of the patient's chest. Lidocaine 1% was injected through a 25-G needle into the subcutaneous tissues at the level of the marked cross. The syringe was detached from the local anesthetic needle that was left in the subcutaneous tissues. A repeat limited axial scan was performed to confirm that the local anesthetic needle was correctly positioned.

Choosing the Coaxial Needle

The distance between the skin and pleura along the needle trajectory was measured. The distance between the skin and nodule was also measured in order to enable the correct length choice of the 17-G coaxial needle.

Figure 28: Sample images of gauge 16 semi-automatic biopsy gun and a gauge 17 coaxial needle, used to obtain lung biopsy samples at MTRH, interventional radiology department.

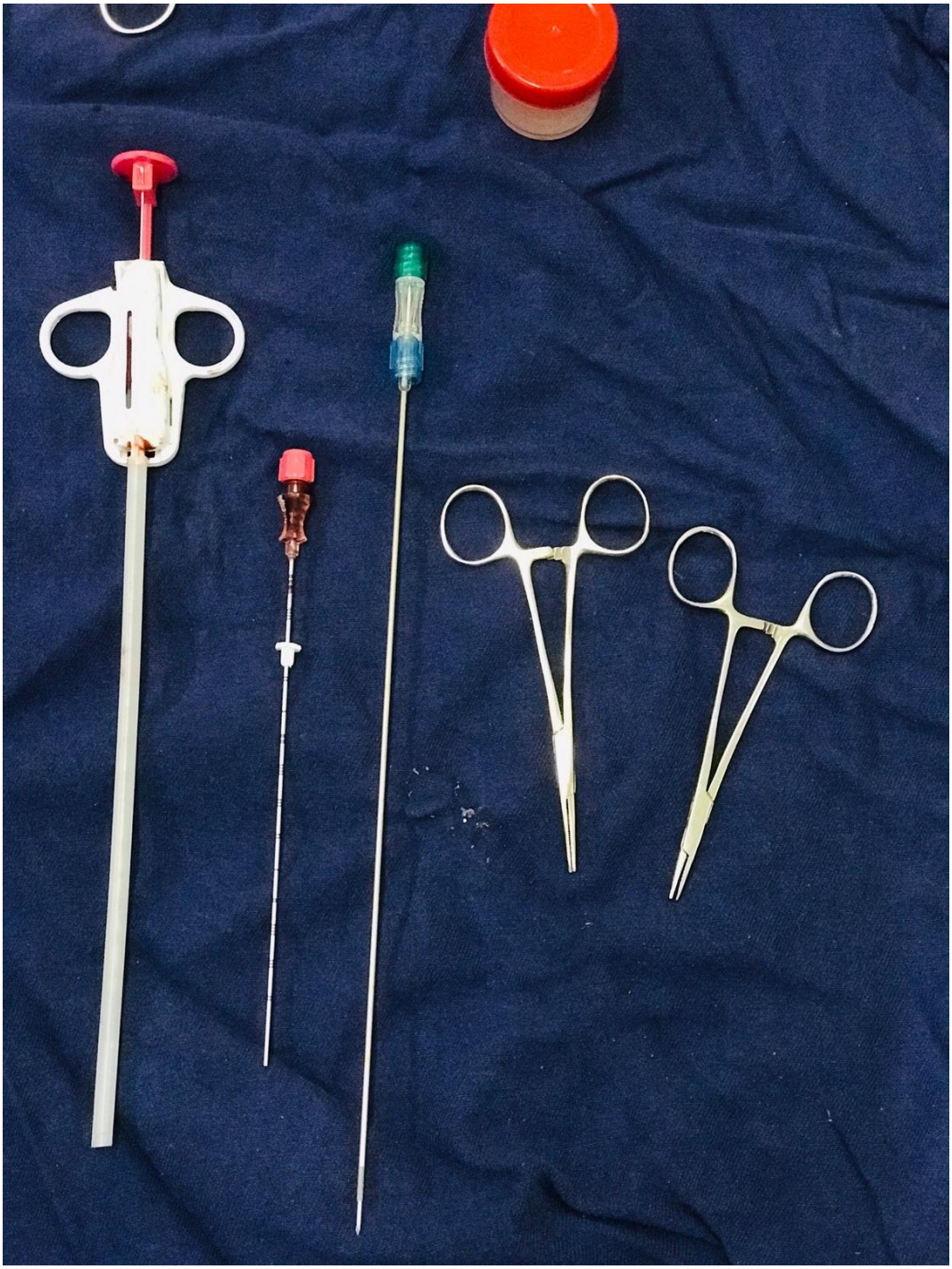

Figure 29: Sample images of the biopsy needles that are commonly used for PTNB at MTRH interventional radiology department. From the left: 17-gauge semiautomatic biopsy gun, 18 - gauge coaxial needle through which the core biopsy is obtained, small artery forceps and needle holder. Top – A sample collection bottle with formalin preservative.

Advancing the Coaxial Needle into the Nodule

A 4-mm incision was made in the sterilized skin with a scalpel blade and the coaxial needle was advanced into the subcutaneous tissues at the confirmed skin entry site. The coaxial needle was supported by gauze when the subcutaneous tissue was limited. A repeat stack of axial images with the same gantry angulation was performed to confirm the correct position of the coaxial needle. A line was drawn on the workstation along the length of the needle and extending into the nodule. The needle was then advanced through the muscles and up to the pleural surface then pleural puncture after 1 to 2 mL of local anesthetic injection. Following confirmation of the needle trajectory remaining on course toward the lung nodule, the needle was advanced incrementally until the tip was within the nodule.

Obtaining Biopsy Material

The central stylet was exchanged for the 17-G coaxial needle over a saline seal to prevent air embolism. A 2-mL syringe with a blunt-ended needle was filled with injectable saline and was used to drip saline into the central core of the coaxial needle as the inner stylet was slowly removed. The coaxial needle was completely filled with saline before a rapid exchange of the inner stylet with the FNA needle. The FNA needle was allowed to fall to the level of the nodule and advanced rapidly in and out of the coaxial needle by a few millimeters while aspirating with a syringe placed on the end of the needle. Short, sharp jabbing movements cut into the nodule and negative pressure on the syringe was used to aspirate cells into the needle. Saline was again dripped into the trocar of the coaxial needle and the FNA needle was rapidly exchanged with the central stylet. A repeat limited CT scan confirmed that the position of the coaxial needle remained within the nodule and that no complications occurred during aspiration for instance pneumothorax or hemothorax.

Safe Removal of the Biopsy Needle and Recovery

Once adequate samples were obtained, a final limited scan with the needle in the nodule was performed to exclude complications. Once all the specimens were obtained, the patient's skin was cleaned and monitoring equipment, sterile towels, and drapes were removed. Then the radiologist swiftly removed the needle, applied a dressing over the skin incision, and the patient was rolled over onto the stretcher to lie on the puncture site for a few minutes. Patient was taken to recovery area for observation for two-three hours, to check for any post-biopsy complications.

Percutaneous transthoracic needle biopsy technique, step by step

Action	Steps
Sedation	None/conscious sedation/general anesthesia with cardiorespiratory monitoring
Patient position	Supine/prone if possible. Stabilize with straps
Needle	Coaxial 18-G/19-G needle at least 3–4 cm longer than distance from skin to nodule
Find the nodule	Review imaging, place radio-opaque skin grid, scout views, limited 5-mm axial sections
Find the window	2.5 mm axial ± gantry angulation. Mark skin entry site
Insert needle	Sterilize field/local anesthetic infiltration, image 25-G needle to confirm window, measure skin to pleura distance, advance coaxial needle to pleural surface
Pierce nodule	Confirm correct trajectory toward nodule. Local anesthetic injected into the extrapleural space/intravenous fentanyl dose before pleural puncture. Cross pleura, advance into nodule
Biopsy	Inject saline into coaxial needle, rapid exchange of stylet with FNA or core biopsy needle, FNA/core biopsy, refill saline during each exchange
Specimen	FNA smear onto slides (on-site cytology), or into saline (flow cytometry and cell block)/transport medium; cores in formalin; microbiology aspirate in saline
Needle removal	Remove all monitoring leads/blood pressure cuff first. Remove needle, rapid rollover
Recovery	Recover in dependent position for 3 h, chest radiograph at 1 and 3 h
Discharge	Home with overnight support. Postbiopsy/sedation instructions

Figure 30: CT Guided biopsy of lung mass step by step procedure.

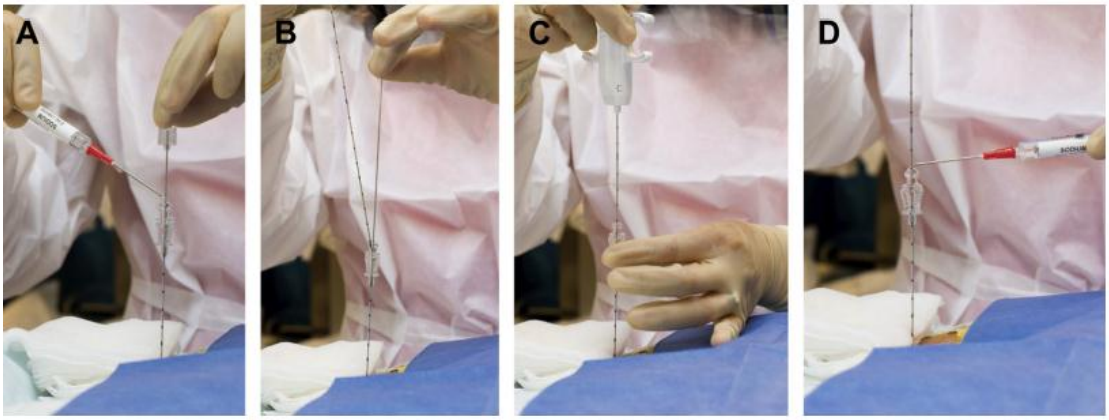

Figure 31: The saline injection technique used to reduce risk of air embolism during needle exchanges. (A) Once the coaxial needle is positioned within the nodule, the central trocar is exchanged with the aspiration needle or core biopsy needle. Before the central stylet of the coaxial needle is removed, a 2-mL syringe with a blunt-tipped needle is used to drip sterile saline into the hollow bore of the coaxial needle until saline is visible at the top of the trocar. (B) A rapid exchange of the central stylet with the biopsy needle is performed through the saline seal. (C) The biopsy is performed. (D) Before removal of the biopsy needle, the saline is dripped again into the bore of the coaxial needle. A rapid exchange of the biopsy needle with the central stylet is performed through the saline seal.

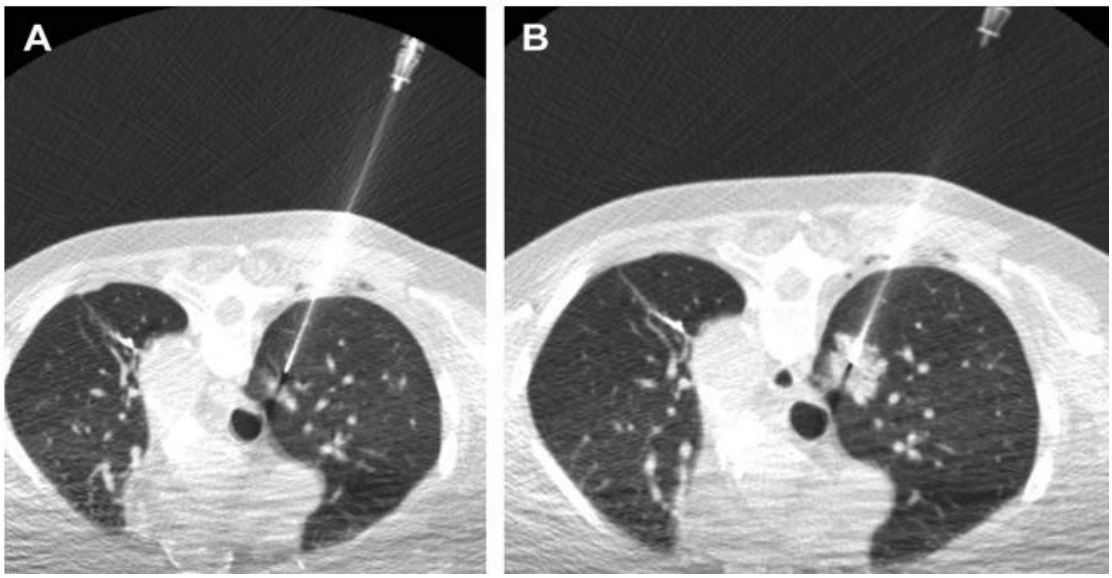

Figure 32: 70-year-old man with right upper lobe adenocarcinoma. (A) Axial prone lung window CT image obtained during PTNB shows the coaxial needle proximal to the 1.4-cm nodule. (B) Following FNA, a repeat image shows development of minor pulmonary hemorrhage that obscures the nodule. This hemorrhage may have been caused by the needle tip lying in lung rather than within the lesion at the time of biopsy. The patient was asymptomatic

Figure 33: A 70 year old female patient with a left sided anterior lung tumour undergoing ultrasound guided biopsy under local anesthesia, at the IR department in MTRH. (A) Demonstrates continuous monitoring of vital signs and (B) Real time ultrasound images are being taken during the procedure.

Ultrasound guided biopsy

The supplies that were used included the Coaxial Needles Gauge 17 and a Semi-automatic Biopsy Guns Gauge 18.

Medications that were used were analgesics e.g. Morphine, local anaesthetic agents eg Lignocaine (for procedure use), formalin for biopsy tissue preservation and oral antibiotics and analgesics for post-procedure infection prophylaxis.

Patients were instructed to lie supine. The lung area for biopsy was exposed, and then cleaning and draping were done aseptically.

The local anaesthesia was infiltrated subcutaneously to numb the pain, then into the lung mass under ultrasound guidance/ CT guidance as planned. The access to the mass was under coaxial biopsy needle gauge 17 and then the semi-automatic biopsy gun gauge 18 was used to obtain multiple samples from the lung mass till sufficient samples were obtained (about 8-10). The core biopsy samples were preserved in

formalin solution in a clearly labelled container and accompanied with a well written request form to be taken to the histopathology lab.

After the procedure, the needles were retracted and then post procedure chest ultrasound/CT done to check for any immediate complications such as hemothorax, pneumothorax or hematoma.

Nick site was dressed and patient put in the observation room for two hours to monitor for mentioned complications.

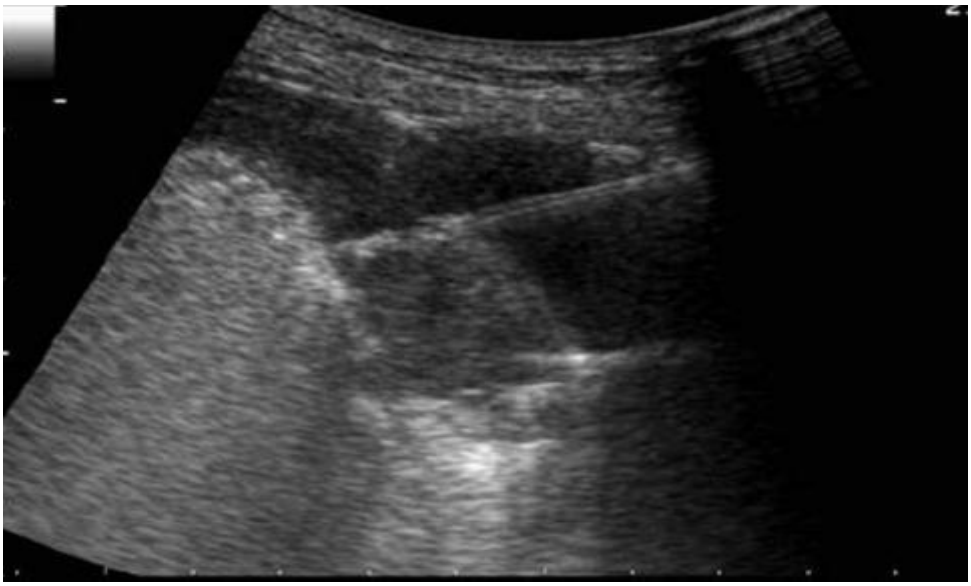

Figure 34: Image of an ultrasound guided lung tumor biopsy. The needle passes over the pleural effusion penetrating the tumor.

Immediate post-biopsy complications:

Few of the immediate post biopsy complications that occurred (within two hours) included: pneumothorax, hemothorax, pulmonary hemorrhage, non-diagnostic sample and air embolism.

Histopathology for lung mass biopsy

The lung biopsy samples from the Interventional Radiology Department were preserved in formalin solution in a clearly labelled container and a well elaborated laboratory request form. The samples were handled by two qualified independent

pathologists who prepared the specimens and viewed them under microscopy. The respective pathologists concluded on the histopathology findings in line with possible CT chest diagnosis of the lung tumor in question. Those biopsy specimens that brought about inconclusive results were taken for further studies such as immunohistochemistry to confirm the final diagnosis.

3.8 Data collection

Data was collected using a data collection tool. Comprehensive data were obtained regarding patient's age, gender, occupation and residence. CT chest imaging findings were recorded onto the data form after a detailed review by the two radiologists. The histopathological findings from lung biopsies were recorded after obtaining results in patients file, compiled from a qualified pathologist at the histopathology laboratory. Information gathered was entered into a computer database.

3.9 Data Analysis and Interpretation.

Data was analyzed using the STATA version 16. Continuous variables were summarized as mean and standard deviation as well as median and associated interquartile ranges, while categorical variables were expressed as frequencies and percentages. Data was presented using frequency tables, charts and graphs. The level of significance was set at $p \leq 0.05$.

Objective1: To describe the CT chest findings, frequencies and percentages were used.

Objective 2: To describe the histopathological findings, frequencies and percentages were used.

Objective 3: To evaluate the diagnostic accuracy of chest CT in the diagnosis of lung tumors, measures of diagnostic accuracy were used i.e. sensitivity, specificity, negative predictive value, positive predictive value and likelihood ratio.

3.10 Data Quality and Security

Data was entered into a computer via double entry to ensure accuracy. The entry screen had check codes included to minimize errors. The computers had password protection and access was only allowed to the authorized persons. The databases obtained were stored electronically and the copies of filled questionnaires were stored in a locked shelf within the principal investigators residence.

3.11 Data Presentation

The data obtained was presented in the form of tables, charts and graphs.

3.12 Ethical consideration

Prior to the commencement of the study, ethical approval and permission were sought from Moi University Institutional Research Ethics Committee (IREC) – Approval No. 0003849 and Permission was obtained from the MTRH administration. NACOSTI approval was obtained - Ref No. 377897.

Participants were required to sign a consent form with details on the rationale for, the procedure, the benefits and any anticipated risks of the study (appendix 2).

Respect for autonomy was considered by giving all the necessary information as well as freedom to withdraw from the study at any point, without any need for justification. Participants were assured of privacy and confidentiality. All the data obtained was maintained in a confidential manner and no individual was identified during the dissemination of findings. Codes of alphanumeric nature were used in the data collection tool to protect the privacy of participants. Computers used for data entry

and analysis had password-enabled access only to the principal investigator. Printed research data were kept in a locked office with limited access.

3.13 Dissemination of Data

Study findings have been presented to Moi University in partial fulfillment for the award of degree in Master of Medicine (Radiology and Imaging).A copy of thesis will be made available at the institutional Library for public access and consumption.

The study finding will also be shared in peer reviewed journals for publication.

CHAPTER FOUR: RESULTS.

Table 4.1: Sociodemographic Characteristics of patients with lung tumors

The Mean age of the participants was 55years with a range of 23-86 years. Female gender was more affected 52.3:47.7. Most of the study participants were unemployed with 54.7% living in semi urban areas**.**

Variable	**N**	Frequency (n)	Percent (%)
	86		
Gender			
Female		45	52.3
Male		41	47.7
Age in Years	**86**		
Mean 55			
Range 23-86			
Occupation	**86**		
Unemployed		42	48.8
Self Employed		27	31.4
Employed		17	19.8
Residence	**86**		
Rural		20	23.3
Semi-urban		47	54.7
Urban		19	22.1

Table 4.2: Risk factors for patients with lung tumors

Majority of the study participants (60.5%) had no history of smoking with 62.8% having used unprocessed biomass. A few of them (17.4%) were exposed to occupational hazards and 34.9% participants had poor diet.

Variable	**N**	Frequency (n)	Percent (%)
	86		
Smoking history	**86**		
No		52	60.5
Yes		34	39.5
Use of unprocessed biomass	86		
No		32	37.2
Yes		54	62.8
Exposure to occupational hazards	86		
No		71	82.6
Yes		15	17.4
1st Degree relative with lung cancer	**86**		
No		67	77.9
Yes		19	22.1
Poor diet	**86**		
No		56	65.1
Yes		30	34.9

Table 4.3: Clinical Presentation of patients with lung tumors

Most of the patients presented with persistent cough (88.4), chest pain (83.7%), Hemoptysis (54.7%) and General body malaise (65.1%). Other clinical presentations are detailed in table 4.3 below.

Variable	N	Frequency (n)	Percent (%)
	86		
Persistent cough	**86**		
No		10	11.6
Yes		76	88.4
Chest pain	86		
No		14	16.3
Yes		72	83.7
Difficulty in breathing	86		
No		34	39.5
Yes		52	60.5
Hemoptysis (Blood-stained sputum)	**86**		
No		39	45.3
Yes		47	54.7
Unexplained weight loss	**86**		
No		32	37.2
Yes		54	62.8
Hoarseness of voice	**86**		
No		50	58.1
Yes		36	41.9
General body malaise	**86**		
No		30	34.9
Yes		56	65.1
Loss of appetite	**86**		
No		37	43.0
Yes		49	57.0
Incidental finding on chest X-ray	**86**		
No		60	69.8
Yes		26	30.2

Table 4.4: Clinical Examination Findings for patients with lung tumors

The most common clinical findings were decreased breath sounds and tachycardia. The other findings are shown in table 4.4 below.

Variable	N	Frequency (n)	Percent (%)
	86		
Decreased/absent breath sounds	**86**		
No		15	17.4
Yes		71	82.6
Low grade fever	86		
No		41	47.7
Yes		45	52.3
Decreased oxygen saturation	86		
No		38	44.2
Yes		48	55.8
Tachycardia (increased heart rate)	**86**		
No		23	26.7
Yes		63	73.3
Hypotension	**86**		
No		43	50.0
Yes		43	50.0
Lymphadenopathy	**86**		
No		63	73.3
Yes		23	26.7

Objective 1- Table 4.5: Lung tumor description on chest CT scan

The most affected lobe was the left upper lobe (22.1%). Most of the tumors had irregular margins (45.3%) and mild enhancement pattern (44.2%). There were satellite pulmonary nodules in most of the lung tumors (27.9%).

Variable	Frequency (n)	Percent (%)
Site		
bilateral lung bases	5	5.8
both entire lungs	2	2.3
entire left lung	4	4.7
Entire right lung	3	3.5
left lower lobe	14	16.3
Left upper lobe	19	22.1
right lower lobe	16	18.6
right middle lobe	11	12.8
right upper lobe	12	14.0
Largest Dimension of solid component(cm)		
Mean 4 cm		
SD 6.07		
Margins		
Irregular	39	45.3
Smooth	33	38.4
Spiculated	14	16.3
Configuration		
Lobulated	41	47.7
Multilobulated	26	30.2
None	19	22.1
Characteristics		
Cavitatory	4	4.7
Central	55	64.0
Central necrosis	11	12.8
Eccentric	16	18.6
Inner Wall		
Calcification	4	4.7

Irregular	23	26.7
Smooth	12	14.0
Soft tissue	47	54.7
Enhancement Pattern		
Mild enhancement	38	44.2
Moderate enhancement	22	25.6
Non enhancement	12	14.0
Rim enhancement	3	3.5
Intense homogenous enhancement	11	12.8
Interstitial Pattern Spread		
Consolidation (part GGO)	47	54.7
Nodular/Solid	39	45.3
Satellite Mass Effect		
Absent	54	62.8
Present	32	37.2
Satellite Lesions		
Atelectasis	12	14.0
Fibrosis	19	22.1
Pulmonary nodules	24	27.9
None	31	36.0

Objective 1-Table 4.6: Other extra-pulmonary masses on chest CT scan

Thyroid masses were common among the other masses in patients with lung tumor (3.5%). The most involved local nodes were mediastinal (32.6%) while the distant nodes were left axillary (10.5%).

Variable	Frequency (n)	Percent (%)
Other Masses		
Hepatic	1	1.2
Breast mass	1	1.2
Neck	1	1.2
Mesenteric	2	2.3
None	71	82.6
Pelvic mass	2	2.3
Pericardial mass	2	2.3
Esophageal	1	1.2
Colon	1	1.2
Gluteal mass	1	1.2
Thyroid mass	3	3.5
Local		
Intercostal	4	4.7
Mediastinal	28	32.6
None	40	46.5
Para tracheal	12	14.0
Retro cardiac	2	2.3
Distant		
Both axillary	5	5.8
Cervical	8	9.3
Left axillary nodes	9	10.5
None	58	67.4
Right axillary nodes	6	7.0

Objective 1-Table 4.7: Pleura Involvement

Pleural thickening (24.4%), ipsilateral pleural effusion (25.6%) and emphysema (8.1%) were the more common types of pleural involvement.

Variable	Frequency (n)	Percent (%)
Pleura		
Infiltration	12	14.0
Mass	1	1.2
Nodules	3	3.5
None	49	57.0
Thickening	21	24.4
Pleural Fluid Collection		
Bilateral effusion	4	4.7
Ipsilateral effusion	22	25.6
Empyema	6	7.0
None	54	62.8
Pleural Air Collection		
Emphysema	7	8.1
None	78	90.7
Pneumothorax	1	1.2

Objective 1-Table 4.8: Vascular and osseous involvement of the lung masses.

Vascular invasion involved mostly the major vessels (9.3%) while osseous involvement was more common on the sternum (3.5%).

Variable	Frequency (n)	Percent (%)
Vascular Invasion		
Major (pulmonary artery and vein)	7	8.1
Minor (segmental arteries)	1	1.2
None	78	90.7
Osseous involvement		
Cervical vertebrae	1	1.2
None	77	89.5
Ribs	2	2.3
Sternum	3	3.5
Thoracic vertebrae	2	2.3
Trachea	1	1.2

Objective 1-Table 4.9: Chest CT Findings for the lung tumors

Variable	Frequency (n)	Percent (%)
CT FINDINGS		
1. Malignant lesions		
Primary	55	64.0
Secondary distant metastasis	6	7.0
Secondary infiltrative	5	5.8

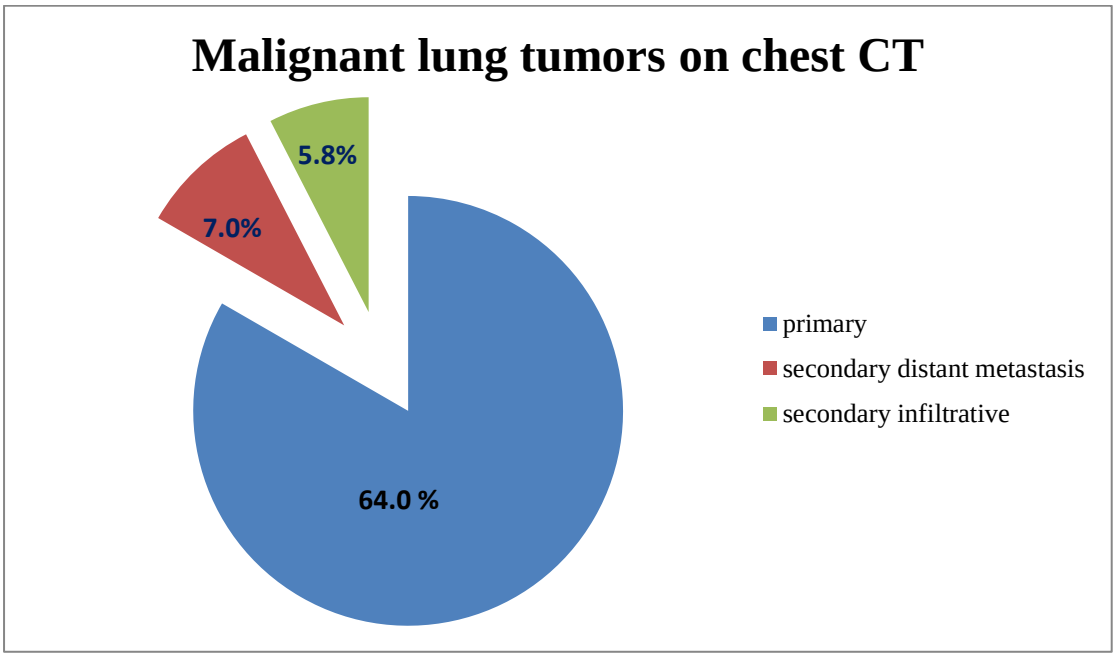

Objective 1: Figure 35: Malignant lesions distribution on CT (%).

Primary malignant lesions accounted for majority of the cases (64.0%), followed by lesions from secondary distant metastases (7.0%) then secondary infiltrative lesions (5.8%).

2. Benign lesions		
Indeterminate lung lesion (for IHC)	1	1.2
Inflammatory lung lesions	17	19.7
Lesion with mixed components (scarring, inflammation, or infection)	2	2.3

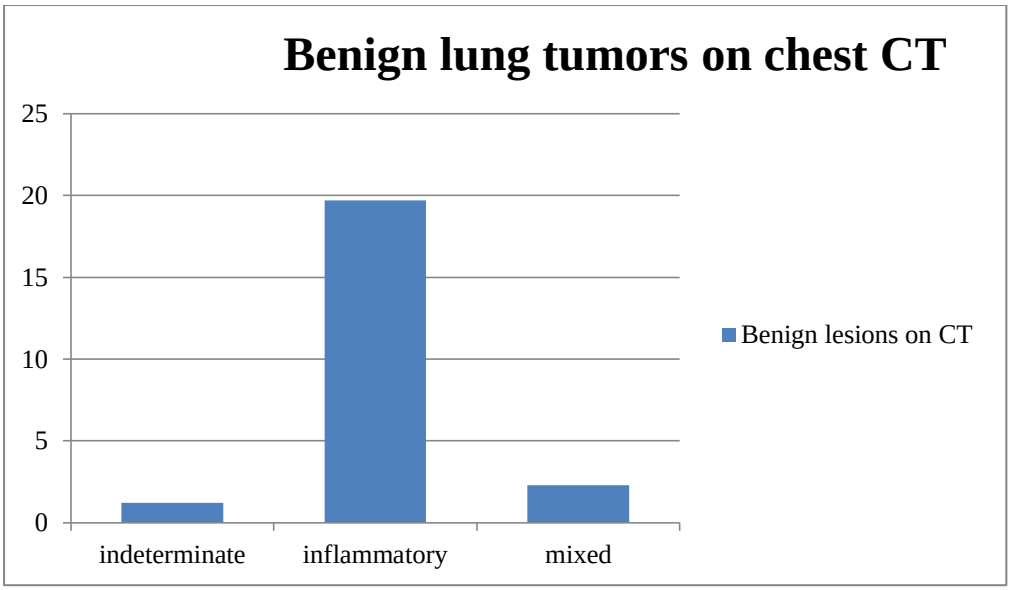

Objective 1- Figure 36: Benign lesions distribution on chest CT (%).

Inflammatory lung lesions were the commonest (19.7%) followed by mixed component lung lesions (2.3%) and there was one indeterminate lung lesion (1.7%) i.e. needed immunohistochemistry studies.

Objective 2- Histopathology findings of the lung masses

Malignant	74	86.0
Benign	12	14.0

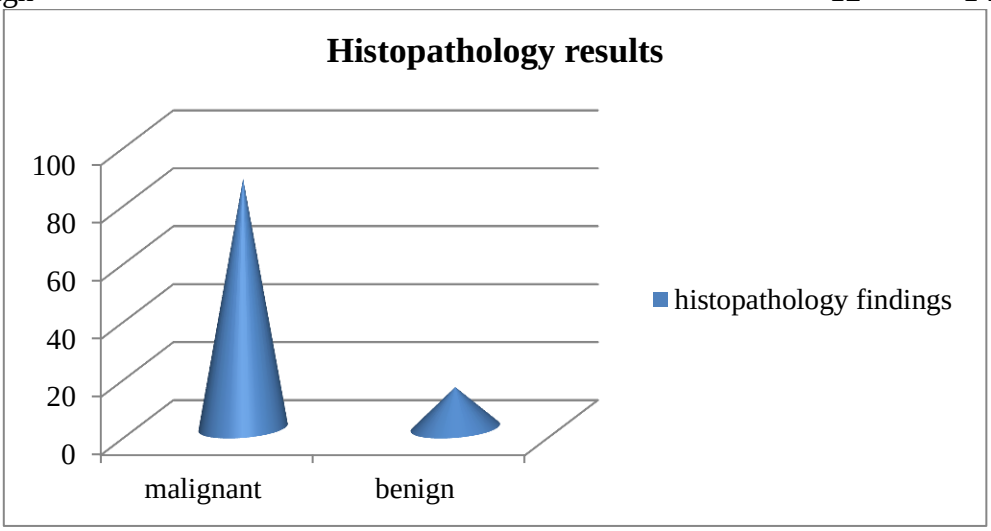

Objective 2- Figure 37: Histopathology results (%)

Most of the lung tumors were malignant in nature upon histopathology studies (86%) while few were benign (14%).

Objective 2-Table 4.10: Malignant histopathology sub-types of the lung masses.

Adenocarcinoma was the more common subtype of the malignant lesions (51.23%) followed by squamous cell carcinoma (10.5%).

Variable	Frequency (n)	Percent (%)
Adenocarcinoma	44	51.2
Broncho-alveolar carcinoma	1	1.2
Hodgkin's lymphoma	2	2.3
Plasmacytoma	1	1.2
Sarcoma	4	4.7
Small cell carcinoma	3	3.5
Squamous cell carcinoma	9	10.5
Thymoma	1	1.2
Non-small cell carcinoma	1	1.2

Objective 2- Table 4.11: Benign histopathology sub-types of the lung masses.

The more common subtypes of benign lesions were chronic interstitial pneumonitis and necrotizing granulomatous inflammation from TB, both at 5.8%.

Variable	Frequency (n)	Percent (%)
Chronic granulomatous inflammatory process	3	3.5
Chronic inflammatory process	4	4.7
Chronic interstitial pneumonitis	5	5.8
COVID	1	1.2
Necrotizing granulomatous inflammation TB	5	5.8
Non-specific inflammatory process	2	2.3

Table 4.12: Modalities for image guided biopsy for the lung tumors.

Majority of the patients underwent ultrasound guided biopsy (87.2%) while 12.8% underwent CT guided biopsy of the lung tumors.

CT guided	11	12.8%
Ultrasound guided	75	87.2%

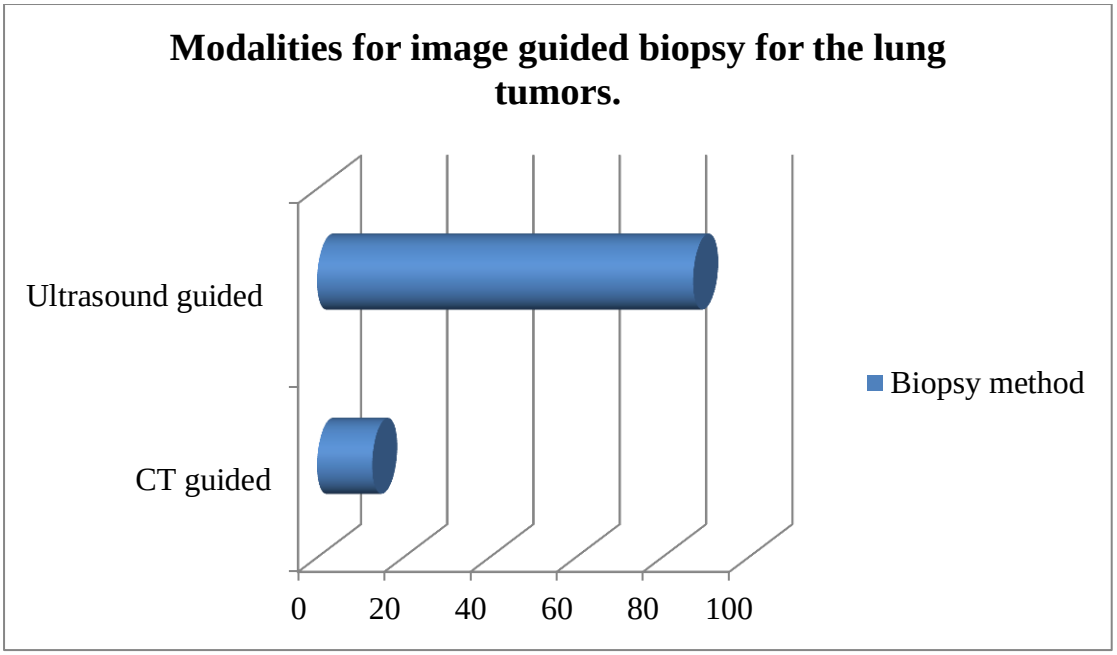

Figure 38: Modalities for image guided biopsy of the lung tumors. (%)

Most of the patients, 87.2%, underwent ultrasound guided biopsy due to the easy accessibility of the lung tumors. A few underwent CT guided biopsy (12.8%), likely the small lesions and those that were inaccessible via ultrasound guidance.

Table 4.13: Immediate complications of the image guided lung tumor biopsy

Most of the patients did not develop post biopsy complications (88.3%). However, the commonest post-biopsy complication noted was hemoptysis (5.8%), followed by desaturation (4.7%) and pneumothorax (1.2%).

Variable	Frequency (n)	Percent (%)
Desaturation	4	4.7
Hemoptysis	5	5.8
Pneumothorax	1	1.2

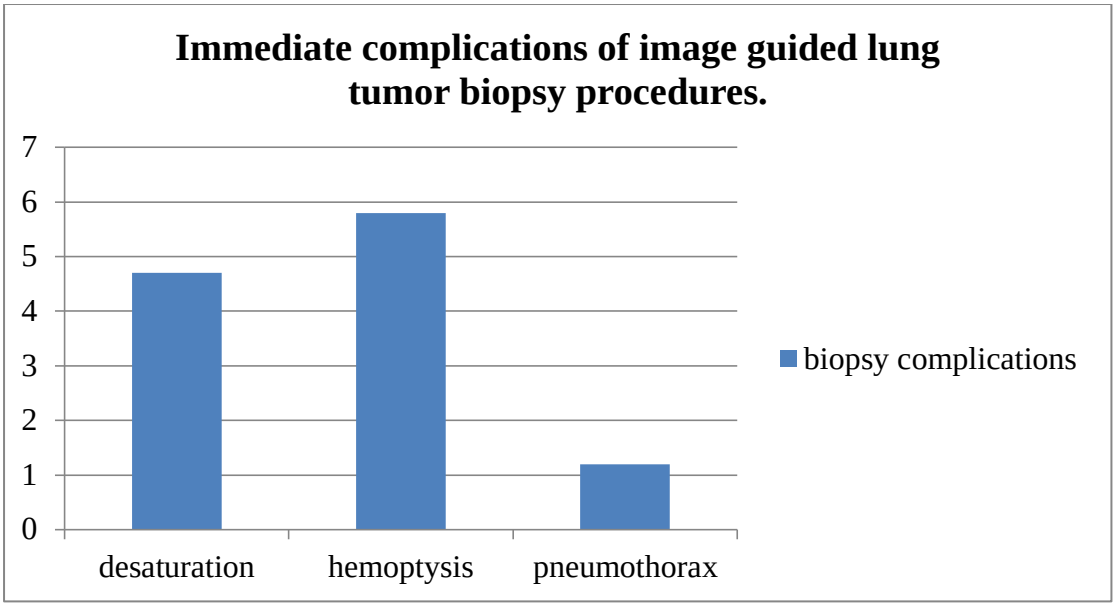

Figure 39: Immediate complications of the image guided lung tumor biopsy procedures (%)

Most of the patients did not develop post biopsy complications (88.3%). However, the commonest post-biopsy complication noted was hemoptysis (5.8%), followed by desaturation (4.7%) and pneumothorax (1.2%).

Objective 3- Table 4.14: Evaluation of diagnostic accuracy of chest CT in the diagnosis of lung tumors based on histopathology findings.

True positive were 64, false positive 6, false negative 1 and true negative 15 in number.

		Histopathology findings (Gold standard)		Total
		Positive	Negative	
CT Findings	Positive	64 (TP)	6 (FP)	70
	Negative	1 (FN)	15 (TN)	16
Total		65	21	86

Cohen's Kappa was run to determine if there was agreement between computed tomography and histopathology findings. There was a substantial agreement between the two examinations $\kappa = 0.764$ (0.646-0.882), $p < 0.0001$

Objective 3-Table 4.15: Sensitivity and Specificity tests

Validation of the CT scan diagnosis in this case found a surprising result that the sensitivity value found was quite high at 98%, with a specificity value of 71%, then PPV, NPV, LR +, LR-, and accuracy were 91.4%, 93.8%, 3.38, 0.17 and 91.9% respectively.

Variable	Value
Sensitivity	98.46%
Specificity	71.43%
Negative Predictive Value	93.75%
Positive Predictive Value	91.43%
Accuracy	91.86%
Negative Likelihood Ratio	0.17
Positive Likelihood Ratio	3.38

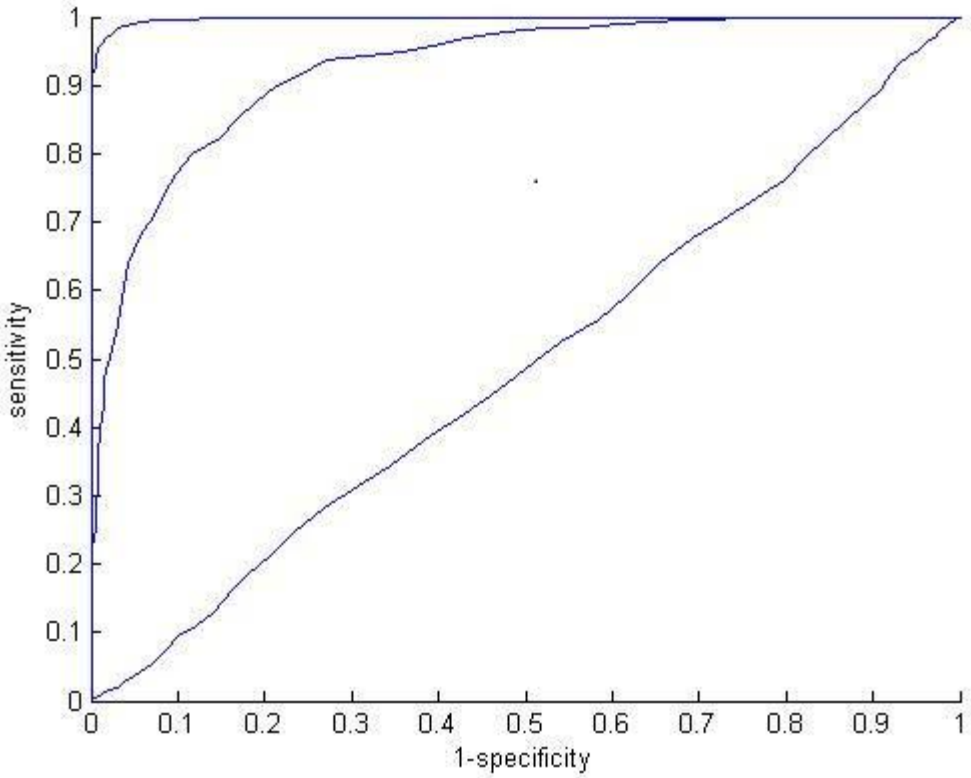

Objective 3- Figure 40: Sensitivity and Specificity curve

Sample images lung masses as seen on chest CT and their corresponding histopathology slides.

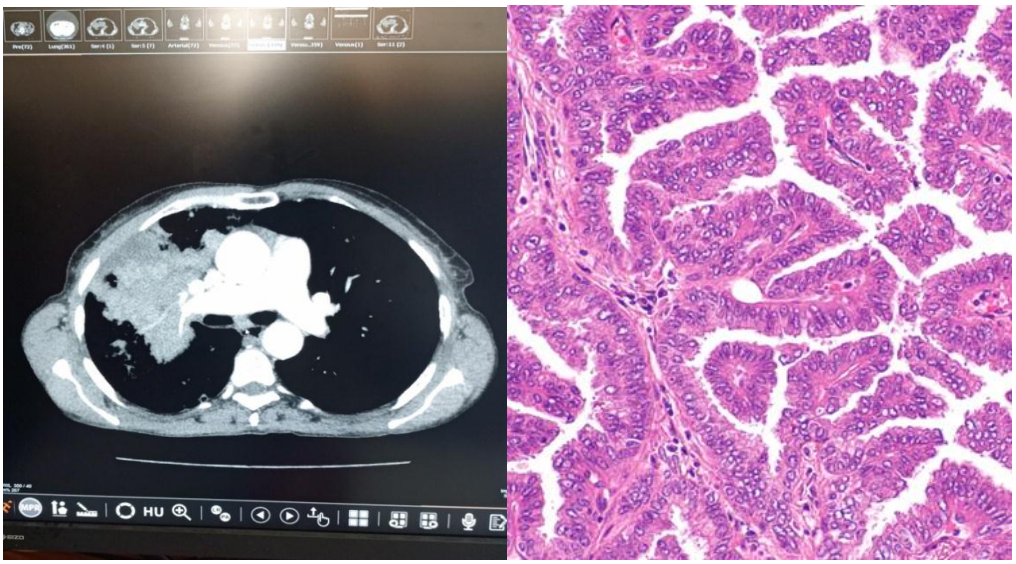

Sample Image 1: An axial CT scan image of a 55 year old female presenting with history of cough, weight loss and hemoptysis. The CT image showed a right upper lobe lung tumor. Histopathology slide of the same patient demonstrated features of papillary adenocarcinoma.

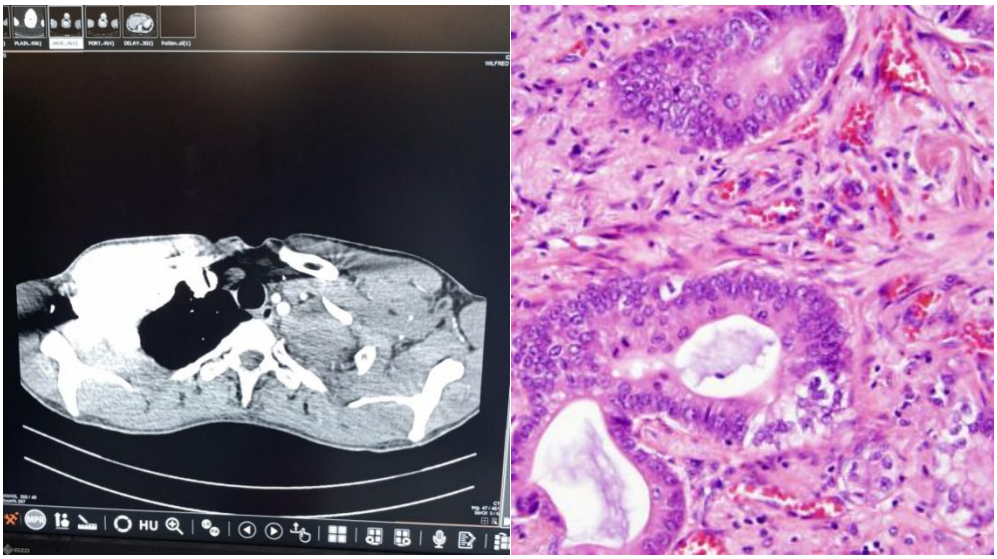

Sample Image 2: An axial CT scan image of a 48 year old male who had progressive weight loss, dyspnea and cough, showing a left upper lobe mass. Histopathology result showed features of non-small cell lung cancer.

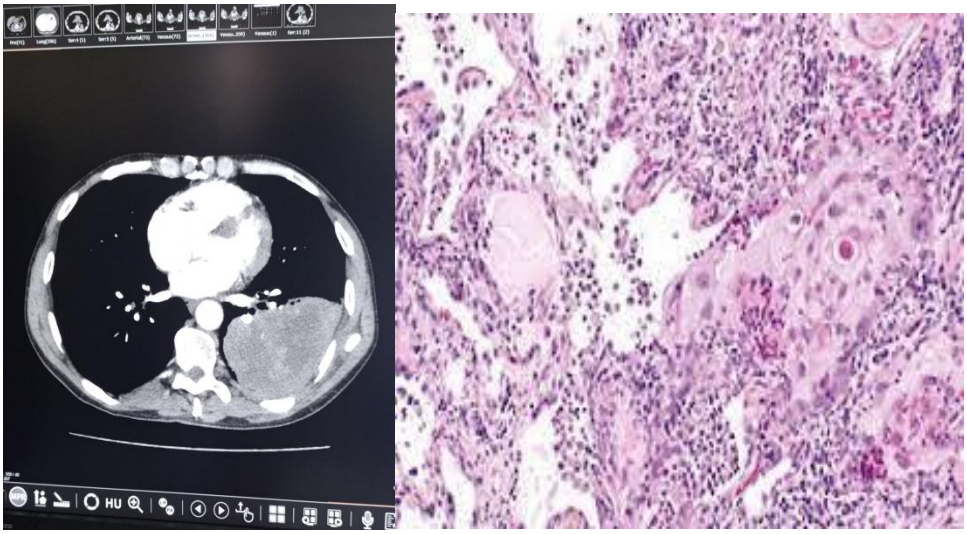

Sample Image 3: An axial CT scan image of a 56 year old male with chest pain, tachycardia and hotness of body, showing a left lower lobe lung mass. Histopathology studies showed features of invasive squamous cell carcinoma.

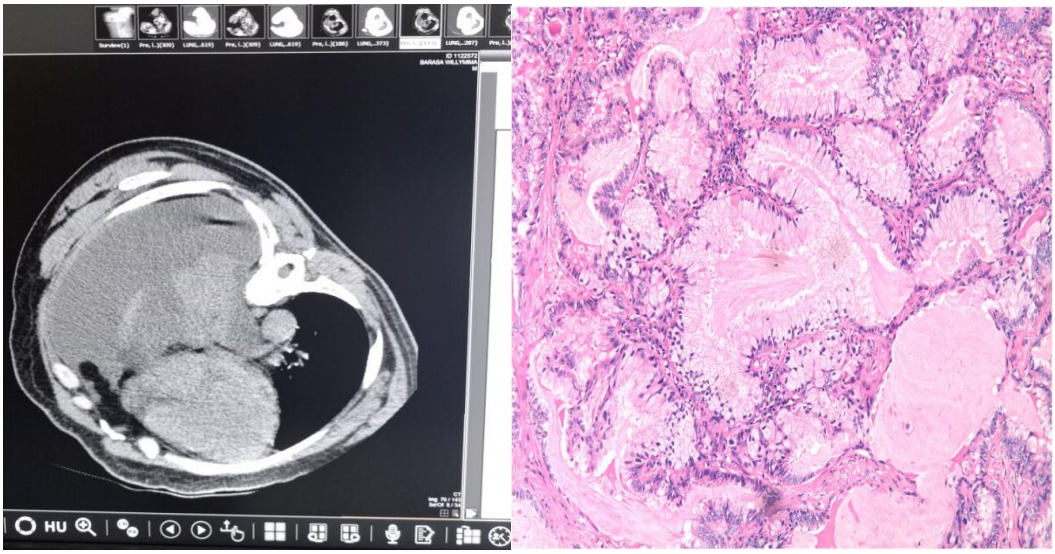

Sample size 4: An axial CT scan image of the left lower lobe lung mass in a 52 year old male who had hemoptysis, difficulty in breathing and positive history of smoking. It demonstrates displacement of mediastinal structures and a midline shift to the right. Histopathology showed features of a moderately differentiated invasive adenocarcinoma.

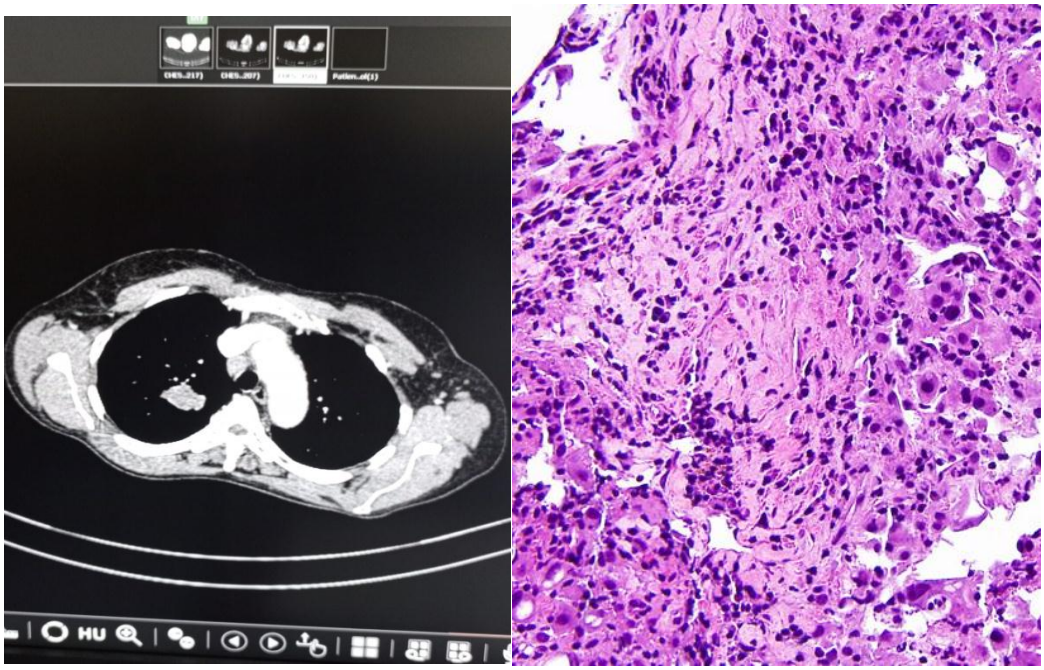

Sample Image 5: An axial CT scan image of a 43 year old female showing a right middle lobe lung mass. She had history of longstanding biomass use, cough and intermittent chest pains. Histopathology studies revealed invasive adenocarcinoma of the lung.

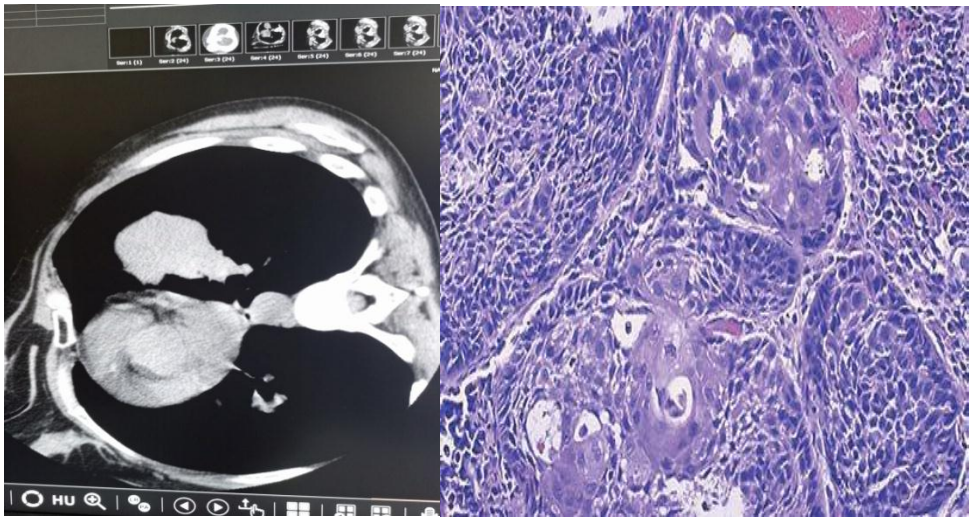

Sample Image 6: An axial CT scan image of a 50 year old female who had hemoptysis, hotness of body and weight loss. It shows a left upper lobe lung mass near the hilar region. Histopathology demonstrated squamous cell carcinoma of the lung.

CHAPTER FIVE: DISCUSSION

5.1 Introduction

The incidence of lung cancer is continuously increasing globally in both men and women. Availability of newer imaging techniques has made it possible to diagnose lung cancer in the earlier stages and thus improve the prognosis of the patients.

This study was carried out with an aim to determine the diagnostic accuracy of chest CT in the diagnosis of lung tumors based on histopathology as the gold standard among adults at MTRH.

5.2 Demographics

In the present study, the mean age of adults affected with lung tumors was 55 years with a range of 23-86 years, (SD 15.57). This contrasts with a study done by (Bade & Dela Cruz, 2020) where it was found that lung cancer was more common in men and women aged 70 years and older, and that the median age at lung cancer diagnosis was 70 years. In this study, there was female predominance among the patients for susceptibility to lung cancer at 52.3%. The study contrasts with that done by (Bain et al., 2004) which concluded that women did not appear to have a greater susceptibility than men to lung cancer upon equal smoking exposure.

5.3 Risk Factors

In the present study, there was no association found between smoking and incidence of lung tumors. This could be due to adenocarcinoma being the commonest histopathological sub-type in our study, which is generally rising in incidence and often not associated with history of smoking. This contradicts other studies where smoking, especially of cigarettes, has been clearly established in the literature as a major risk factor for the development of lung cancer (Biesalski et al., 1998). This

contrasts with a study by (O'Keeffe et al., 2018) who found tobacco use to be the leading cause of lung cancer, in which 55% and over 70% of lung cancer deaths in women and men were due to smoking. Majority of the study participants with lung cancer in our study (62.8%), had exposure to the use of unprocessed biomass.

This is similar to a study done in rural China, which showed that women who were exposed to smoke from coal fires in their homes had an elevated risk of lung cancer (Lissowska et al., 2005). It was also similar to a study by (Kaplan, 2010) who found indoor air pollution, derived primarily from burning coal, was a highly significant risk factor for lung cancer in women. A study done among the non-smoking women in India found that of all the cooking fuels used, the risk of developing lung cancer was highest among those exposed to biomass fuel, in comparison to the use of Liquefied petroleum gas (LPG) and kerosene. It concurs with a study by (Hernández-Garduño et al., 2004) in Mexico who found out that long-term exposure to wood smoke from cooking contributes significantly to the development of lung cancer. These studies compare well with our study findings where lung cancer incidence was slightly higher among the females in our population, with regard to use of biomass.

In our study, there was a significant finding of patients with lung cancer who reported poor diet in their lifestyle (34.9%). The findings in our study concur with the study done by (Yong et al., 1997) where there was a notable decrease in lung cancer risk with associated high vitamin intake from fruits and vegetables among those with few or reducing pack years of smoking.

5.4 Clinical Features – Symptoms and Signs

Persistent cough was found to be the most common symptom followed by chest pain in this current study. The symptoms are similar to those found by (Ettinger et al., 2015) who found the respiratory symptoms to include cough, hemoptysis and dyspnoea (Ettinger et al., 2015). However, the findings differ from a study done by (Krech et al., n.d.), where the most common and severe symptoms were chest pain, dyspnoea and anorexia. This could be explained by recall bias as most patients reported what they could recall and the symptoms were varied over the long duration of the disease.

Most clinical signs in our study were identified as decreased breath sounds and tachycardia , followed by decreased oxygen saturation, low grade fever hypotension and lymphadenopathy in the order of decreasing frequency. These findings differed from a study done by (Prado et al., 2022) where hemoptysis, chest crackles or wheeze and weight loss were common. This could be explained by their large sample size (698) and longer duration of study (8years).

5.5 Objective 1- Chest CT Scan Findings of Lung Tumors

The most common lobe affected in our study was found to be left upper lobe. The current study findings compare well with a study by (Celikoglu et al., 2006), which discovered that epidermoid carcinoma was found more frequently in the two upper lobes, while small cell carcinomas showed predilection for the right main bronchus and the left upper lobe.

The mean largest dimension of solid component of lung tumor obtained in our study was 4cm with SD of 6.07 This contrasts with the findings in a five year lung cancer screening retrospective study done by (Rosado de Christenson, 2008), where the mean

tumor size was found to be 16.4 mm (range, 5.5–52.5 mm). The difference can be explained by the fact that the later study was a screening programme and it was done retrospectively hence the smaller size of nodules seen.

Most of the lung masses in our current study had solid attenuation and irregular margins (45.3%) while others had smooth (38.4%) and speculated (16.3%) margins. This agrees with a study done on the CT appearance of lung tumors where most of the tumors demonstrated solid and semi-solid attenuation and margins that were irregular and spiculated for most of the non-bronchoalveolar carcinoma types. The bronchoalveolar carcinomas types in that study had ground glass attenuation (Rosado de Christenson, 2008).

There was an equal distribution between the lobulated and multilobulated configuration of the masses. Most of the lung tumors were located centrally on the lung parenchymal tissue (64%) and a few had features of central necrosis (12.8%) and cavitation (4.7%) the inner walls of most of the lung tumors were of soft tissue attenuation (54.7%) and irregular in outline (26.7%). This agrees with a study done by (Goto et al., 2011) which found the frequency of cavity formation in primary lung cancer to be around 2-16%. In that study, squamous cell carcinoma and adenocarcinoma accounted for 45-63 and 30-53% of the cavitation, respectively. Our study concurs with another retrospective study in China where the pseudo-cavitation was noted to be 5.8% (S. K. Kim et al., 2018).

Majority of the lung tumors demonstrated mild (44.2%) to moderate (25.6%) enhancement on contrast enhanced CT (CECT) scans. A few demonstrated intense homogenous enhancement (12.8%) and 3.5 % of the cases showed rim enhancement. Only 14.0% of them did not enhance. In a study done on the comparison of contrast enhanced and non-contrast enhanced helical CT of the chest, CECT was found to

enable visualization of additional hilar and mediastinal nodes. The findings may not have been a true representative of lung tumor stage and may not have had any effect on patient management. Thus the findings on enhancement majorly focused on the radiological staging of the lung tumor (Patz et al., 1999).

Most of the interstitial pattern spread was consolidation and nodularity at 54.7% and 45.3% respectively. This study compares well with a study done by (S. K. Kim et al., 2018) which found the solid nodules to be commonest (50%) followed by part-solid pattern 37.7% and ground glass pattern in 12.3%.

In our study, the satellite mass effect was absent in most cases at 62.8%. This compares well with (Kim et al., 2018) who found a higher incidence of absent satellite lesions. In our study, the pulmonary nodules were the most common satellite lesions (27.9%) while pulmonary lung fibrosis was less common (22.1%). The tumors that demonstrated features of atelectasis accounted for 14.0% of the cases.

Local adenopathy was more on the mediastinal nodes followed by paratracheal nodes at 32.6% and 14.0% respectively. The other infiltrated nodes were intercostal and retro-cardiac nodes, but to a lesser extent at 4.7% and 23% respectively. Majority of the lung masses did not have distant nodal metastasis. However, the few cases which demonstrated distant nodal metastases were mostly on the left axillary nodes (10.5%) followed by cervical neck nodes (9.3%) and right axillary nodes (7.0%). A few lung tumors had bilateral axillary adenopathy (5.8%). This compares with a study done on lympho-vascular invasion where overall nodal metastasis was present in 72/381 patients (18.9%) (S. K. Kim et al., 2018).

The commonest forms of pleural involvement in our study were pleural thickening at 24.4% and pleural infiltration 14.0%. Ipsilateral pleural effusion was the most notable pleural fluid collection (25.6%) besides empyema (7.0%). Bilateral effusion was at 4.7%. Only a few cases had emphysema (8.1%) and pneumothorax (1.2%). Our study differs from the study done by (Kim et al., 2018) where pleural retraction was reported as the commonest pleural involvement at 39.9%.

Most of the lung tumors did not have vascular invasion in this study (90.7%). About 8.1% demonstrated major vascular involvement and 1.2 % invaded minor vessels. This differs from a retrospective study by (Oka et al., 2017) whereby analysis was done for 48 participants with suspected major vascular involvement in lung cancer. It was found that 30% (9 out of 30) had invasion of the pulmonary artery and 18%(2 out of 11) had pulmonary vein invasion.

Osseous involvement was mostly on the sternum (3.5%), and the thoracic vertebra and ribs in equal frequency (2.3%) This differs significantly from a retrospective study of 259 non-small-cell lung cancer (NSCLC) patients by (Tsuya et al., 2007) in which about one half of the patients had the most common site of skeletal metastases as being the spine.

In the overall chest CT findings, most of the lung tumors were primary lung tumors at 76.7%. The tumors originating within the lung parenchyma accounted for (64.0%), the distant metastatic types were (7.0%) and the secondary infiltrative lesions from other primary sites (such as thyroid, mediastinum, pericardium and breasts) accounted for 5.8%, in that order of reducing frequency. Benign tumors accounted for 23.3% on chest CT. This compares well with a study by (Dinesh et al., 2019) where the results from CT revealed that 37(82.2%) of the patients had malignant features of lung tumor and 8(17.7%) showed benign features.

5.6 Objective 2 - Histopathology Findings of Lung Tumors

On the histopathology findings of this study, 60.9% of the cases were found to be malignant lung tumors and benign cases accounted for 19.5%.

This compares well with a study by (Gupta et al., 2019), where malignancy was found in 38 cases (84.4%) & benign lesions were in 7cases (15.5%).

It is also similar to a study done at the Kenyatta National Hospital in Kenya by (John, 2017) among 49 patients where histopathology yielded 36(73.5%) malignant lesions and 13(26.5%) benign lesions.

It is also similar to another study where 311 patients were evaluated and 72.3% had carcinomas, 25.1% had benign lesions, and 2.6% inconclusive lesions (Yang et al., 2015).

The commonest histopathological type of lung malignancy in this study was adenocarcinoma (51.2%) followed by squamous cell carcinoma (10.5%) and large cell carcinoma (1.2%). The findings are similar to a study by (Cruz et al., 2011) where adenocarcinoma accounted for 38.5% of all lung cancer cases, with squamous cell carcinoma accounting for 20% and the large cell carcinoma subtype accounting for 2.9%. This compares well with a study by (John, 2017) who found 94.1% NSCLC and 5.9% SCLC, whereby SCC accounted for 70.6%, adenocarcinoma 23.5% and small cell carcinoma 5.9%.

Regarding benign lung tumors, the more common types were necrotizing granulomatous inflammatory process (TB sequelae) and chronic interstitial pneumonitis both at 5.80%, followed by chronic inflammatory changes (4.70%). Chronic granulomatous inflammatory process accounted for 3.50%. There were two cases of non-specific inflammatory process and one case of COVID-19. This differs

from a study done by (Takahashi et al., 1989) where the more common benign tumors were as below: hamartomas (76%), benign fibrous mesothelioma/solitary fibrous tumor at (12.3%), the inflammatory pseudo-tumor (5.4%), lipoma (1.5%), leiomyoma (1.5%), and single cases of adenoma of the mucous glands, hemangioma and mixed tumor.

5.7 Objective 3- CT Chest and Histopathology Correlation Findings

In our present study, there was a substantial agreement between computed tomography and histopathology findings whereby the two examinations demonstrated a Cohen's Kappa, $\kappa = 0.764$, $p < 0.0001$. Validation of the CT scan diagnosis in this case found a surprising result that the sensitivity value found was quite high at 98.46%, with a specificity value of 71.43%, then PPV, NPV, LR +, LR-, and accuracy were 91.4%, 93.8%,3.38, 0.17and 91.9% respectively.

This compares well with a study done in 2019 in Mahatma Gandhi Medical College in Jaipiur to establish the role of chest CT in the comprehensive lung mass evaluation. In that study, the sensitivity of CT in the diagnosis of malignancy was 97.36%, with a specificity of 100%, a PPV of 100% and NPV of 88.89%. The final diagnosis upon histopathology studies showed malignancy in 38(84.4%) &benign lesions in 7(15.5%), with both having the sensitivity and specificity at 100%. (Sudha et al., 2019)

It is also similar to a study by Japan Clinical Oncology Group where 545 patients were evaluated from 31 institutions between December 2002 and May 2004. It was found to have a high specificity and moderate sensitivity for diagnosis of pathologically diagnosed invasive cancer at 96.4% (161/167, 95% with CI: 92.3–98.7%) and 30.4% (115/378, 95% with CI: 25.8–35.3%) respectively (Suzuki et al., 2011).

This is also comparable to a study done by (Yang et al., 2015) among 311 patients over a 6 year duration. They found the diagnostic accuracy, sensitivity, and specificity of CT-guided percutaneous transthoracic needle biopsy to be 92.9%, 95.3%, and 95.7%, respectively.

A lung cancer screening study was done in America, where 108 patients underwent transthoracic sonographic guided biopsy following chest CT suspicion of lung tumors. This resulted in histopathology features that showed obvious malignant cells in 79 of the cases (73%), benign cells in five of the cases (5%), and inconclusive or unsatisfactory results in 24 cases (Sartori et al., 2007). These results closely mimic the results obtained in our present study.

5.8 Image Guided Modalities for Biopsy of Lung Tumors

Ultrasound guided biopsy was done in majority of the patients (87.2%) while CT guided was done in 12.8% of the patients. This contrasts with a study by (Singh et al., 2004) where CT guided biopsy was used for the diagnosis of most of their thoracic masses. It also contrasts with a study by (Planchard et al., 2018) who did biopsy under CT guidance. This could be explained by the fact that most of their lesions were small and peripherally located.

Some of the immediate post biopsy complications encountered during this study were hemoptysis (6.1%), desaturation (4.9%) and hemothorax (1.2%). The complications encountered differ from those of a study by (Planchard et al., 2018) where the most significant complication of transthoracic needle biopsy was pneumothorax, with rates ranging from 17% to 50%.

This contrasts with a study by (Yang et al., 2015) where they recorded pneumothorax in 17.7% and pulmonary hemorrhage in 11.6% of the cases. This could be explained by their larger sample size of 311 patients.

However, the complications from our study were handled within the department by administration of medications i.e. antifibrinolytics such as intravenous tranexamic acid, antibiotics like metronidazole and amoxicillin-clavulanic acid and analgesics such as morphine, tramadol or paracetamol. Oxygen therapy was administered to the patients developing desaturation and aspiration of any hemothorax under ultrasound guidance was done in some cases.

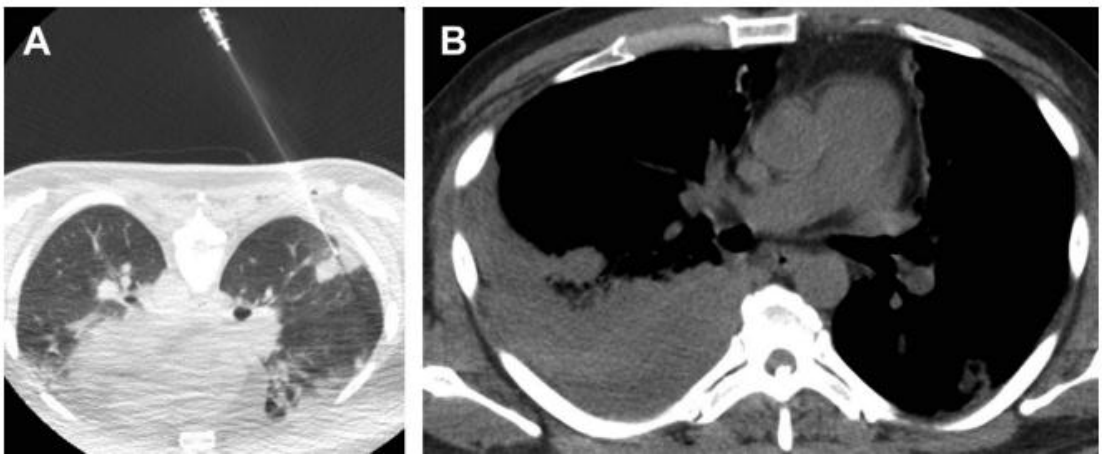

Figure 41: Axial CT scans of chest showing a 49-year-old man with acute myeloid leukemia and fungal pneumonia. **(A) Prone axial lung window CT image during PTNB shows the tip of the coaxial needle in the nodule. (B) Immediately following removal of the coaxial needle the patient developed pleuritic chest pain. Chest CT done showed high-density fluid in the right pleural space secondary to hemothorax that required emergency drainage.**

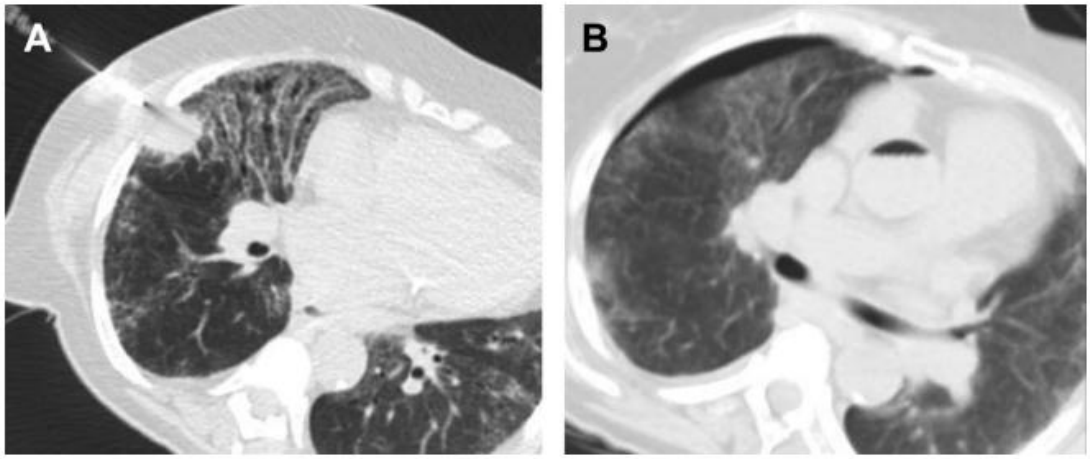

Figure 42: Axial CT scans of the chest showing a 60-year-old woman with air embolism after PTNB (A) Axial lung window CT image shows coaxial needle in the chest wall and a 2.5-cm middle lobe nodule. (B) Repeat CT after the patient's condition deteriorated shows a small right pneumothorax and air in the ascending aorta secondary to an air embolus.

CHAPTER SIX: CONCLUSIONS, LIMITATIONS AND RECOMENDATIONS

6.1 Conclusions

1. The common tumour on chest CT findings was the malignant type with salient features being irregular margins, intense enhancement, mediastinal adenopathy and osseous involvement.
2. Histo-pathologically, the malignant lesions were majority. The more common malignant subtype was adenocarcinoma and benign subtypes were necrotizing granulomatous inflammatory process (TB sequelae) and chronic interstitial pneumonitis.
3. Chest CT had a high diagnostic accuracy, sensitivity and specificity with a substantial kappa agreement in detecting lung tumors based on the obtained histopathology results.

6.2 Limitations of the study

1. This study was conducted in a level 6 teaching and referral hospital, and the results may not be a representative of the entire population and other hospitals both in the public and private sector. Therefore the results may not be generalizable.

6.3 Recommendations

1. Increase awareness to clinicians and radiologists on use of chest CT scan for detecting salient features of the more aggressive malignant lung tumours, for timely interventions.
2. Emphasis to be made to clinicians on the use of histopathology studies for detection of the subtypes of lung tumours prior to treatment.
3. Both chest CT scan and histopathology to be used together for increasing the accuracy of diagnosis of the lung tumours.

REFERENCES

Aoki, T., Nakata, H., Watanabe, H., Nakamura, K., Kasai, T., Hashimoto, H., Yasumoto, K., & Kido, M. (2000). Evolution of Peripheral Lung Adenocarcinomas. *American Journal of Roentgenology*, *174*(3), 763–768. https://doi.org/10.2214/ajr.174.3.1740763

Asamura, H., Suzuki, K., Watanabe, S. I., Matsuno, Y., Maeshima, A., & Tsuchiya, R. (2003). A clinicopathological study of resected subcentimeter lung cancers: A favorable prognosis for ground glass opacity lesions. *Annals of Thoracic Surgery*, *76*(4), 1016–1022. https://doi.org/10.1016/S0003-4975(03)00835-X

Atundo, L., Chite, F., Chesumbai, G., & Kosgei, A. (2018). Incidences and Trends of Lung Cancer in Western Kenya for the Period Between 2012-2016. *Journal of Global Oncology*, *4*(Supplement 2), 201s-201s. https://doi.org/10.1200/jgo.18.81400

Bade, B. C., & Dela Cruz, C. S. (2020). Lung Cancer 2020: Epidemiology, Etiology, and Prevention. *Clinics in Chest Medicine*, *41*(1), 1–24. https://doi.org/10.1016/j.ccm.2019.10.001

Bain, C., Feskanich, D., Speizer, F. E., Thun, M., Hertzmark, E., Rosner, B. A., & Colditz, G. A. (2004). Lung cancer rates in men and women with comparable histories of smoking. *Journal of the National Cancer Institute*, *96*(11), 826–834. https://doi.org/10.1093/jnci/djh143

Barta, J. A., Powell, C. A., & Wisnivesky, J. P. (2019). Global epidemiology of lung cancer. *Annals of Global Health*, *85*(1), 1–16. https://doi.org/10.5334/aogh.2419

Biesalski, H. K., de Mesquita, B. B., Chesson, A., Chytil, F., Grimble, R., Hermus, R. J., Kohrle, J., Lotan, R., Norpoth, K., Pastorino, U., & Thurnham, D. (1998). European Consensus Statement on Lung Cancer: risk factors and prevention. Lung Cancer Panel. *CA: A Cancer Journal for Clinicians*, *48*(3), 167–176. https://doi.org/10.3322/canjclin.48.3.167

Blegen, M. A., Goode, C. J., Spetz, J., Vaughn, T., Hye, S., Care, S. M., & April, N. (2019). *Lippincott Williams & Wilkins*. *49*(4), 406–414.

Bueno, J., Landeras, L., & Chung, J. H. (2018). Updated fleischner society guidelines for managing incidental pulmonary nodules: Common questions and challenging scenarios. *Radiographics*, *38*(5), 1337–1350. https://doi.org/10.1148/rg.2018180017

Cardoso, J. R., Pereira, L. M., Iversen, M. D., & Ramos, A. L. (2014). What is gold standard and what is ground truth? *Dental Press Journal of Orthodontics*, *19*(5), 27–30. https://doi.org/10.1590/2176-9451.19.5.027-030.ebo

Celikoglu, S. I., Aykan, T. B., Karayel, T., Demirci, S., & Göksel, F. M. (1986). The frequency of distribution according to histological types of lung cancer in the tracheobronchial tree among Turkish patients. *Panminerva Medica*, *28*(4), 349–351.

Cohen, J. G., Reymond, E., Jankowski, A., Brambilla, E., Arbib, F., Lantuejoul, S., & Ferretti, G. R. (2016). Lung adenocarcinomas: correlation of computed tomography and pathology findings. *Diagnostic and Interventional Imaging*, *97*(10), 955–963. https://doi.org/10.1016/j.diii.2016.06.021

de Groot, P. M., Wu, C. C., Carter, B. W., & Munden, R. F. (2018). The epidemiology of lung cancer. *Translational Lung Cancer Research*, *7*(3), 220–233. https://doi.org/10.21037/tlcr.2018.05.06

Dela Cruz, C. S., Tanoue, L. T., & Matthay, R. A. (2011). Lung Cancer: Epidemiology, Etiology, and Prevention. *Clinics in Chest Medicine*, *32*(4), 605–644. https://doi.org/10.1016/j.ccm.2011.09.001

Delruei L, Gosselin R, Ilsen B, Landeghem A Van, Mey J De, D. P. (2001). Difficulties in The Interpretation of Chest Radiography. *EurResp*, *Mon17*, 86–119. https://doi.org/10.1007/978-3-540-79942-9

Detterbeck, F. C., Boffa, D. J., Kim, A. W., & Tanoue, L. T. (2017). The Eighth Edition Lung Cancer Stage Classification. *Chest*, *151*(1), 193–203. https://doi.org/10.1016/j.chest.2016.10.010

Dr. Dinesh K. Gupta , Dr. Sudha Gupta, D. S. K. (2019). *Original Research Article Original Research Article*. *6*(34), 2299–2305.

Ettinger, D. S., Wood, D. E., Akerley, W., Bazhenova, L. A., Borghaei, H., Camidge, D. R., Cheney, R. T., Chirieac, L. R., Amico, T. A. D., & Demmy, T. L. (2015). *Non – Small Cell Lung Cancer , Featured Updates to the NCCN Guidelines*. *13*(5), 515–524.

Franco, F., & Di Napoli, A. (2016). Evaluation of diagnostic tests in parallel and in series. *Giornale Di Tecniche Nefrologiche e Dialitiche*, *28*(3), 212–215. https://doi.org/10.5301/gtnd.2016.15992

Gaafar, R. (2017). SC17.05 Lung Cancer in Africa: Challenges and Perspectives. *Journal of Thoracic Oncology*, *12*(1), S115–S116. https://doi.org/10.1016/j.jtho.2016.11.102

Goto, T., Maeshima, A., Oyamada, Y., & Kato, R. (2011). Cavitary lung cancer lined with normal bronchial epithelium and cancer cells. *Journal of Cancer*, *2*(1), 503–506. https://doi.org/10.7150/jca.2.503

Grainger 2019, G. A. D. R. (Ed.). (n.d.). *Grainger & Allison's Diagnostic Radiology Essentials 2nd Edition*.

Hernández-Garduño, E., Brauer, M., Pérez-Neria, J., & Vedal, S. (2004). Wood smoke exposure and lung adenocarcinoma in non-smoking Mexican women. *International Journal of Tuberculosis and Lung Disease*, *8*(3), 377–383.

Islami, F., Torre, L. A., & Jemal, A. (2015). Global trends of lung cancer mortality and smoking prevalence. *Translational Lung Cancer Research*, *4*(4), 327–338. https://doi.org/10.3978/j.issn.2218-6751.2015.08.04

Jazieh, A. R., Algwaiz, G., Errihani, H., Elghissassi, I., Mula-Hussain, L., Bawazir, A. A., & Gaafar, R. (2019). Lung Cancer in the Middle East and North Africa Region. *Journal of Thoracic Oncology*, *14*(11), 1884–1891. https://doi.org/10.1016/j.jtho.2019.02.016

John, W. (2017). *Percutaneous 17/18-gauge Coaxial Ct Guided Core Needle Biopsies of Lung Nodules and Masses at Kenyatta National Hospital: Diagnostic Yield, Complication Rates and Radiological Pattern of Histologically Proven Primary Lung Cancer Histological Subtypes*.

Kaplan, C. (2010). Indoor air pollution from unprocessed solid fuels in developing countries. *Reviews on Environmental Health*, *25*(3), 221–242. https://doi.org/10.1515/REVEH.2010.25.3.221

Kim, S. K., Kim, T. J., Chung, M. J., Kim, T. S., Lee, K. S., Zo, J. I., & Shim, Y. M. (2018). Lung adenocarcinoma: CT features associated with spread through air spaces. *Radiology*, *289*(3), 831–840. https://doi.org/10.1148/radiol.2018180431

Kim, T. H., Kim, S. J., Ryu, Y. H., Lee, H. J., Goo, J. M., Im, J. G., Kim, H. J., Lee, D. Y., Cho, S. H., & Choe, K. O. (2004). Pleomorphic carcinoma of lung: Comparison of CT features and pathologic findings. *Radiology*, *232*(2), 554–559. https://doi.org/10.1148/radiol.2322031201

Kishi, K., Homma, S., Kurosaki, A., Motoi, N., Kohno, T., Nakata, K., & Yoshimura, K. (2004). Small lung tumors with the size of 1 cm or less in diameter: Clinical, radiological, and histopathological characteristics. *Lung Cancer*, *44*(1), 43–51. https://doi.org/10.1016/j.lungcan.2003.09.024

KNCCS. (2017). Ministry of Health National Cancer Control Strategy 2017-2022. *National Cancer Control Strategy*, 1–76. http://www.health.go.ke/wp-content/uploads/2017/10/NATIONAL-CANCER-CONTROL-STRATEGY-2017-2022-KENYA-.pdf

Korir, A., Okerosi, N., Ronoh, V., Mutuma, G., & Parkin, M. (2015). Incidence of cancer in Nairobi, Kenya (2004-2008). *International Journal of Cancer*, *137*(9), 2053–2059. https://doi.org/10.1002/ijc.29674

Krech, R. L., Care, P., Clinic, C., Davis, J., & Information, M. (n.d.). *Symptoms lung*. 309–315.

Li, F., & Abe, H. (2004). Radiology Malignant versus Benign Nodules at CT Screening for Lung Cancer : Comparison of. *Lung*, *1*, 793–798.

Liao, J. H., Amin, V. B., Kadoch, M. A., Beasley, M. B., & Jacobi, A. H. (2015). Subsolid pulmonary nodules: CT-pathologic correlation using the 2011 IASLC/ATS/ERS classification. *Clinical Imaging*, *39*(3), 344–351. https://doi.org/10.1016/j.clinimag.2014.12.009

Liao, W. Y., Liaw, Y. S., Wang, H. C., Chen, K. Y., Luh, K. T., & Yang, P. C. (2000). Bacteriology of infected cavitating lung tumor. *American Journal of Respiratory and Critical Care Medicine*, *161*(5), 1750–1753. https://doi.org/10.1164/ajrccm.161.5.9905103

Lissowska, J., Bardin-Mikolajczak, A., Fletcher, T., Zaridze, D., Szeszenia-Dabrowska, N., Rudnai, P., Fabianova, E., Cassidy, A., Mates, D., Holcatova, I., Vitova, V., Janout, V., Mannetje, A. A. T., Brennan, P., & Boffetta, P. (2005). Lung cancer and indoor pollution from heating and cooking with solid fuels: The IARC international multicentre case-control study in Eastern/Central Europe and the United Kingdom. *American Journal of Epidemiology*, *162*(4), 326–333. https://doi.org/10.1093/aje/kwi204

Macharia, L. W., Mureithi, M. W., & Anzala, O. (2019). Cancer in Kenya: types and infection-attributable. Data from the adult population of two National referral hospitals (2008-2012). *AAS Open Research*, *1*, 25. https://doi.org/10.12688/aasopenres.12910.5

Mittal, A., Hooda, R., & Sofat, S. (2017). Lung field segmentation in chest radiographs: A historical review, current status, and expectations from deep learning. *IET Image Processing*, *11*(11), 937–952. https://doi.org/10.1049/iet-ipr.2016.0526

Molinaro, A. M. (2015). Diagnostic tests: How to estimate the positive predictive value. *Neuro-Oncology Practice*, *2*(4), 161–165. https://doi.org/10.1093/nop/npv030

Moore, K. L. (2019). *Clinically Oriented Embryology Ninth Edition*.

Moore, K. L., Dalley, I. I. A. F., & Agur, A. M. R. (n.d.). *Clinically Oriented Anatomy EIGHTH EDITION*. Wolters Kluwer Health.

Munden, R. F., Carter, B. W., Chiles, C., MacMahon, H., Black, W. C., Ko, J. P., McAdams, H. P., Rossi, S. E., Leung, A. N., Boiselle, P. M., Kent, M. S., Brown, K., Dyer, D. S., Hartman, T. E., Goodman, E. M., Naidich, D. P., Kazerooni, E. A., Berland, L. L., & Pandharipande, P. V. (2018). Managing Incidental Findings on Thoracic CT: Mediastinal and Cardiovascular Findings. A White Paper of the ACR Incidental Findings Committee. *Journal of the American College of Radiology*, *15*(8), 1087–1096. https://doi.org/10.1016/j.jacr.2018.04.029

Nanavaty, P., Alvarez, M. S., & Michael Alberts, W. (2014). Lung Cancer Screening: Advantages, controversies, and applications. *Cancer Control*, *21*(1), 9–14. https://doi.org/10.1177/107327481402100102

Nicholson, A. G., Tsao, M. S., Beasley, M. B., Borczuk, A. C., Brambilla, E., Cooper, W. A., Dacic, S., Jain, D., Kerr, K. M., Lantuejoul, S., Noguchi, M., Papotti, M., Rekhtman, N., Scagliotti, G., van Schil, P., Sholl, L., Yatabe, Y., Yoshida, A., & Travis, W. D. (2022). The 2021 WHO Classification of Lung Tumors: Impact of Advances Since 2015. *Journal of Thoracic Oncology*, *17*(3), 362–387. https://doi.org/10.1016/j.jtho.2021.11.003

Noguchi, M., Morikawa, A., Kawasaki, M., Matsuno, Y., Yamada, T., Hirohashi, S., Kondo, H., & Shimosato, Y. (1995). Small adenocarcinoma of the lung. Histologic characteristics and prognosis. *Cancer*, *75*(12), 2844–2852. https://doi.org/10.1002/1097-0142(19950615)75:12<2844::AID-

CNCR2820751209>3.0.CO;2-#

Nwagbara, U. I., Ginindza, T. G., & Hlongwana, K. W. (2020). Health systems influence on the pathways of care for lung cancer in low- And middle-income countries: A scoping review. *Globalization and Health*, *16*(1), 1–11. https://doi.org/10.1186/s12992-020-00553-8

O'Keeffe, L. M., Taylor, G., Huxley, R. R., Mitchell, P., Woodward, M., & Peters, S. A. E. (2018). Smoking as a risk factor for lung cancer in women and men: A systematic review and meta-analysis. *BMJ Open*, *8*(10), 1–12. https://doi.org/10.1136/bmjopen-2018-021611

Oka, S., Shinohara, S., Kuwata, T., Takenaka, M., Chikaishi, Y., Hirai, A., Ichiki, Y., Shimajiri, S., Aoki, T., & Tanaka, F. (2017). The major thoracic vascular invasion of lung cancer. *Annals of Medicine and Surgery*, *20*, 13–18. https://doi.org/10.1016/j.amsu.2017.06.025

Patz, E. F., Erasmus, J. J., McAdams, H. P., Connolly, J. E., Marom, E. M., Goodman, P. C., Leder, R. A., Keogan, M. T., & Herndon, J. E. (1999). Lung cancer staging and management: Comparison of contrast-enhanced and nonenhanced helical CT of the thorax. *Radiology*, *212*(1), 56–60. https://doi.org/10.1148/radiology.212.1.r99jl1956

Planchard, D., Popat, S., Kerr, K., Novello, S., Smit, E. F., Faivre-Finn, C., Mok, T. S., Reck, M., Van Schil, P. E., Hellmann, M. D., & Peters, S. (2018). Metastatic non-small cell lung cancer: ESMO Clinical Practice Guidelines for diagnosis, treatment and follow-up. *Annals of Oncology*, *29*(Supplement 4), iv192–iv237. https://doi.org/10.1093/annonc/mdy275

Prado, M. G., Kessler, L. G., Au, M. A., Burkhardt, H. A., Suchsland, M. Z., Kowalski, L., Otr, L., Walter, F. M., Lybarger, K., Turner, G., & Farjah, F. (2022). *Symptoms and signs of lung cancer prior to diagnosis : Comparative study using electronic health records*.

Rosado de Christenson, M. L. (2008). Five-year Lung Cancer Screening Experience: CT Appearance, Growth Rate, Location, and Histologic Features of 61 Lung Cancers. *Yearbook of Diagnostic Radiology*, *2008*(2), 8–10. https://doi.org/10.1016/s0098-1672(08)79004-0

Said, N. S. (2023). *Assessment of survival outcomes among lung cancer patients at the National and Referral Hospital in Kenya*. *January*, 9194–9201. https://doi.org/10.1002/cam4.5658

Said, N. S., & Degu, A. (2023). Assessment of survival outcomes among lung cancer patients at the National and Referral Hospital in Kenya. *Cancer Medicine*, *September 2022*, 9194–9201. https://doi.org/10.1002/cam4.5658

Sartori, S., Tombesi, P., Trevisani, L., Nielsen, I., Tassinari, D., & Abbasciano, V. (2007). Accuracy of transthoracic sonography in detection of pneumothorax after sonographically guided lung biopsy: Prospective comparison with chest radiography. *American Journal of Roentgenology*, *188*(1), 37–41.

https://doi.org/10.2214/AJR.05.1716

Sharma, A., & Shepard, J. O. (2018). Lung Cancer Biopsies. *Radiologic Clinics of NA*. https://doi.org/10.1016/j.rcl.2018.01.001

Singh, J., Garg, L., & Setia, V. (2004). Computed tomography (Ct) guided transthoracic needle aspiration cytology in difficult thoracic mass lesions-not approachable by USG. *Indian Journal of Radiology and Imaging*, *14*. https://link.gale.com/apps/doc/A158965232/HRCA?u=anon~d2bee3e4&sid=googleScholar&xid=3400a10f

Stapelfeld, C., Dammann, C., & Maser, E. (2020). Sex-specificity in lung cancer risk. *International Journal of Cancer*, *146*(9), 2376–2382. https://doi.org/10.1002/ijc.32716

Stephanie, R. (2011). anatomy for diagnostic imaging by Stephanie Ryan. In *Elseviers: Vol. 3rd editio* (Issue 3). https://doi.org/10.5843/jsot.32.171

Suzuki, K., Koike, T., Asakawa, T., Kusumoto, M., Asamura, H., Nagai, K., Tada, H., Mitsudomi, T., Tsuboi, M., Shibata, T., Fukuda, H., & Kato, H. (2011). A prospective radiological study of thin-section computed tomography to predict pathological noninvasiveness in peripheral clinical ia lung cancer (Japan Clinical Oncology Group 0201). *Journal of Thoracic Oncology*, *6*(4), 751–756. https://doi.org/10.1097/JTO.0b013e31821038ab

Takahashi, T., Ogasawara, A., Yano, S., Ikeda, J., Hishiyama, M., Masuda, T., Okayasu, T., Hashimoto, M., & Tanabe, T. (1989). 38 Cases of Benign Tumors and Tumor-Like Lesions of the Lung. *Haigan*, *29*(3), 253–262. https://doi.org/10.2482/haigan.29.253

Travis, W. D., Brambilla, E., Noguchi, M., Nicholson, A. G., Geisinger, K. R., Yatabe, Y., Beer, D. G., Powell, C. A., Riely, G. J., Van Schil, P. E., Garg, K., Austin, J. H. M., Asamura, H., Rusch, V. W., Hirsch, F. R., Scagliotti, G., Mitsudomi, T., Huber, R. M., Ishikawa, Y., … Yankelewitz, D. (2011). International association for the study of lung cancer/American Thoracic Society/European Respiratory Society international multidisciplinary classification of lung adenocarcinoma. *Journal of Thoracic Oncology*, *6*(2), 244–285. https://doi.org/10.1097/JTO.0b013e318206a221

Tsuya, A., Kurata, T., Tamura, K., & Fukuoka, M. (2007). Skeletal metastases in non-small cell lung cancer: A retrospective study. *Lung Cancer*, *57*(2), 229–232. https://doi.org/10.1016/j.lungcan.2007.03.013

Viera, A. J., & Garrett, J. M. (2005). Anthony J. Viera, MD; Joanne M. Garrett, PhD (2005). Understanding interobserver agreement: the kappa statistic. Fam Med 2005;37(5):360-63. *Family Medicine*, *37*(5), 360–363. http://www1.cs.columbia.edu/~julia/courses/CS6998/Interrater_agreement.Kappa_statistic.pdf

Warui, L. W., Suleman, M. A., Makokha, F. W., & Kamita, M. (2021). *Trend in Cancer Cases Diagnosed at Kiambu and Gatundu Level 5 Hospitals , Kiambu County Kenya between 2013 and 2017*. *4*(1), 36–48.

Wheless, L., Brashears, J., & Alberg, A. J. (2013). Epidemiology of lung cancer. *Lung Cancer Imaging*, 1–15. https://doi.org/10.1007/978-1-60761-620-7_1

Winokur, R. S., Pua, B. B., Sullivan, B., & Madoff, D. C. (2013). Percutaneous lung biopsy: Technique, efficacy, and complications. *Seminars in Interventional Radiology*, *30*(2), 121–127. https://doi.org/10.1055/s-0033-1342952

Yang, W., Sun, W., Li, Q., Yao, Y., Lv, T., Zeng, J., Liang, W., Zhou, X., & Song, Y. (2015). Diagnostic accuracy of CT-guided transthoracic needle biopsy for solitary pulmonary nodules. *PLoS ONE*, *10*(6), 1–9. https://doi.org/10.1371/journal.pone.0131373

Yong, L. C., Brown, C. C., Schatzkin, A., Dresser, C. M., Slesinski, M. J., Cox, C. S., & Taylor, P. R. (1997). Intake of vitamins E, C, and A and risk of lung cancer. *American Journal of Epidemiology*, *146*(3), 231–243. https://doi.org/10.1093/oxfordjournals.aje.a009258

APPENDICES

Appendix I: Client Explanation Form

Akora Rosemary Moraa

SM/PGR/08/18

Phone: 0728474285

Dear Client,

I am a Resident Registrar currently pursuing a Master of Medicine Degree in Radiology and Imaging at Moi University.

As part of the fulfillment of the M.Med program requirements, I am conducting a study entitled '**DIAGNOSTIC ACCURACY OF CHEST COMPUTED TOMOGRAPHY IN THE DIAGNOSIS OF LUNG TUMORS AMONG ADULTS BASED ON HISTOPATHOLOGY AT MOI TEACHING AND REFERRAL HOSPITAL.'**

The study population includes the patients who have been diagnosed with suspected or confirmed lung tumor by CT scan of the chest and undergone lung biopsy to get a histopathology result. The study will be carried over a period of one year. The information which will be obtained will provide local data regarding the incidence and types of lung tumors from the histopathological and give the diagnostic accuracy of chest CT to in the diagnosis of the same. This will help the healthcare providers to improve quality service and care for patients who have been diagnosed with lung tumors, as well as aid in health policy formulation on the management protocols for the same.

I am requesting for 5 minutes of your time to fill the attached consent form. I will be obtaining information from using by using a data collection form. Please answer the

questions as truthfully and I will be recording the answers on the data collection sheet.

I assure you that confidentiality will be maintained.

You are at liberty to ask for any clarification on any issues regarding this particular survey at any time.

The study findings will be presented to the IREC committee and the department of Radiology and Imaging, MTRH, for the use of CT in aiding the diagnosis and management of lung tumors.

Withdrawal from the study at any given point is allowed since this is a voluntary exercise.

No monetary payment will be given or asked for volunteering to participate in this study.

Thank you,

Rosemary Akora.

Appendix II: Consent Form

I……. (Initials) hereby consent to be included in the study titled:

DIAGNOSTIC ACCURACY OF CHEST COMPUTED TOMOGRAPHY IN THE DIAGNOSIS OF LUNG TUMORS AMONG ADULTS BASED ON HISTOPATHOLOGY AT MOI TEACHING AND REFERRAL HOSPITAL.

I confirm that I have read the cover letter that clearly outlines the nature of the study and I understand that confidentiality will be maintained at all times.

In case any problem or questions arise in the course of duration of the study, I am at liberty to contact the primary researcher Dr. Rosemary Akora on 0728474285 or akorarosemary@gmail.com for any clarification and further information or instructions as need be.

I fully understand the right of withdrawal from the study at any point.

I hereby give my consent.

Name: ……. (Initials)

Signature…….....Date…….

Statement by the researcher

I confirm that the participant has been explained to about the study and been given an opportunity to ask questions. All the questions raised have been answered extensively.

I confirm that the participant has not been coerced to participate in the study and that the consent has been given freely and voluntarily.

Name: ……...

Signature of the researcher: …….

Date: …….

Appendix III: Data Collection Form

Part I:

Date …… Medical Record No. …….....

Serial No. …….....

A. Participant Socio-demographics

1. Age (years)

Age years	Age bracket (tick)	Exact years
18-28		
29-38		
39-48		
49-58		
59-68		
69-78		
>79		

2. Gender

Male	
Female	
Other	

3. Occupation

Employed	
Informal employment	
Business person	
Other(s)	

4. Residence

Urban	
Semi-urban	
Rural	
Other(s)	

B. Risk factors for lung cancer

Risk factor	**Present**	**Absent**
History of cigarette smoking		
Use of unprocessed biomass		
Exposure to occupational hazards e.g., asbestos		
1st degree relative with lung cancer		
Poor diet		
Other(s)		
Total		

C. Clinical presentation of lung cancer

Presentation feature	**Present**	**Absent**
Persistent cough		
Chest pain		
Difficulty in breathing		
Hemoptysis (blood-stained sputum)		
Unexplained weight loss		
Hoarseness of voice		
General body malaise		
Loss of appetite		
Incidental finding on chest x-ray		
Other(s)		
Total		

D. Clinical Examination Findings for lung cancer

Examination finding	**Present**	**Absent**
Decreased/absent breath sounds		
Low grade fever		
Decreased oxygen saturation		
Tachypnea (increased respiratory rate)		
Tachycardia (increased heart rate)		
Hypotension (decreased blood pressure)		
Lymphadenopathy (lymph node enlargement)		
Other (s)		

E) Lung mass description on CT chest

Site: RUL……..RML…….RLL……LUL……LLL…….

Size (AP, TRANSV,

CC)……

Largest dimension

……

……..

Margins: Irregular……..Spiculated……..Smooth ……

Configuration: Multi-lobulated……. lobulated…….....

Characteristics: ……Central necrosis …Cavity/eccentric…….Central……

Inner wall: smooth……. Irregular……calcification……mixed …soft tissue…..

Enhancement pattern: Enhancing…….mild ……moderate……vivid……..

Non-enhancing……

Extension/ infiltrative pattern: hilar…….mediastinal……..chest

wall…….parenchyma…..

Interstitial pattern spread: nodular……consolidation……

Satellite mass effect: present…….absent…….

Associated features

Satellite lesions……pulmonary nodules…….fibrosis……. atelectasis ……

Other masses……

Nodes: Local

PARATRACHEAL……

RETROCARDIAC……

MEDIASTINAL……..

INTERCOSTAL……

PREAORTIC …….

PARAAORTIC……

Distant……

Pleural involvement

Pleura: Thickening …….nodules…..mass ……..infiltration……

Pleural fluid collections:

Effusion……hemothorax……..empyema……

Pleural air collections: pneumothorax…….. Emphysema…….

Mixed: …….

Vascular invasion:

Major……

Minor……

Osseous involvement: vertebra: cervical …… thoracic……

Ribs……

Sternum……

Muscle involvement: Yes……No……..

Subcutaneous tissue involvement: yes…..……..No……...

F) CT Findings Conclusion

Neoplastic: Primary……..

Secondary: infiltrative…….distant……

Inflammatory ……**.....**

Mixed……

Indeterminate…….

G) Histopathology findings

Malignant: ……**.....**

Benign: ……

Mixed (scarring/inflammation/infection)……

Indeterminate (IHC required)…..……

H) Biopsy method

Ultrasound guided……

CT scan guided…….

I) Immediate complications post biopsy

Hemothorax……..

Pneumothorax……

Hemoptysis……

Desaturation…….

Mixed…….

Others …….

J) Immunohistochemistry done:

Yes……..No……

Name of data collector…….Signature……..Date

Name of Supervisor……Signature…….Date

Appendix IV: Budget

Items	Quantity	Unit Price (Kshs)	Total (Kshs)
Stationery & Equipment			
Printing papers	5 reams	500.00	2,500.00
Flash drive	1	2,000.00	2,000.00
Black ink cartridges	2	2,000.00	4,000.00
Writing pens	1 packet	500.00	500.00
Box files	2	200.00	400.00
Document wallets	2	50.00	100.00
Sub-total			**9,500**

Research proposal development			
Printing drafts & final proposal	10 copies	500.00	5,000.00
Photocopies of final proposal	6 copies	100.00	600.00
Binding of copies of proposal	5 copies	100.00	500.00
Sub-total			**6,100.00**
Personnel			
Biostatistician	1	15,000	15,000.00
Research assistant 1	2	5,000	10,000.00
Sub-total			**25,000.00**
Thesis Development			
Printing of drafts and final thesis	10 copies	800.00	8,000.00
Photocopy of final thesis	6 copies	200.00	1,200.00
Binding of thesis	6 copies	300.00	1,800.00
Publication	1	20,000	20,000.00
Sub-total			**31,000.00**
Total			**71,600.00**
Miscellaneous expenditure			**20,000.00**
Grand total			**91,600.00**

Appendix V: Work Plan

	2021	**2022**						
ACTIVITY	**JAN-MAR 2021**	**APR-JUN 2021**	**JUL-SEPT 2021**	**OCT-DEC 2021**	**JAN-MAR 2022**	**APR-JUN 2022**	**JUL-SEP 2022**	**OCT-DEC 2022**
Proposal Concept development								
Proposal writing								
Ethical approval + Nacosti certification								
Data collection								
Data analysis								
Report writing								

Appendix VI: IREC Approval

INSTITUTIONAL RESEARCH AND ETHICS COMMITTEE (IREC)

MOI TEACHING AND REFERRAL HOSPITAL
P.O. BOX 3
ELDORET
Tel: 33471//2/3

MOI UNIVERSITY
COLLEGE OF HEALTH SCIENCES
P.O. BOX 4606
ELDORET
Tel: 33471/2/3

Reference: IREC/2021/46
Approval Number: 0003849

15th April, 2021

Dr. Akora Rosemary Moraa,
Moi University,
School of Medicine,
P.O. Box 4606-30100,
ELDORET-KENYA.

Dear Dr. Akora,

DIAGNOSTIC ACCURACY OF CHEST COMPUTED TOMOGRAPHY IN THE DIAGNOSIS OF LUNG TUMORS BASED ON HISTOPATHOLOGY AMONG ADULTS AT MOI TEACHING AND REFERRAL HOSPITAL

This is to inform you that ***MTRH/MU-IREC*** has reviewed and approved your above research proposal. Your application approval number is ***FAN: 0003849.*** The approval period is **15th April, *2021 – 14th April, 2022.***
This approval is subject to compliance with the following requirements;

i. Only approved documents including (informed consents, study instruments, MTA) will be used.
ii. All changes including (amendments, deviations, and violations) are submitted for review and approval by ***MTRH/MU-IREC***.
iii. Death and life threatening problems and serious adverse events or unexpected adverse events whether related or unrelated to the study must be reported to ***MTRH/MU-IREC*** within 72 hours of notification.
iv. Any changes, anticipated or otherwise that may increase the risks or affected safety or welfare of study participants and others or affect the integrity of the research must be reported to ***MTRH/MU-IREC*** within 72 hours.
v. Clearance for export of biological specimens must be obtained from ***MTRH/MU-IREC*** for each batch of shipment.
vi. Submission of a request for renewal of approval at least 60 days prior to expiry of the approval period. Attach a comprehensive progress report to support the renewal.
vii. Submission of an executive summary report within 90 days upon completion of the study to ***MTRH/ MU-IREC.***

Prior to commencing your study; you will be required to obtain a research license from the National Commission for Science, Technology and Innovation (NACOSTI) https://oris.nacosti.go.ke and other relevant clearances. Further, a written approval from the CEO-MTRH is mandatory for studies to be undertaken within the jurisdiction of Moi Teaching & Referral Hospital (MTRH), which includes 22 Counties in the Western half of Kenya.

Sincerely,

INSTITUTIONAL RESEARCH & ETHICS COMMITTEE
15 APR 2021
APPROVED
P. O. Box 4606-30100 ELDORET

PROF. E. WERE
CHAIRMAN
INSTITUTIONAL RESEARCH AND ETHICS COMMITTEE

cc CEO - MTRH Dean - SOP Dean - SOM
Principal - CHS Dean - SON Dean - SOD

Appendix VII: Hospital Approval (MTRH)

An ISO 9001:2015 Certified Hospital

MOI TEACHING AND REFERRAL HOSPITAL

Telephone :(+254)053-2033471/2/3/4
Mobile: 722-201277/0722-209795/0734-600461/0734-683361
Fax: 053-2061749
Email: ceo@mtrh.go.ke/directorsofficemtrh@gmail.com

Nandi Road
P.O. Box 3 – 30100
ELDORET, KENYA

Ref: ELD/MTRH/R&P/10/2/V.2/2010

16th April, 2021

Dr. Akora Rosemary Moraa
Moi University
School of Medicine
P.O .Box 4606-30100
ELDORET-KENYA

DIAGNOSTIC ACCURACY OF CHEST COMPUTED TOMOGRAPHY IN THE DIAGNOSIS OF LUNG TUMORS BASED ON HISTOPATHOLOGY AMONG ADULTS AT MOI TEACHING AND REFERRAL HOSPITAL

In order to conduct research within the jurisdiction of Moi Teaching and Referral Hospital (MTRH) this includes 22 counties in the Western half of Kenya. You are required to strictly adhere to the regulations stated below in order to safeguard the safety and well-being of staff and patients seen at MTRH involved research studies.

1. The study shall be under Moi Teaching and Referral Hospital regulation.
2. A copy of MU/MTRH-IREC approval shall be provided.
3. Studies dealing with collection, storage and transportation of Human Biological Material (HBM) will not be allowed to export the HBM outside the jurisdiction of **MTRH.**
4. For those tests which are unavailable locally the PI is tasked to ensure sourcing of equipment and subsequent training of staff to build their capacity.
5. No data collection will be allowed without an approved consent form(s) to participants to sign.
6. Take note that **data** collected must be treated with due confidentiality and anonymity.

Permission to conduct research shall only be provided once all the requirements stated above have been met.

MOI TEACHING AND REFERRAL HOSPITAL
CEO
APPROVED
16 APR 2021
P. O. Box 3-30100, ELDORET

16/04/2021
DR. WILSON K. ARUASA, *EBS*
CHIEF EXECUTIVE OFFICER
MOI TEACHING AND REFERRAL HOSPITAL

c.c. - Senior Director, Clinical Services
- Director of Nursing Services
- HOD, HRISM

Appendix VIII: Nacosti Approval

REPUBLIC OF KENYA

NATIONAL COMMISSION FOR SCIENCE,TECHNOLOGY & INNOVATION

Ref No: 377897

Date of Issue: 18/May/2021

RESEARCH LICENSE

This is to Certify that Dr.. ROSEMARY MORAA AKORA of Moi University, has been licensed to conduct research in Uasin-Gishu on the topic: DIAGNOSTIC ACCURACY OF CHEST COMPUTED TOMOGRAPHY IN DIAGNOSIS OF LUNG TUMORS BASED ON HISTOPATHOLOGY AMONG ADULTS AT MOI TEACHING AND REFERRAL HOSPITAL. for the period ending : 18/May/2022.

License No: NACOSTI/P/21/10501

377897

Applicant Identification Number

Director General
NATIONAL COMMISSION FOR SCIENCE,TECHNOLOGY & INNOVATION

Verification QR Code

NOTE: This is a computer generated License. To verify the authenticity of this document, Scan the QR Code using QR scanner application.